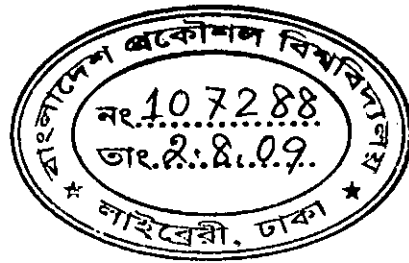


**MIXED CONVECTION IN TRAPEZOIDAL CAVITIES AT  
VARIOUS ASPECT RATIOS WITH A MOVING LID**

**by**

**Tanvir Reza Tanim**

Submitted in partial fulfillment of the requirements for the degree of  
**MASTER OF SCIENCE IN MECHANICAL ENGINEERING**



Department of Mechanical Engineering

**BANGLADESH UNIVERSITY OF ENGINEERING AND TECHNOLOGY**

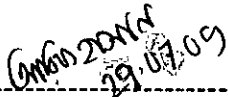

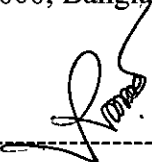
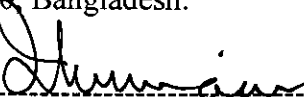
Dhaka-1000, Bangladesh

July 2009



The thesis titled “**Mixed Convection in Trapezoidal cavities at various aspect ratios with a moving lid**”, submitted by **Tanvir Reza Tanim**, Roll no: 100710006P Session October, 2007 has been accepted as satisfactory in partial fulfillment of the requirement for the degree of MASTER OF SCIENCE IN MECHANICAL ENGINEERING on July 29, 2009.

## BOARD OF EXAMINERS

1.   
-----  
**Dr. Md. Arif Hasan Mamun**  
Associate Professor  
Department of Mechanical Engineering  
Bangladesh University of Engineering and Technology (BUET)  
Dhaka-1000, Bangladesh.  
Chairman
2.   
-----  
**Dr. Abu Rayhan Md. Ali**  
Professor  
Department of Mechanical Engineering  
Bangladesh University of Engineering and Technology (BUET)  
Dhaka-1000, Bangladesh.  
Member  
(Ex-officio)
3.   
-----  
**Dr. Chowdhury Md. Feroz**  
Professor  
Department of Mechanical Engineering  
Bangladesh University of Engineering and Technology (BUET)  
Dhaka-1000, Bangladesh.  
Member
4.   
-----  
**Dr. A. K. M Iqbal Hussain**  
Professor  
Department of Mechanical and Chemical Engineering  
Islamic University Technology (IUT)  
Gazipur, Bangladesh.  
External

## CANDIDATE'S DECLARATION

It is hereby declared that this thesis or any part of it has not been submitted elsewhere for any degree or diploma.



---

**Tanvir Reza Tanim**

## CERTIFICATE OF RESEARCH

This is to certify that the work presented in this thesis is carried out by the author under the supervision of Dr. Md. Arif Hasan Mamun, Associate Professor of the Department of Mechanical Engineering, Bangladesh University of Engineering & Technology, Dhaka.

Gm6n2014  
29.07.09

-----  
**Dr. Md. Arif Hasan Mamun**



-----  
**Tanvir Reza Tanim**

*Dedicated to My Parents*

## **ACKNOWLEDGEMENT**

I recall with sincere gratitude my supervisor Dr. Md. Arif Hasan Mamun, Associate Professor, Department of Mechanical Engineering, Bangladesh University of Engineering and Technology, who has brought the CFD concept to my attention and contributed by his constructive suggestions and criticism to the improvement of this research work. Without his assistance, the research work could not have been completed in time.

I owe a debt of gratitude to Tofiqul Islam who has assisted me by providing useful advices.

Special thanks also go to all of my colleagues and friends.

## ABSTRACT

Two dimensional steady, mixed convection heat transfer in a trapezoidal cavity with constant heat flux from the bottom wall while the isothermal moving top wall in the horizontal direction has been studied numerically. Firstly the problem is defined as a two dimensional enclosure. Control Volume based finite volume method (FVM) has been used to discretize the governing differential equations. The pressure- velocity coupling in the governing equations is obtained using the well known SIMPLE method for numerical computations. The set of governing equations are solved sequentially. A second order upwind differencing scheme is used for the formulation of the coefficients in the finite-volume equations. All computations are done for a range of Richardson number,  $Ri$  from 0.1 to 10 and the aspect ratio,  $A$  has been changed from 0.5 to 2 for a fluid having Prandtl number equal to 0.71 (air). First the optimum configuration of the trapezoidal cavity has been obtained by changing the inclination angle,  $\gamma$  of the side walls. Then the effect of Richardson number, aspect ratio, and Rotation angle,  $\Phi$  ( $30^\circ, 45^\circ$  and  $60^\circ$ ) of the optimum trapezoidal cavity has been studied by changing the desired parameter. Results have been presented in the form of streamline and isotherm plots as well as the variation of the Nusselt number at the heat source surface under different conditions. The results shows that with increasing  $Ri$ , the heat transfer rate increases as natural convection dominates. The rotational angle of the trapezoidal cavity and the direction of the lid motion affect the heat transfer rate significantly. Optimum heat transfer rate is obtained for aiding flow condition having higher values of  $Ri$ .

## NOMENCLATURE

$h$	convective heat transfer coefficient ( $\text{W}/\text{m}^2 \text{K}$ )
$q''$	Heat Flux ( $\text{W}/\text{m}^2$ )
$C_P$	specific heat at constant pressure ( $\text{J}/\text{kg K}$ )
$g$	gravitational acceleration ( $\text{m}/\text{s}^2$ )
$k$	thermal conductivity of the fluid ( $\text{W}/\text{m K}$ )
$Nu$	Nusselt number, $hW/k$
$Pr$	Prandtl number, $\nu/\alpha$
$Gr$	Grashof number, $g\beta\Delta TW^3/\nu^2$
$Re$	Reynolds number, $U_0W/\nu$
$Ri$	Richardson number, $Gr/Re^2$
$A$	Aspect Ratio, $H/W$
$R$	length of the inclined sidewalls (m)
$T$	temperature of the fluid, ( $^{\circ}\text{C}$ )
$u$	velocity component at x-direction (m/s)
$U$	dimensionless velocity component at X-direction
$v$	velocity component at y-direction (m/s)
$V$	dimensionless velocity component at Y-direction
$W$	length of the cavity, (m)
$x$	distance along the x-coordinate
$X$	distance along the non-dimensional x-coordinate
$Y$	distance along the non-dimensional y-coordinate

### ***Greek Symbols***

$\alpha$	thermal diffusivity of the fluid ( $\text{m}^2/\text{s}$ )
$\beta$	volumetric coefficient of thermal expansion ( $\text{K}^{-1}$ )
$\gamma$	inclination angle of the sidewalls of the cavity
$\theta$	dimensionless temperature, $(T_H - T_C)/\Delta T$
$\mu$	dynamic viscosity of the fluid (Pa s)
$\nu$	kinematic viscosity of the fluid ( $\text{m}^2/\text{s}$ )
$\rho$	density of the fluid ( $\text{kg}/\text{m}^3$ )
$\phi$	rotational angle of the cavity



***Subscripts***

<i>av</i>	average value
<i>c</i>	value of cold temperature
<i>H</i>	value of hot temperature

# Contents

CANDIDATE'S DECLARATION.....	iii
CERTIFICATE OF RESEARCH.....	iv
ACKNOWLEDGEMENT.....	vi
ABSTRACT.....	vii
NOMENCLATURE.....	viii
LIST OF FIGURES.....	xii
<b>CHAPTER 1: INTRODUCTION.....</b>	<b>1</b>
1.1 GENERAL.....	1
1.2 FLOW WITHIN AN ENCLOSURE.....	3
1.3 TILTED ENCLOSURE.....	3
1.4 LID DRIVEN ENCLOSURE.....	4
1.5 APPLICATION.....	4
1.6 MOTIVATION BEHIND THE SELECTION OF PROBLEM.....	5
1.7 MAIN OBJECTIVE OF THE WORK.....	6
<b>CHAPTER 2: LITERATURE REVIEW.....</b>	<b>7</b>
<b>CHAPTER 3 MATHEMATICAL MODELING.....</b>	<b>11</b>
3.1 PHYSICAL MODEL.....	11
3.2.1 GOVERNING EQUATIONS IN DIMENSIONAL FORM.....	14
3.2.2 DIMENSIONAL ANALYSIS.....	15
3.2.3 BOUNDARY CONDITIONS.....	16

<b>CHAPTER 4 COMPUTATIONAL DETAILS.....</b>	<b>17</b>
4.1 CFD PROCESSES AT A GLANCE .....	19
4.2 FINITE VOLUME METHOD .....	21
4.3 SOLUTION OF A CFD ANALYSIS USING FVM METHOD .....	22
4.4 STEPS FOR SOLVING THE PROBLEM USING FVM METHOD .....	24
4.5 GRID INDEPENDENCE TEST .....	25
4.6 INITIALIZATION THE SIMULATION .....	26
4.7 SOLVER SETTING.....	27
4.8 CONVERGENCE CRITERIA.....	27
4.9 CODE VALIDATION.....	27
<b>CHAPTER 5 RESULTS AND DISCUSSION .....</b>	<b>29</b>
5.1 EFFECT OF INCLINATION ANGLES .....	29
5.2 EFFECT OF RICHARDSON NUMBER.....	30
5.3 EFFECT OF ASPECT RATIO .....	31
5.4 EFFECT OF REYNOLDS NUMBER.....	32
5.5 EFFECT OF ROTATIONAL ANGLES .....	33
<b>CHAPTER 6 CONCLUSION.....</b>	<b>90</b>
<b>CHAPTER 7 FURTHER RECOMMENDATIONS.....</b>	<b>91</b>
<b>REFERENCES.....</b>	<b>92</b>
APPENDIX : AVERAGE NUSSELT NUMBER FOR A TRAPEZOIDAL ENCLOSURE.....	95

## LIST OF FIGURES

Figure 3.1 Schematic diagram of the physical system considering opposing flow condition:.....	12
Figure 3.2 Schematic diagram of the physical system considering aiding flow condition.....	12
Figure 4.1 Finite Volume discretization of a domain:.....	24
Figure 4.2 Current mesh structure .....	25
Figure 4.3: Convergence of the $Nu_{av}$ with grid refinement for rectangular cavity at $Ri=1.0$ , $Re=400$ and $A=1$ .....	25
Figure 4.4: Grid sensitivity test for Trapezoidal cavity at $Ri=1.0$ , $Re=400$ and $A=1$ .....	27
Figure 4.5: Variation of the Average Nusselt number with different Aspect Ratio at $Ri=10$ , $Re=100$ and $\epsilon =0.6$ .....	28
Figure 5.1: Contours of Streamlines and isotherms at $Re=400$ , $A=1.0$ and $\gamma=30^\circ$ .....	35
Figure 5.2: Contours of Streamlines and isotherms at $Re=400$ , $A=1.0$ and $\gamma=45^\circ$ .....	36
Figure 5.3: Contours of Streamlines and isotherms at $Re=400$ , $A=1.0$ and $\gamma=60^\circ$ .....	37
Figure 5.4: Average Nusselt number, $Nu_{av}$ vs Richardson number at $Re=400$ , $A=1$ .....	38
Figure 5.5: Average Nusselt number, $Nu_{av}$ vs Richardson number at $Re=600$ , $A=1$ .....	38
Figure 5.6: Contours of Streamlines and isotherms at $Re=400$ , $A=0.5$ and $\Phi=0^\circ$ .....	39
Figure 5.7: Contours of Streamlines and isotherms at $Re=400$ , $A=1.0$ and $\Phi=0^\circ$ .....	40
Figure 5.8: Contours of Streamlines and isotherms at $Re=400$ , $A=1.5$ and $\Phi=0^\circ$ .....	41
Figure 5.9: Contours of Streamlines and isotherms at $Re=400$ , $A=2.0$ and $\Phi=0^\circ$ .....	42
Figure 5.10: Contours of Streamlines and isotherms at $Re=600$ , $A=0.5$ and $\Phi=0^\circ$ .....	43
Figure 5.11: Contours of Streamlines and isotherms at $Re=600$ , $A=1.0$ and $\Phi=0^\circ$ .....	44
Figure 5.12: Contours of Streamlines and isotherms at $Re=600$ , $A=1.5$ and $\Phi=0^\circ$ .....	45

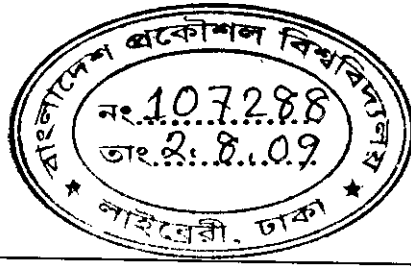
Figure 5.13: Contours of Streamlines and isotherms at $Re=600$ , $A=2$ and $\Phi=0^\circ$ .....	46
Figure 5.14: Variation of $Nu_{av}$ with $Ri$ at $Re=400$ and $\Phi=0^\circ$ .....	47
Figure 5.15: Variation of $Nu_{av}$ with $Ri$ at $Re=600$ and $\Phi=0^\circ$ .....	47
Figure 5.16: Variation of $Nu_{av}$ with $A$ at $Re=400$ and $\Phi=0^\circ$ .....	48
Figure 5.17: Variation of $Nu_{av}$ with $A$ at $Re=600$ and $\Phi=0^\circ$ .....	48
Figure 5.18: Contours of Streamlines and isotherms at $Re=400$ , $A=0.5$ and $\Phi=30^\circ$ , Opposing Flow .....	49
Figure 5.19: Contours of Streamlines and isotherms at $Re=400$ , $A=1$ and $\Phi=30^\circ$ , Opposing Flow .....	50
Figure 5.20: Contours of Streamlines and isotherms at $Re=400$ , $A=1.5$ and $\Phi=30^\circ$ , Opposing Flow .....	51
Figure 5.21: Contours of Streamlines and isotherms at $Re=400$ , $A=2$ and $\Phi=30^\circ$ , Opposing Flow .....	52
Figure 5.22: Contours of Streamlines and isotherms at $Re=400$ , $A=0.5$ and $\Phi=45^\circ$ , Opposing Flow .....	53
Figure 5.23: Contours of Streamlines and isotherms at $Re=400$ , $A=1$ and $\Phi=45^\circ$ , Opposing Flow .....	54
Figure 5.24: Contours of Streamlines and isotherms at $Re=400$ , $A=1.5$ and $\Phi=45^\circ$ , Opposing Flow .....	55
Figure 5.25: Contours of Streamlines and isotherms at $Re=400$ , $A=2$ and $\Phi=45^\circ$ , Opposing Flow .....	56
Figure 5.26: Contours of Streamlines and isotherms at $Re=400$ , $A=0.5$ and $\Phi=60^\circ$ , Opposing Flow .....	57
Figure 5.27: Contours of Streamlines and isotherms at $Re=400$ , $A=1$ and $\Phi=60^\circ$ , Opposing Flow .....	58
Figure 5.28: Contours of Streamlines and isotherms at $Re=400$ , $A=1.5$ and $\Phi=60^\circ$ , Opposing Flow .....	59

Figure 5.29: Contours of Streamlines and isotherms at $Re=400$ , $A=2$ and $\Phi=60^\circ$ , Opposing Flow.....	60
Figure 5.30: Contours of Streamlines and isotherms at $Re=600$ , $A=1$ and $\Phi=30^\circ$ , Opposing Flow.....	61
Figure 5.31: Contours of Streamlines and isotherms at $Re=600$ , $A=1$ and $\Phi=45^\circ$ , Opposing Flow.....	62
Figure 5.32: Contours of Streamlines and isotherms at $Re=600$ , $A=1$ and $\Phi=60^\circ$ , Opposing Flow.....	63
Figure 5.33: Contours of Streamlines and isotherms at $Re=400$ , $A=0.5$ and $\Phi=30^\circ$ , Aiding Flow.....	64
Figure 5.34: Contours of Streamlines and isotherms at $Re=400$ , $A=1$ and $\Phi=30^\circ$ , Aiding Flow.....	65
Figure 5.35: Contours of Streamlines and isotherms at $Re=400$ , $A=1.5$ and $\Phi=30^\circ$ , Aiding Flow.....	66
Figure 5.36: Contours of Streamlines and isotherms at $Re=400$ , $A=2$ and $\Phi=30^\circ$ , Aiding Flow.....	67
Figure 5.37: Contours of Streamlines and isotherms at $Re=400$ , $A=0.5$ and $\Phi=45^\circ$ , Aiding Flow.....	68
Figure 5.38: Contours of Streamlines and isotherms at $Re=400$ , $A=1$ and $\Phi=45^\circ$ , Aiding Flow.....	69
Figure 5.39: Contours of Streamlines and isotherms at $Re=400$ , $A=1.5$ and $\Phi=45^\circ$ , Aiding Flow.....	70
Figure 5.40: Contours of Streamlines and isotherms at $Re=400$ , $A=2$ and $\Phi=45^\circ$ , Aiding Flow.....	71
Figure 5.41: Contours of Streamlines and isotherms at $Re=400$ , $A=0.5$ and $\Phi=60^\circ$ , Aiding Flow.....	72

Figure 5.42: Contours of Streamlines and isotherms at $Re=400$ , $A=1$ and $\Phi=60^\circ$ , Aiding Flow.....	73
Figure 5.43: Contours of Streamlines and isotherms at $Re=400$ , $A=1.5$ and $\Phi=60^\circ$ , Aiding Flow.....	74
Figure 5.44: Contours of Streamlines and isotherms at $Re=400$ , $A=2$ and $\Phi=60^\circ$ , Aiding Flow.....	75
Figure 5.45: Contours of Streamlines and isotherms at $Re=600$ , $A=1$ and $\Phi=30^\circ$ , Aiding Flow.....	76
Figure 5.46: Contours of Streamlines and isotherms at $Re=600$ , $A=1$ and $\Phi=45^\circ$ , Aiding Flow.....	77
Figure 5.47: Contours of Streamlines and isotherms at $Re=600$ , $A=1$ and $\Phi=60^\circ$ , Aiding Flow.....	78
Figure 5.48: Variation of $Nu_{av}$ with $Ri$ at $\Phi=30^\circ$ , $Re=400$ , Opposing Flow.....	79
Figure 5.49: Variation of $Nu_{av}$ with $Ri$ at $\Phi=30^\circ$ , $Re=600$ , Opposing Flow.....	79
Figure 5.50: Variation of $Nu_{av}$ with $Ri$ at $\Phi=45^\circ$ , $Re=400$ , Opposing Flow.....	80
Figure 5.51: Variation of $Nu_{av}$ with $Ri$ at $\Phi=45^\circ$ , $Re=600$ , Opposing Flow.....	80
Figure 5.52: Variation of $Nu_{av}$ with $Ri$ at $\Phi=60^\circ$ , $Re=400$ , Opposing Flow.....	81
Figure 5.53: Variation of $Nu_{av}$ with $Ri$ at $\Phi=60^\circ$ , $Re=600$ , Opposing Flow.....	81
Figure 5.54: Variation of $Nu_{av}$ with $Ri$ at $\Phi=30^\circ$ , $Re=400$ , Aiding Flow.....	82
Figure 5.55: Variation of $Nu_{av}$ with $Ri$ at $\Phi=30^\circ$ , $Re=600$ , Aiding Flow.....	82
Figure 5.56: Variation of $Nu_{av}$ with $Ri$ at $\Phi=45^\circ$ , $Re=400$ , Aiding Flow.....	83
Figure 5.57: Variation of $Nu_{av}$ with $Ri$ at $\Phi=45^\circ$ , $Re=600$ , Aiding Flow.....	83
Figure 5.58: Variation of $Nu_{av}$ with $Ri$ at $\Phi=60^\circ$ , $Re=400$ , Aiding Flow.....	84
Figure 5.59: Variation of $Nu_{av}$ with $Ri$ at $\Phi=60^\circ$ , $Re=600$ , Aiding Flow.....	84
Figure 5.60: Variation of $Nu_{av}$ with $Ri$ at $A=0.5$ , $Re=400$ .....	85
Figure 5.61: Variation of $Nu_{av}$ with $Ri$ at $A=1$ , $Re=400$ .....	85

Figure 5.62: Variation of $Nu_{av}$ with $Ri$ at $A=1.5$ , $Re=400$ .....	86
Figure 5.63: Variation of $Nu_{av}$ with $Ri$ at $A=2$ , $Re=400$ .....	86
Figure 5.64: Variation of $Nu_{av}$ with $Ri$ at $A=0.5$ , $Re=600$ .....	87
Figure 5.65: Variation of $Nu_{av}$ with $Ri$ at $A=1$ , $Re=600$ .....	87
Figure 5.66: Variation of $Nu_{av}$ with $Ri$ at $A=1.5$ , $Re=600$ .....	88
Figure 5.67: Variation of $Nu_{av}$ with $Ri$ at $A=2$ , $Re=600$ .....	88





# CHAPTER 1

## INTRODUCTION

### 1.1 GENERAL

Convection is the heat transfer mechanism affected by the flow of fluids. The amount of energy and matter are conveyed by the fluid can be predicted through the convective heat transfer. The convective heat transfer may be the natural convection or forced convection or the combination of two. Forced convection is characterized by the heat transport by induced fluid motion. This induced flow needs consistent mechanical power. Natural convection differs from the forced convection as the driving force of fluid flow happens naturally. The flows are driven by the buoyancy effect due to the presence of density gradient and gravitational field. As the temperature distribution in the natural convection depends on the intensity of the fluid currents which is dependent on the temperature potential itself, the qualitative and quantitative analysis of natural convection heat transfer is very difficult. Numerical investigation instead of theoretical analysis is more needed in this field.

Two types of natural convection heat transfer phenomena can be observed in the nature. One is that external free convection that is caused by the heat transfer interaction between a single wall and a very large fluid reservoir adjacent to the wall. Another is that internal free convection which befalls within an enclosure. Mathematically, the tendency of a particular system towards natural convection relies on the Grashof number,

$(Gr = \frac{g\beta\Delta TW^3}{\nu^2})$ , which is the ratio of buoyancy force to viscous force. The parameter  $\beta$

is the rate of change of density with respect to the change in temperature ( $T$ ) per unit density, and  $\nu$  is kinematic viscosity. Thus, the Grashof number can be thought of as the ratio of the upwards buoyancy of the heated fluid to the internal friction slowing it down. In very sticky, viscous fluids, the fluid movement is restricted, along with natural convection. In the extreme case of infinite viscosity, the fluid could not move and all heat transfer would be through conductive heat transfer.

Forced convection is often encountered by engineers designing or analyzing heat exchangers, pipe flow, and flow over flat plate at a different temperature than the stream (the case of a shuttle wing during re-entry, for example). However, in any forced convection situation, some amount of natural convection is always present. When the natural convection is not negligible, such flows are typically referred to as mixed convection.

When analyzing potentially mixed convection, a parameter called the Richardson number ( $Ri = Gr / Re^2$ ) parametrizes the relative strength of free and forced convection. The Richardson number is the ratio of Grashof number and the square of the Reynolds number, which represents the ratio of buoyancy force and inertia force, and which stands in for the contribution of natural convection. When  $Ri \gg 1$ , natural convection dominates and when  $Ri \ll 1$ , forced convection dominates and when  $Ri = 1$ , mixed convection dominates.

The thermo-fluid fields developed inside the cavity depend on the orientation and the geometry of the cavity. Reviewing the nature and the practical applications, the enclosure phenomena can loosely be organized into two classes. One of these is enclosure heated from the side which is found in solar collectors, double wall insulations, laptop cooling system and air circulation inside the room and the another one is enclosure heated from below which is happened in geophysical system like natural circulation in the atmosphere, the hydrosphere and the molten core of the earth.

## 1.2 FLOW WITHIN AN ENCLOSURE

The flow within an enclosure consisting of two horizontal walls, at different temperatures, is an important circumstance encountered quite frequently in practice. In all the applications having this kind of situation, heat transfer occurs due to the temperature difference across the fluid layer, one horizontal solid surface being at a temperature higher than the other. If the upper plate is the hot surface, then the lower surface has heavier fluid and by virtue of buoyancy the fluid would not come to the lower plate. Because in this case the heat transfer mode is restricted to only conduction. But if the fluid is enclosed between two horizontal surfaces of which the upper surface is at lower temperature, there will be the existence of cellular natural convective currents which are called as Benard cells. For fluids whose density decreases with increasing temperature, this leads to an unstable situation. Benard [1] mentioned this instability as a "top heavy" situation. In that case fluid is completely stationary and heat is transferred across the layer by the conduction mechanism only. Rayleigh [2] recognized that this unstable situation must break down at a certain value of Rayleigh number above which convective motion must be generated. Jeffreys [3] calculated this limiting value of  $Ra$  to be 1708, when air layer is bounded on both sides by solid walls.

## 1.3 TILTED ENCLOSURE

The tilted enclosure geometry has received considerable attention in the heat transfer literature because of mostly growing interest of solar collector technology. The angle of tilt has a dramatic impact on the flow housed by the enclosure. Consider an enclosure heated from below is rotated about a reference axis. When the tilted angle becomes  $90^\circ$ , the flow and thermal fields inside the enclosure experience the heating from side condition. Thereby convective currents may pronounce over the diffusive currents. When the enclosure rotates to  $180^\circ$ , the heat transfer mechanism switches to the diffusion because the top wall is heated.

## 1.4 LID DRIVEN ENCLOSURE

Flow and heat transfer analysis in lid-driven cavities is one of the most widely studied problems in thermo-fluids area. Numerous investigations have been conducted in the past on lid-driven cavity flow and heat transfer considering various combinations of the imposed temperature gradients and cavity configurations. This is because the driven cavity configuration is encountered in many practical engineering and industrial applications. Such configurations can be idealized by the simple rectangular geometry with regular boundary conditions yielding a well-posed problem. Combined forced-free convection flow in lid-driven cavities or enclosures occurs as a result of two competing mechanisms. The first is due to shear flow caused by the movement of one of the walls of the cavity while the second is due to buoyancy flow produced by thermal non homogeneity of the cavity boundaries. Understanding these mechanisms is of great significance from technical and engineering standpoints.

## 1.5 APPLICATION

Air-cooling is one of the preferred methods for the cooling of computer systems and other electronic equipments, due to its simplicity and low cost. It is very important that such cooling systems should be designed in the most efficient way and the power requirement for the cooling should be minimized. The electronic components are treated as heat sources embedded on flat surfaces [4]. A small fan blows air at low speeds over the heat sources. This gives rise to a situation where the forced convection due to shear driven flow and the natural convection due to buoyancy driven flow are of comparable magnitude and the resulting heat transfer process is categorized as mixed convection. Mixed convection flow and heat transfer also occur frequently in other engineering and natural situations. One important configuration is a lid-driven (or shear-driven) flow in a differentially heated/cooled cavity, which has applications in crystal growth, flow and heat transfer in solar ponds [5], dynamics of lakes [6], thermal-hydraulics of nuclear reactors [7], industrial processes such as food processing, and float glass production [8]. The interaction of the shear driven flow due to the lid motion and natural convective flow due to the buoyancy effect is quite complex and warrants

comprehensive analysis to understand the physics of the resulting flow and heat transfer process.

## 1.6 SELECTION OF PROBLEM

Two dimensional steady, mixed convection heat transfers in a trapezoidal cavity, with constant heat flux from heated bottom wall while the isothermal moving top wall has been studied numerically. The present study is based on the configuration of Aydin and Yang [9] where the isothermal heat source at the bottom wall is replaced by a constant flux heat source, which is physically more realistic. The main attribute for choosing the trapezoidal shape cavity is to enhance the heat transfer rate as it could be said intuitively due to its extended cold top surface. The inclination angle,  $\gamma$  of the sidewalls of the trapezoid has been changed (  $30^\circ$ ,  $45^\circ$  and  $60^\circ$  ) to get the maximum heat transfer in terms of maximum Nusselt number. Then the trapezoid has been rotated ( $30^\circ$ ,  $45^\circ$  and  $60^\circ$ ) and the results have been studied. The tilted position of the enclosure shows a significant influence on the heat transfer. Results are obtained for both the aiding and opposing flow conditions by changing the direction of the lid motion. This study includes additional computations for cavities at various aspect ratios,  $A$ , ranging from 0.5 to 2 and their effects on the heat transfer process is analyzed in terms of average Nusselt number. Contextually the present study will focus on the computational analysis of the influence of inclination angle of the sidewalls of the cavity, rotational angle of the cavity, Aspect ratio, direction of the lid motion and Richardson number.

## 1.7 MAIN OBJECTIVES OF THE WORK

The investigation is carried out in a two dimensional lid driven trapezoidal enclosure filled with air. The inclined side walls are kept adiabatic and the bottom wall of the cavity is kept at uniform heat flux. The cooled top wall having constant temperature will move with a constant velocity. The specific objectives of the present research work are as follows:

- (a) To study the variation of average heat transfer in terms of Nusselt number with the variation of Richardson number of the rectangular enclosure and compare the results with those earlier.
- (b) To find out the optimum configuration by changing the inclination angle of the side walls of the trapezoidal cavity for maximum heat transfer.
- (c) To study the variation of average heat transfer in terms of Nusselt number with the variation of Richardson number of the optimum trapezoidal cavity.
- (d) To study the variation of average heat transfer in terms of Nusselt number at different aspect ratios of the optimum trapezoidal cavity.
- (e) To study the variation of average heat transfer in terms of Nusselt number with the variation of Richardson number at different aspect ratios of the optimum trapezoidal enclosure by changing the rotation angle for both aiding and opposing flow conditions..
- (f) To analyze the flow pattern inside the trapezoidal enclosures in terms of Streamlines and isotherms.

## CHAPTER 2

### REVIEW OF PREVIOUS WORKS

---

There have been many investigations in the past on mixed convective flow in lid-driven cavities. Many different configurations and combinations of thermal boundary conditions have been considered and analyzed by various investigators. Torrance et al. [10] investigated mixed convection in driven cavities as early as in 1972. Papaniclaou and Jaluria [11-14] carried out a series of numerical studies to investigate the combined forced and natural convective cooling of heat dissipating electronic components, located in rectangular enclosures, and cooled by an external through flow of air. The results indicate that flow patterns generally consists of high of low velocity re-circulating cells because of buoyancy forces induced by the heat source. Koseff and Street [15] studied experimentally as well as numerically the recirculation flow patterns for a wide range of Reynolds ( $Re$ ) and Grashof ( $Gr$ ) numbers. Their results showed that the three dimensional features, such as corner eddies near the end walls, and Taylor- Gortler like longitudinal vortices, have significant effects on the flow patterns for low Reynolds numbers. Khanafer and Chamakha [16] examined numerically mixed convection flow in a lid-driven enclosure filled with a fluid-saturated porous medium and reported on the effects of the Darcy and Richardson numbers on the flow and heat transfer characteristics.

G. A. Holtzman et. al [17] have studied laminar natural convection in isosceles triangular enclosures heated from below and symmetrically cooled from above. This problem is examined over aspect ratios ranging from 0.2 to 1.0 and Grashoff numbers from  $10^3$  to  $10^5$ . Its is found that a pitchfork bifurcation occurs at a critical Grashoff number for each of the aspect ratios considered, above which the symmetric solutions are unstable to finite perturbations and asymmetric solutions are instead obtained. Results are presented detailing the occurrence of the pitchfork bifurcation in each of the aspect ratios considered, and the resulting flow patterns are described. A flow visualization study is

used to validate the numerical observations. Difference in local values of the Nusselt number between asymmetric and symmetric solutions are found to be more than 500 percent due to the shifting of the buoyancy-driven cells. The phenomenon of natural convection in trapezoidal enclosures where upper and lower walls are not parallel, in particular a triangular geometry, is examined by H. Asan, L. Namli [18] over a parameter domain in which the aspect ratio of the enclosure ranges from 0.1 to 1.0, the Rayleigh number varies between  $10^2$  to  $10^5$  and Prandtl number correspond to air and water. It is found that the numerical experiments verify the flow features that are known from theoretical asymptotic analysis of this problem (valid for shallow spaces) only over a certain range of the parametric domain.

Moallemi and Jang [19] numerically studied mixed convective flow in a bottom heated square driven cavity and investigated the effect of Prandtl number on the flow and heat transfer process. They found that the effects of buoyancy are more pronounced for higher values of Prandtl number. They also derived a correlation for the average Nusselt number in terms of the Prandtl number, Reynolds number, and Richardson number. Mohammad and Viskanta [20] performed numerical investigation and flow visualization study on two and three-dimensional laminar mixed convection flow in a bottom heated shallow driven cavity filled with water having a Prandtl number of 5.84. They concluded that the lid motion destroys all types of convective cells due to heating from below for finite size cavities. They also implicated that the two-dimensional heat transfer results compare favorably with those based on a three-dimensional model for  $Gr/Re < 1$ . Later, Mohammad and Viskanta [21] experimentally and numerically studied mixed convection in shallow rectangular bottom heated cavities filled with liquid Gallium having a low Prandtl number of 0.022. They found that the heat transfer rate is rather insensitive to the lid velocity and an extremely thin shear layer exists along the major portion of the moving lid. The flow structure consists of an elongated secondary circulation that occupies a third of the cavity.



Mansour and Viskanta [22] studied mixed convective flow in a tall vertical cavity where one of the vertical sidewalls, maintained at a colder temperature than the other, was moving up or downward thus assisting or opposing the buoyancy. They observed that when shear assisted the buoyancy a shear cell developed adjacent to the moving wall while the buoyancy cell filled the rest of the cavity. When shear opposed buoyancy, the heat transfer rate reduced below that for purely natural convection. Iwatsu et al. [23] and Iwatsu and Hyun [24] conducted two-dimensional and three-dimensional numerical simulation of mixed convection in square cavities heated from the top moving wall. Mohammad and Viskanta [25] conducted three-dimensional numerical simulation of mixed convection in a shallow driven cavity filled with a stably stratified fluid heated from the top moving wall and cooled from below for a range of Rayleigh number and Richardson number.

Prasad and Koseff [26] reported experimental results for mixed convection in deep lid-driven cavities heated from below. In a series of experiments which were performed on a cavity filled with water, the heat flux was measured at different locations over the hot cavity floor for a range of  $Re$  and  $Gr$ . Their results indicated that the overall (i.e. area-averaged) heat transfer rate was a very weak function of  $Gr$  for the range of  $Re$  examined ( $2200 < Re < 12000$ ). The data were correlated by Nusselt number vs Reynolds number, as well as Stanton number vs Reynolds number relations.

They observed that the heat transfer is rather insensitive to the Richardson number. Hsu and Wang [27] investigated the mixed convective heat transfer where the heat source was embedded on a board mounted vertically on the bottom wall at the middle in an enclosure. The cooling air flow enters and exits the enclosure through the openings near the top of the vertical sidewalls. The results show that both the thermal field and the average Nusselt number depend strongly on the governing parameters, position of the heat source, as well as the property of the heat-source-embedded board.

Aydin and Yang [28] numerically studied mixed convection heat transfer in a two-dimensional square cavity having an aspect ratio of 1. In their configuration the

isothermal sidewalls of the cavity were moving downwards with uniform velocity while the top wall was adiabatic. A symmetrical isothermal heat source was placed at the otherwise adiabatic bottom wall. They investigated the effects of Richardson number and the length of the heat source on the fluid flow and heat transfer. Shankar et al. [29] presented analytical solution for mixed convection in cavities with very slow lid motion. The convection process has been shown to be governed by an inhomogeneous biharmonic equation for the stream function. Oztop and Dagtekin [30] performed numerical analysis of mixed convection in a square cavity with moving and differentially heated sidewalls. Sharif [31] investigates heat transfer in two-dimensional shallow rectangular driven cavity of aspect ratio 10 and Prandtl number 6.0 with hot moving lid on top and cooled from bottom. They investigated the effect of Richardson number and inclination angle. G. Guo and M. A. R. Sharif [32] studied mixed convection in rectangular cavities at various aspect ratios with moving isothermal sidewalls and constant heat source on the bottom wall. They plotted the streamlines and isotherms for different values of Richardson number and also studied the variation of the average Nu and maximum surface temperature at the heat source with Richardson number with different heat source length. They simulated streamlines and isotherms for asymmetric placements of the heat source and also the effects of asymmetry of the heating elements on the average Nu and the maximum source length temperature.

## CHAPTER 3

# MATHEMATICAL MODELING

---

Two dimensional steady, mixed convection heat transfer in a lid driven trapezoidal cavity with constant heat flux from heated bottom wall while the isothermal moving top wall in the horizontal direction has been studied numerically. Natural convection heat transfer within such an enclosure is a function of the temperature difference between the hot and cold walls, the boundary conditions, the inclination angle of the side walls of the cavity, the rotational angle of the cavity and the direction of lid motion whether it is opposing flow or aiding flow condition.

The generalized governing equations are used based on the conservation laws of mass, momentum and energy. As the heat transfer depends upon a number of factors, a dimensional analysis is presented to show the important non-dimensional parameters which will influence the dimensionless heat transfer parameter, i.e. Nusselt number.

### 3.1 PHYSICAL MODEL

The physical model considered here is shown in fig. 3.1 and fig. 3.2, along with the important geometric parameters. It consists of a trapezoidal cavity filled with air, whose bottom wall and top wall are subjected to hot  $T_H$  and cold  $T_C$  temperatures respectively while the side walls are kept adiabatic. Two cases of thermal boundary conditions for the top moving wall have been considered here. The first case is (fig. 3.1) when the moving cold wall is moving in the positive  $x$  direction (opposing flow condition). In that case the shear flow caused by moving top wall opposes the buoyancy driven flow caused by the thermal nonhomogeneity of the cavity boundaries. The second case is (fig. 3.2) when the moving cold wall is moving in the negative  $x$  direction (aiding flow condition). In that case the shear flow assists the buoyancy flow. The cavity height is  $H$ , width of the bottom hot wall is  $W$ , is inclined at angle  $\Phi$  with the horizontal reference axis.  $\gamma$  is the inclination angle of the sidewalls of the cavity. The flow and heat transfer phenomena in the cavity are investigated for inclination angle  $\gamma$ , a series of Richardson numbers ( $Ri$ ), aspect ratio ( $A=H/W$ ), rotation angle of the cavity  $\Phi$ .

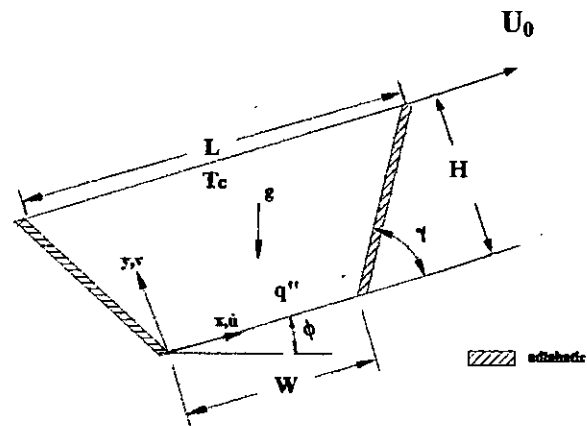


Figure 3.1: Schematic diagram of the physical system considering opposing flow condition

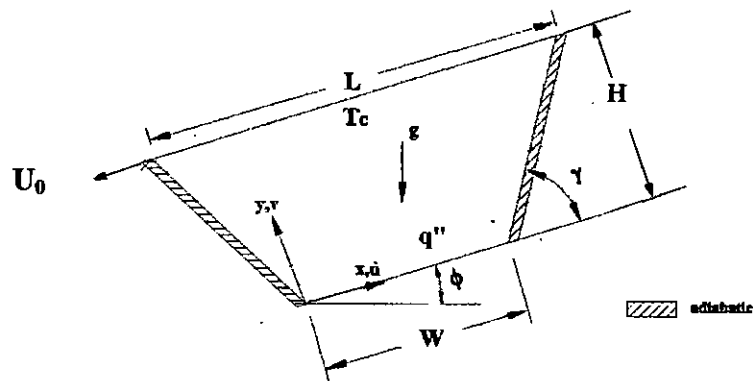


Figure 3.2: Schematic diagram of the physical system considering aiding flow condition

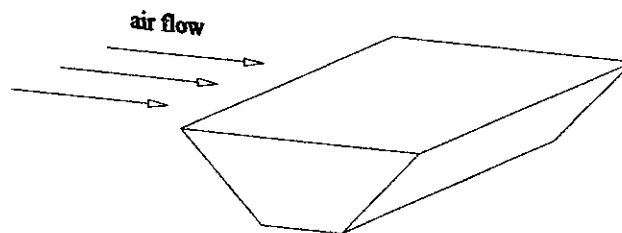


Figure 3.3: 3D view of the cavity

Natural convection flow of a thermal viscous fluid assumed to be Newtonian is considered under the Oberbeck-Boussineq approximation in the presence of a gravitational field. The Oberbeck-Boussineq approximation is based on the assumptions that the temperature variations are small enough in order to consider the density  $\rho$  as a constant except in the buoyancy term  $\rho \bar{g}$ , where  $\bar{g}$  is the gravitational force and  $\rho$  is given linearly by  $\rho = \rho_o [1 - \beta(T - T_o)]$  where  $T$  is the temperature and  $\rho_o$  and  $T_o$  denote reference density and temperature respectively. The density change due to changes in pressure is neglected.. Fluid properties such as viscosity  $\mu$ , thermal expansion  $\beta = -\frac{1}{\rho_o} \left( \frac{\partial \rho}{\partial T} \right)_p$ , the thermal diffusivity  $\alpha$  and the specific heat  $C_p$  are assumed to be constants. Prandtl number is assumed to be 0.71 for air.

### 3.2.1 GOVERNING EQUATIONS IN DIMENSIONAL FORM

Using the Boussinesq approximation and neglecting the viscous dissipation effect and compressibility effect the governing equations for two dimensional laminar incompressible flow can be written as follows:

Continuity equation:

$$\frac{\partial u}{\partial x} + \frac{\partial v}{\partial y} = 0 \quad (1)$$

X- Momentum equation:

$$u \frac{\partial u}{\partial x} + v \frac{\partial u}{\partial y} = -\frac{1}{\rho} \frac{\partial p}{\partial x} + \nu \left( \frac{\partial^2 u}{\partial x^2} + \frac{\partial^2 u}{\partial y^2} \right) \quad (2)$$

Y-momentum equation:

$$u \frac{\partial v}{\partial x} + v \frac{\partial v}{\partial y} = -\frac{1}{\rho} \frac{\partial p}{\partial y} + \nu \left( \frac{\partial^2 v}{\partial x^2} + \frac{\partial^2 v}{\partial y^2} \right) + g\beta(T - T_i) \quad (3)$$

Energy equation:

$$u \frac{\partial T}{\partial x} + v \frac{\partial T}{\partial y} = \frac{k}{\rho C_p} \left( \frac{\partial^2 T}{\partial x^2} + \frac{\partial^2 T}{\partial y^2} \right) \quad (4)$$

### 3.2.2 DIMENSIONAL ANALYSIS

To get the non dimensional form of the above governing equations, all distances are normalized by the cavity width,  $W$  and all velocities are normalized by the lid velocity  $U_0$  and the pressure is normalized by  $\rho U_0^2$ . The governing equation in the non dimensional form can be written by using the following non dimensional variables and parameters:

$$X = \frac{x}{W}, Y = \frac{y}{W}, \theta = \frac{T_H - T_C}{\Delta T}, \Delta T = \frac{q'' W}{k}, U = \frac{u}{U_0}, V = \frac{v}{U_0}, P = \frac{p}{\rho U_0^2}$$

$$\frac{\partial U}{\partial X} + \frac{\partial V}{\partial Y} = 0 \quad (5)$$

$$U \frac{\partial U}{\partial X} + V \frac{\partial U}{\partial Y} = -\frac{\partial P}{\partial X} + \frac{1}{\text{Re}} \left( \frac{\partial^2 U}{\partial X^2} + \frac{\partial^2 U}{\partial Y^2} \right) \quad (6)$$

$$U \frac{\partial V}{\partial X} + V \frac{\partial V}{\partial Y} = -\frac{\partial P}{\partial Y} + \frac{1}{\text{Re}} \left( \frac{\partial^2 V}{\partial X^2} + \frac{\partial^2 V}{\partial Y^2} \right) + \frac{Gr}{\text{Re}^2} \theta \quad (7)$$

$$U \frac{\partial \theta}{\partial X} + V \frac{\partial \theta}{\partial Y} = \frac{1}{\text{RePr}} \left( \frac{\partial^2 \theta}{\partial X^2} + \frac{\partial^2 \theta}{\partial Y^2} \right) \quad (8)$$

The dimensionless parameters, appearing in Eqs. (6)-(8) are Reynolds number  $Re = U_0 W / \nu$ , the Prandtl number  $Pr = \nu / \alpha$ , the Grashof number  $Gr = \frac{g \beta \Delta T W^3}{\nu^2}$ . The ratio of  $Gr/Re^2$  is the mixed convection parameter and is called Richardson number  $Ri$  and is a measure of the relative strength of the natural convection and forced convection for a particular problem. If  $Ri \ll 1$  the forced convection is dominant while if  $Ri \gg 1$ , then natural convection is dominant. For problems with  $Ri \sim 1$  then the natural convection effects are comparable to the forced convection effects.

### 3.2.3 BOUNDARY CONDITIONS

The boundary conditions for the present problem are specified as follows:

Top wall:  $U=U_0, V=0, \theta=0$

Bottom wall:  $U=V=0, \theta=1$

Right and Left wall:  $U=V=0, \frac{\partial \theta}{\partial X} = 0$

Convection heat transfer co-efficient  $h$  can be defined as the rate of heat transfer between a solid surface and a fluid per unit surface area per unit temperature difference. Since, as in the case, the flux is often variable over the surface, even for a uniform temperature difference, the surface coefficient  $h$  varies over the surface. Mathematically the local convection heat transfer coefficient can be written as:

$$h_x = \frac{q''}{T_s(x) - T_c}$$

Here,  $T(x)$  is the local temperature on the base of trapezoid.

So, the convection heat transfer coefficient, in general, varies along the flow direction. The average or mean convection heat transfer coefficient for a surface in such cases is determined by properly averaging the local convection heat transfer coefficient over the entire surface, which is:

$$h_{av} = \frac{1}{W} \int_0^W h_x dx$$

In convection studies, it is common practice to nondimensionalize the governing equations and combines the variables, which group together into dimensionless numbers in order to reduce the number of total variables. It is also common practice to nondimensionalize the heat transfer coefficient  $h$  with the Nusselt number, defined as

$$Nu_{av} = \frac{1}{W} \int_0^W \frac{h(x)x}{k} dx = \frac{h_{av}W}{k}$$

$$Nu_{av} = \int_0^1 \left( \frac{\partial \theta}{\partial Y} \right)_{Y=0} dX$$

It is viewed as the dimensionless convection heat transfer coefficient.



## CHAPTER 4

# COMPUTATIONAL DETAILS

---

The governing equations in fluid dynamics and heat transfer, including conservation forms of the Navier-Stokes system of equations as derived from the first law of thermodynamics, are expressed in terms of the control volume / surface integral equations, which represent various physical phenomena. To visualize these thermo-fluid flow scenarios, an approximate numerical solution is needed, which can be obtained by the CFD (Computational Fluid Dynamics) code. It means predicting physical fluid flows and heat transfer using computational methods. Over 40 years ago, this was an emerging field that owed everything to the advent of the modern computer. Although the equations describing fluid flow and heat transfer (i.e. conservation of mass, momentum and energy) had been developed many years earlier, it required the fast automated processing of mathematical instructions before it was considered to be a practical tool. Forty years later on and computers that we carry around in briefcases and handbags are more than powerful enough to perform the required calculations to get a CFD solution in a matter of minutes! As computers get even more powerful in the future then the accessibility and efficiency of CFD will become more and more commonplace.

The partial differential equations of fluid mechanics and heat transfer are discretized in order to obtain a system of approximate algebraic equations, which then can be solved on a computer. The approximations are applied to small domains in space and / or time so the numerical solution provides results at discrete locations in space and time. Much as accuracy of experimental data depends on the quality of the tools used, the accuracy of numerical solution is dependent on the quality of discretization used.

CFD computation involves the creation of a set numbers that constitutes a realistic approximation of a real life system. The outcome of computation process improves the understanding of the behavior of a system. Thereby, engineers need CFD codes that can produce physically realistic results with good accuracy in simulations with finite grids. Contained within the broad field of computational fluid dynamics are activities that cover the range from the automation of well established engineering design methods to the use

of detailed solutions of the Navier-Stokes equations as substitutes for experimental research into the nature of complex flows. CFD have been used for solving wide range of fluid dynamics problem. It is more frequently used in fields of engineering where the geometry is complicated or some important feature that cannot be dealt with standard methods.

The complete Navier-Stokes equations are considered to be the correct mathematical description of the governing equations of fluid motion. The most accurate numerical computations in fluid dynamics come from solving the Navier-Stokes equations. The equations represent the conservation of mass and momentum.

As well as solving plain vanilla fluid flows (such as flows in pipes and around obstacles such as cylinders), CFD can also include additional phenomena such as chemical reactions, phase changes, acoustic noise and thermal radiation, etc. In fact, the speed at which commercial and research codes are progressing means that virtually any kind of real life industrial application, from high speed re-entry vehicles to macroscopic electromagnetic effects can be studied using CFD. Heat transfer within and across solids can also be included. This means that the analysis can include any combination of gas, liquid and solid materials and all appropriate physical effects that would normally occur in reality being included.

There are many different ways by which equations describing fluid flow and heat transfer can be solved using computational methods (but note: the solutions obtained are only approximate, whichever method is used!). Most commercial and research codes rely on one of the following:

- Finite Difference Method (FDM)
- Finite Element Method (FEM)
- Spectral Methods
- Macroscopic Fluid Modeling (Lattice Methods)
- Finite Volume Method (FVM)

Each of these methods requires the definition of discrete points in space at which variables like velocity, pressure, temperature etc. will be computed. While the governing equations are always the same, the particular geometry with initial and boundary conditions determines a unique solution for each particular problem.

Control Volume based finite volume method (FVM) has been used to discretize the governing differential equations, as it is the method used by most of the popular commercial CFD codes currently available. The pressure- velocity coupling in the governing equations is achieved using the well known SIMPLE method for numerical computations. The set of governing equations are to be solved sequentially. A second order upwind differencing scheme is to be used for the formulation of the coefficients in the finite-volume equations.

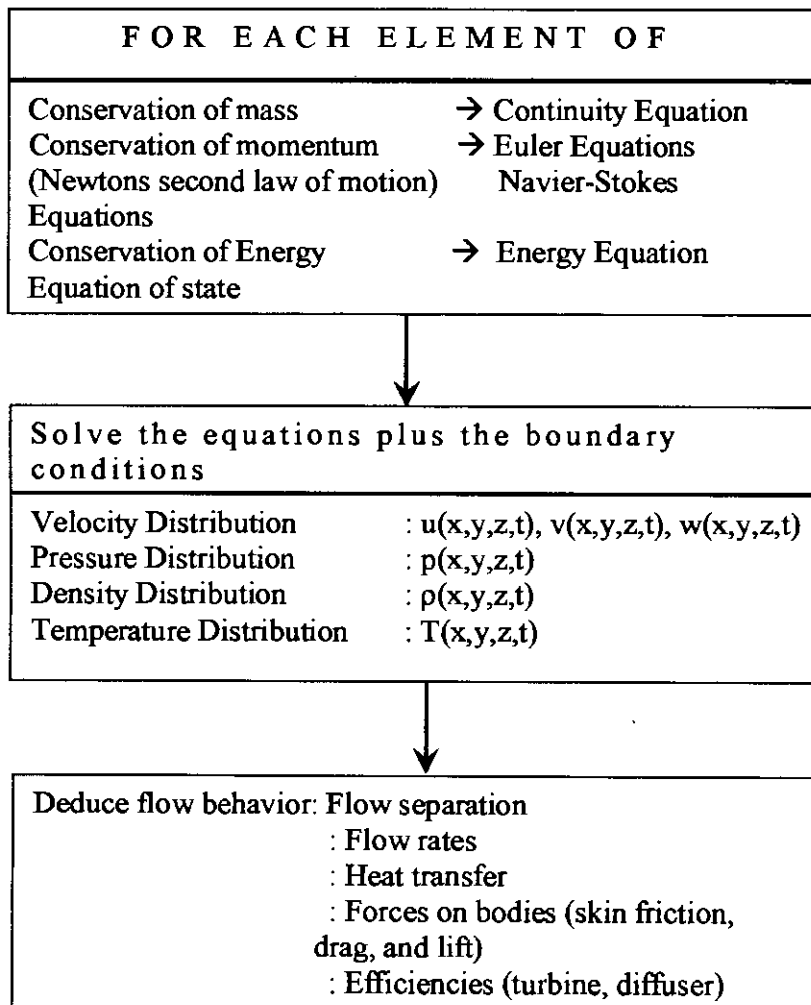
#### **4.1 CFD PROCESSES AT A GLANCE**

The cornerstone of computational fluid dynamics is the fundamental governing equations of fluid dynamics---the continuity, momentum and energy equations. *These equations speak physics.* They are the mathematical statements of three fundamental principles upon which all of fluid dynamics is based:

1. Mass is conserved.
2. Momentum is conserved (Newton's second law).
3. Energy is conserved.

## OVERVIEW OF COMPUTATIONAL FLUID DYNAMICS

The total process of determining practical information about problems involving fluid motion can be represented schematically as below:



## 4.2 THE FINITE VOLUME METHOD

The Finite Volume Method (or FVM as it will hereafter be known) starts with the integral form of the governing equations, involving surface integrals (e.g. convective and diffusive fluxes) and volume integrals (e.g. those describing sources and sinks). In case of a transient flow (ie unsteady flow that changes over time), there is also a rate-of-change term. One of the reason why FVM has succeeded over the other methods is that it is inherently conservative: irrespective of errors in various approximations, the discretized equations still fulfill the conservation laws exactly (e.g. mass entering solution domain equals mass leaving through it). The FVM is also easier to understand by engineers than some of the others, more mathematically involved equation, since the terms that need to be computed have a clear physical meaning.

The FVM represents the integration of the governing equations over (a finite number of) contiguous control volumes (CVs) representing the solution domain. Since variable values are computed only at discrete points (usually centroids of control volumes), approximations must be used to express the integrals in terms of unknowns at discrete locations. Three kinds of approximations are involved:

- Approximation of integrals (usually midpoint rule),
- Interpolation is used to approximate variable values at locations other than the discrete points at which they are computed,
- Finite differences are used to approximate gradients of variables.

In this way, one algebraic equation per CV is obtained, linking variable value at the centroid of that CV with those at neighbor CVs. For the solution domain as a whole, a large system of algebraic equations is obtained. To make things more complicated, one such system is obtained for each governing equation (e.g. for three velocity components, pressure, temperature etc.). Since these equations are in general non-linear and coupled, the solution must be sought using iterative solution methods. Iteration means repeating a

### **4.3 SOLUTION PROCESS OF A CFD ANALYSIS USING FVM APPROACH**

CFD analysis is structured around the numerical algorithms that can tackle fluid flow problems. A CFD analysis mainly works through problems by three different activity stages:

1. A pre-processor.
2. A solver and
3. A post processor.

**The activities at the pre-processor stages involve:**

- Definition of the geometry of the region of interest: the computational domain.
- Solution domain then have to subdivided into a finite number of control volumes or CVs (also called cells) using a suitable grid (also called a mesh). The grid can be composed o hexahedral, tetrahedral, prismatic, pyramid or polyhedral cells. Any of these cell shapes can be used to construct grids suitable for CFD domains.
- Selection of the physical and chemical phenomena that need to be modeled.
- Definition of fluid properties.
- Specification of appropriate boundary conditions at cells which coincide with or touch the domain boundary.

**The activities at the solver stage involves**

- Division of the domain into discrete control volumes using a computational grid.
- Integration of the governing equations on the individual control volumes of the solution domain to construct algebraic equations for the discrete dependent

variables (unknowns) such as velocities, pressure, temperature and conserved scalars.

- Discretization, which involves the substitution of a variety of finite-difference-type approximations for the terms in the integrated equation representing flow processes such as convection, diffusion and sources. This converts the integral equations into a system of algebraic equations.
- Linearization of the discretized equations.
- Solution of the algebraic equations (resultant linear equation system) by an iterative method in order to yield updated values of the dependent variables.

The first step, the control volume integration distinguishes the finite volume method from all other CFD techniques. The resulting statements express the (exact) conservation of relevant properties for each finite size cell. This clear relationship between the numerical algorithm and the underlying physical conservation principle forms one of the main attractions of the finite volume method and makes its concepts much simpler to understand by engineers than finite element and spectral methods.

### **The activities of post-processing stage involves**

- Plotting of results.
- Analysis of results.

## 4.4 NUMERICAL TOOLS/ STEPS FOR SOLVING THE GIVEN PROBLEM USING FVM APPROACH

### Grid/ Mesh generation

The first step, the control volume integration, distinguishes the finite volume method from all other CFD techniques. The resulting statements express the (exact) conservation of relevant properties for each finite size cell. This clear relationship between the numerical algorithm and the underlying physical conservation principle forms one of the main attractions of the finite volume method and makes its concepts much more simple to understand by engineers than finite element and spectral methods. **C**ells are control volumes into which domain is broken up. Computational domain is defined by mesh that represents the fluid and solid regions of interest. **F**ace is the boundary of a cell, **e**dge is the boundary of a face, and **n**odes are grid points. As the sides of the trapezoidal cavity are not parallel, the present numerical techniques will discretize the computational domain into unstructured triangular elements.

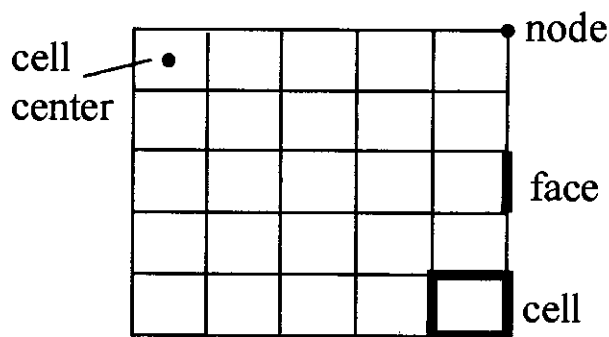


Figure 4.1: Finite Volume discretization of a domain



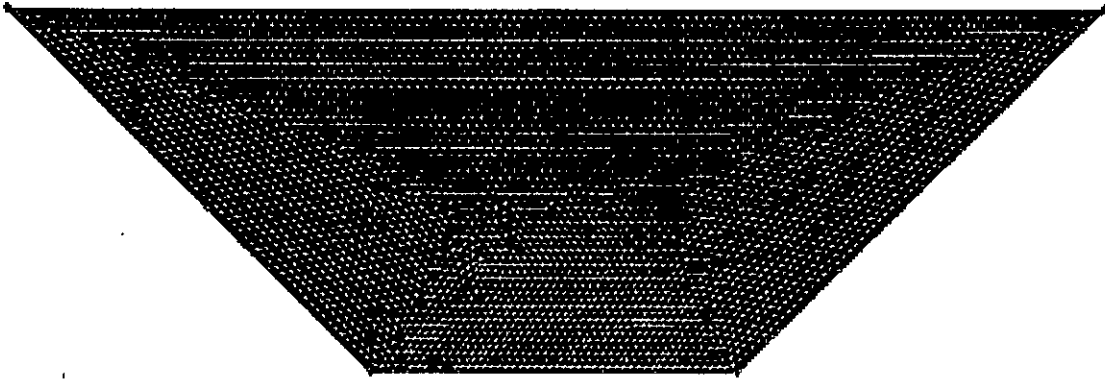


Figure 4.2: Current mesh structure

## 4.5 GRID INDEPENDENCY TEST

In order to obtain the grid independence solution, a grid refinement study is performed for the rectangular and trapezoidal cavity ( $A=1$ ) under constant heat flux condition keeping,  $Re=400$ ,  $Pr=0.71$ ,  $Ri= 1.0$ . fig. 4.3 shows the convergence of the average Nusselt number,  $Nu_{av}$ , at the heated surface with grid refinement. It is observed that grid independence is achieved with  $60 \times 60$  grid for the rectangular enclosure. This grid resolution is therefore used for all subsequent computations for  $A \leq 1$ . For taller cavities with  $A > 1$ , a proportionately large number of grids in the vertical direction is used while keeping the number of grids in the horizontal direction fixed at 60.

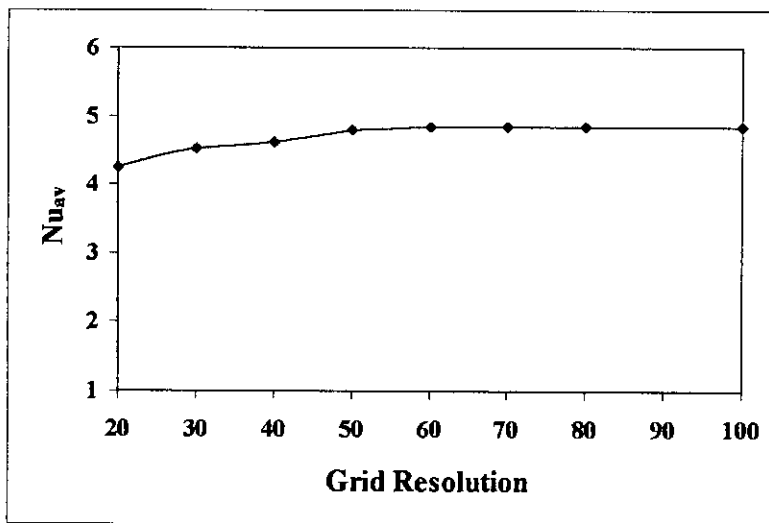


Figure 4.3: Convergence of the  $Nu_{av}$  with grid refinement for rectangular cavity at  $Ri=1.0$ ,  $Re=400$  and  $A=1$

For the trapezoidal cavity, test for the accuracy of grid fineness has been carried out to find out the optimum grid number. It is found in fig. 4.4 that 5496 regular nodes are sufficient to provide accurate results. This grid resolution is therefore used for all subsequent computations for  $A \leq 1$ . For taller cavities with  $A > 1$ , a proportionately large number of grids in the vertical direction is used.

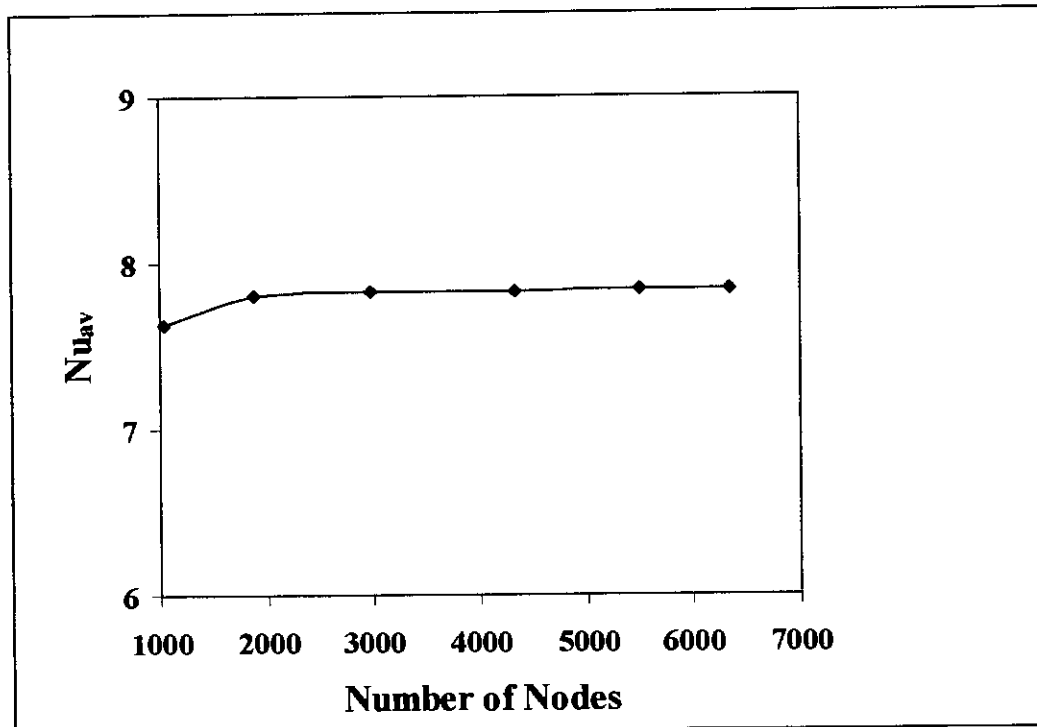


Figure 4.4: Grid sensitivity test for Trapezoidal cavity at  $Ri=1.0$ ,  $Re=400$  and  $A=1$

## 4.6 INITIALIZATION THE SIMULATION

Before stating the CFD simulation the solution flow field is initialized. In many cases, the initial solution is provided so that it will allow the desired final solution to be attained.

There are two methods for initializing the solution:

- Initialize the entire flow field (in all cells)
- Patch values or functions for selected flow variables in selected cell zones or register of cells. (Registers are created with the same functions that are used to mark cells for adaptation.)

## 4.7 SOLVER SETTING

For any given problem using FVM approach two types of solvers can be used.

- Segregated solver
- Coupled solver

The segregated solver traditionally has been used for incompressible and mildly compressible flows. The segregated solver solves the governing integral equations for the conservation of mass and momentum, and (when appropriate) for energy and other scalars.

## 4.8 CONVERGENCE CRITERIA

Convergence is the property of a numerical method to produce a solution, which approaches the exact solution as the grid spacing; control volume size of element size is reduced to zero.

For the current problem, convergence is judged by examining residual levels to reach a predestinated criterion. The convergence criterion was defined by the required scaled residuals to decrease  $10^{-5}$  for all equations except the energy equations, for which the criterion is  $10^{-8}$ .

## 4.9 CODE VALIDATION

The computational procedure is validated against the numerical results of Iwatsu et al.[23] for a top heated moving lid and bottom cooled square cavity filled with air ( $Pr=0.71$ ). A  $60 \times 60$  mesh is used and computations are done for six different  $Re$  and  $Gr$  combinations. Comparisons of the average Nusselt number at the hot lid are shown in Table 1. The general agreement between the present computation and that of Iwatsu et al.[] is seen to be very well with a maximum discrepancy of about 3.9%.

Table 1: Comparison of the computed average Nusselt number at the hot plate

$Re$	$Gr=10^2$			$Gr=10^4$			$Gr=10^6$		
	Present	Iwatsu et al.	Diff. %	Present	Iwatsu et al.	Diff. %	Present	Iwatsu et al.	Diff. %
400	3.97	3.84	3.3	3.75	3.62	3.5	1.18	1.22	3.2
1000	6.25	6.33	1.2	6.32	6.29	0.47	1.70	1.77	3.9

The computational procedure can also be validated against the numerical results of Guo and M. A. R. Sharif [32] shown in the figure below.

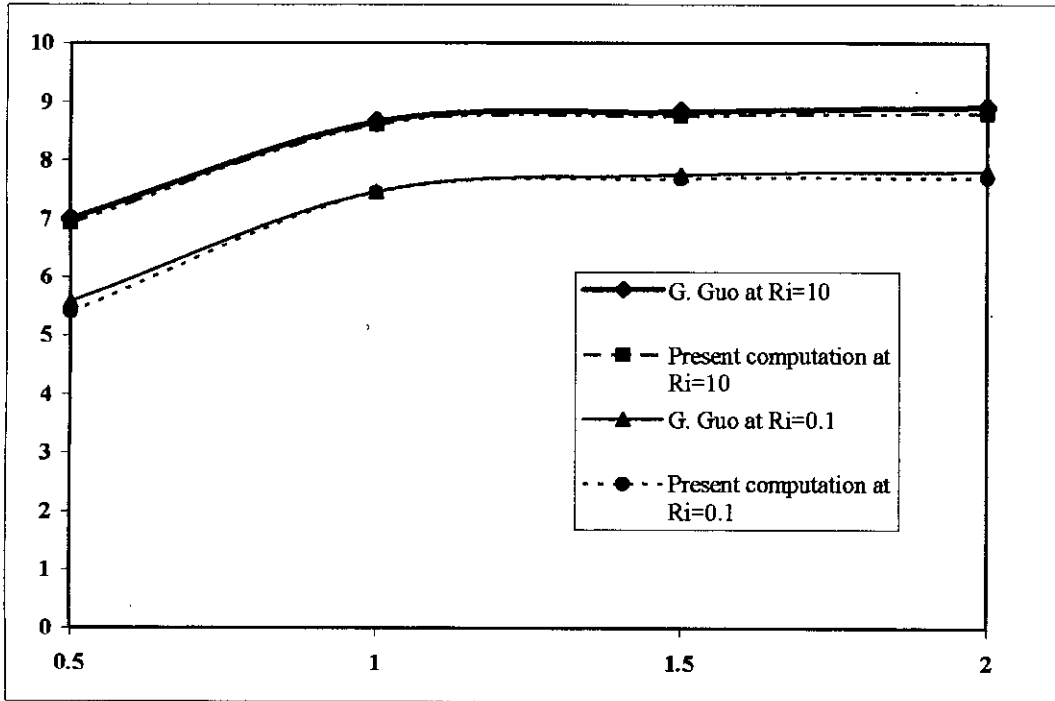


Figure 4.5: Variation of the Average Nusselt number with different Aspect Ratio at  $Ri=10$ ,  $Re=100$  and  $\varepsilon=0.6$

Fig. 4.5, reveals that the Average Nusselt numbers in the present study have excellent agreement with those obtained by Guo and M. A. R. Sharif [32] having a maximum discrepancy of about 2.3%. Therefore, it can be concluded that the numerical code used in this analysis can solve the present problem with reasonable agreement.

## CHAPTER 5

# RESULTS AND DISCUSSION

---

Numerical results are presented in order to determine the effects of the inclination angle of the side walls, Richardson number  $Ri$ , Reynolds number  $Re$ , Aspect ratio  $A$ , the rotational angle of the cavity  $\Phi$  on mixed convection flow in trapezoidal enclosure. The inclination angle of the sidewalls of the trapezoidal enclosure has been changed from  $30^\circ$  to  $60^\circ$  with an interval of  $15^\circ$ . The values of Richardson number varies from 0.1 to 10, Aspect ratio,  $A$  changes from 0.5 to 2.0 taking Rotational angle  $30^\circ$ ,  $45^\circ$ ,  $60^\circ$  for two different Reynolds numbers 400 and 600.

### 5.1 EFFECT OF INCLINATION ANGLE, $\gamma$

In this study the effect of inclination angle of the adiabatic sidewalls has been observed first. The inclination angle of the side walls has been changed to  $30^\circ$ ,  $45^\circ$  and  $60^\circ$ . The Richardson number has been changed from 0.1 to 10. The optimum inclination angle has been selected based on the average Nusselt number which is a non dimensional parameter that indicates the rate of heat transfer between the hot and cold walls. The results are obtained both for  $Re=400$  and  $Re=600$ .

Figure 5.1-5.3 reveals the impact of varying inclination angles of the sidewalls of the trapezoidal cavity. These figures show the contours of streamlines and isotherms at different Richardson numbers. For small values of  $Ri$  number, it can be seen that the shear effect due to the movement of the top wall is dominant. The fluid flow is characterized by a primary recirculation of the size of the cavity generated by the movement of the top lid. The isothermal contour maps are clustered near the bottom and top walls resulting in steep temperature gradient there. In each case as the Richardson number increases the convection current becomes more dominant resulting in stronger flow field. Again at  $\gamma=45^\circ$  (fig. 5.2), the flow field is stronger than the  $\gamma=30^\circ$  and  $\gamma=60^\circ$  (fig. 1 and fig. 3), which is an indication of better heat transfer. The isothermal plots also complies with the flow field, showing minimum value of the maximum isotherms at  $\gamma=45^\circ$ .

From figure 5.4-5.5 the average value of the Nusselt number with respect to the Richardson number has been plotted. Here it can be seen that Nusselt number at  $\gamma=45^\circ$  dominates the other two cases i.e.  $\gamma=30^\circ$  and  $\gamma=60^\circ$ , showing better heat transfer. So it is clearly visible that trapezoid having the inclination angle  $\gamma=45^\circ$  gives better heat transfer and consequently it can be taken as the optimum inclination angle for the rest of the analysis.

## 5.2 EFFECT OF RICHARDSON NUMBER, $Ri$

The value of the Richardson number,  $Ri=Gr/Re^2$  provides a measure of the importance of buoyancy driven natural convection relative to the lid driven forced convection. When the Buoyancy effects are relatively small,  $Ri<1$ , the gross flow features of fig. 5.6-5.13 are similar to those of a conventional non-stratified fluid at comparable values of  $Re$ . In general, the flow field is characterized by a primary clockwise recirculation where the shear driven flow by the lid is impacted on the right adiabatic sidewall and is forced to move downward. The flow then rises along the left side wall due to the buoyancy affect. The main circulation fills the entire cavity of the size of the cavity generated by the movement of the top wall. Minor cells may be visible near the bottom corners. The streamlines and isotherms indicated that the hydrodynamic and thermal boundary layers are not developed fully at low Richardson number. The isothermal lines are mostly undistorted and horizontal lines except the large recirculating area inside the cavity at low Richardson number. In the large recirculating zone temperature gradients are very weak. This implies that, due to the vigorous actions of the mechanically driven circulations, fluids are well mixed; consequently, temperature differences in much of this interior region are very small.

When  $Ri>1$ , natural convection begins to dominate the forced convection. The Buoyancy assists the core flow and thus the convection current becomes more and more strong with increasing Richardson number. As Richardson number increases, the main circulation occupies the whole cavity and it become more symmetrical inside the cavity. If we see the isothermal plots, we can see that as the Richardson number increases the isothermal lines becomes more and more denser at the upper cold lid. The crowded streamlines and isothermal lines indicate that the hydrodynamic and thermal boundary layers have been

developed along the hot wall and cold wall, respectively, reflecting rigorous heat transfer rate occurred. Consequently the maximum temperature reduces due to this large heat transfer rate.

The average Nusselt number as a function of Richardson number has been plotted in fig. 5.14-5.15 for different Reynolds number. It can be observed that as the Richardson number increases the average Nusselt number increases accordingly for all the aspect ratios. When  $Ri < 1$ ,  $Nu_{av}$  grows only slightly with increasing  $Ri$ . After  $Ri$  is more than 1,  $Nu_{av}$  is found to increase more rapidly. Since  $Re$  is kept constant the forced convection effect remains invariant as  $Ri$  increases for a particular case. When  $Ri > 1$ , the natural convection aids more and more in the heat transfer process in addition to the forced convection which results in more rapid increase of  $Nu_{av}$ .

### 5.3 EFFECT OF ASPECT RATIO, $A$

Changing the aspect ratio,  $A$  ( $A=H/W$ ) causes a change in heat transfer characteristics which can be visible in fig. 5.6-5.13. In order to investigate the convection heat transfer at different aspect ratios, computations were done for cavities at aspect ratios of 0.5, 1, 1.5 and 2.0. Keeping Reynolds number fixed at 400 and 600 the Richardson number has been changed from 0.1 to 10. If we compare the flow fields at different aspect ratios from 0.5 to 2.0 (figure 5.6-5.13), it can be revealed that in the convection region adjacent to the heat source, the isotherms become thinner and denser producing higher temperature gradients with increasing aspect ratio. The streamlines become more and more stronger as the aspect ratio increases. The isotherms are also adjusted according to the streamlines and showing lower values as the aspect ratio increases at a particular  $Ri$ . This is due to the fact that the cavity volume increases with aspect ratio and more volume of cooling air is involved in cooling the heat source leading to better cooling effect. The thermal and hydrodynamic boundary layers have been developed completely at high aspect ratios and when natural convection dominates. The average Nusselt number at the heat source surface has been plotted in fig. 5.16-5.17 for a range of  $Ri$  and aspect ratios. For a particular aspect ratio, the  $Nu_{av}$  increases with increasing  $Ri$ . As a result, the maximum temperature decreases monotonously which can be recognized from the isothermal plots. As the aspect ratio increases from 0.5 to 2 the  $Nu_{av}$  increases for a particular  $Ri$ . At higher

Reynolds number i.e.  $Re=600$ , with increasing aspect ratio some secondary eddy at the bottom surface of the cavity has been observed (fig.: 5.12-5.13). This is of frictional losses and stagnation pressure. As the  $Ri$  increases, natural convection dominates more and the bottom secondary eddies blends into the main primary flow. For  $A>1.5$  the variation is almost flat indicating that the aspect ratio does not play a dominant role on the heat transfer process at that range. At high aspect ratios the convection is weak in the upper parts of the taller cavities.

#### **5.4 EFFECT OF REYNOLDS NUMBER, $Re$**

This study has been done at two different Reynolds numbers. They are  $Re=400$  and  $Re=600$ . With a particular case keeping  $Ri$  and  $A$  constant, as the Reynolds number increases the convective current becomes more and more stronger and the maximum value of the isotherms reduces. As we know  $Ri=Gr/Re^2$ .  $Gr$  is square proportional of  $Re$  for a fixed  $Ri$ . So slight change of  $Re$  and  $Ri$  causes huge change of  $Gr$ . For lower  $Gr$  the convection intensity in the cavity is very weak as evident from the stream function values. In that case, viscous forces are more dominant than the buoyant forces at lower  $Gr$  and diffusion is the principle mode of heat transfer. But for higher  $Gr$  the intensity of convection increases significantly, as  $Gr$  increases the buoyancy force. As buoyancy force is increased then heat transfer rate is tremendously high. So changes are very visible to the change of  $Re$ . From fig. 5.14-5.15, it can be observed that as the  $Re$  increases the average Nusselt number also increases for all the aspect ratios.



## 5.5 EFFECT OF ROTATIONAL ANGLE, $\Phi$

Next the effect of rotational angle,  $\Phi$  has been studied. When studying the effect of rotational angle, two distinct cases have been taken into consideration. They are aiding and opposing flow condition. The first one is when the shear driven flow opposes the convective flow and in that case the top moving lid is moving in the positive direction at a specified rotational angle [fig. 3.1]. The second condition is the aiding flow condition where the shear driven flow aids the natural convective flow and the moving top lid moves in the opposite direction unlike the first case [fig. 3.2]. Both these cases have been studied for a rotational angle for  $\Phi=30^\circ$ ,  $45^\circ$  and  $60^\circ$  and their heat transfer characteristics has been studied in terms of streamlines and isothermal plots.

Unlike  $\Phi=0^\circ$ , when the buoyancy is acting only in the y direction, as the rotational angle  $\Phi$  changes, the flow field changes significantly. In opposing flow condition the shear driven flow opposes the natural convective flow, At low Richardson number ( $Ri < 1$ ) the forced convection is dominating, creating a single circulation at the right corner of the top moving lid [fig. 5.18-5.32]. As the Richardson number increases ( $Ri > 1$ ), natural convection becomes dominating creating a large circulation at the bottom of the cavity. This large circulation causing by natural convection goes bigger and stronger as  $Ri$  number increases as well as squeezes the upper circulation, resulting an opposing effect. If we observe the isothermal plots, it changes accordingly with streamlines. As  $Ri$  number increases, the isothermal lines changes significantly indicating that the convection is the dominating heat transfer for the specified case. The shear driven circulation at the upper right side becomes smaller and smaller as the  $Ri$  number increases because of dominating natural convection.

In the case of aiding flow, condition when the forced convection aids the natural convection a different scenario has been observed [fig. 5.33-5.47]. In all the cases, a single circulation of the size of the cavity has been observed. Unlike the opposing flow condition, in that case the natural convection aids the shear driven flow from the smaller value of  $Ri$  number, resulting a much stronger convective current. As the  $Ri$  number increases, the convection flow fields become more and more stronger resulting better and better heat transfer. The isotherms changes significantly as the Richardson number increases and gives the minimum value at higher  $Ri$  number.

As the aspect ratio,  $A$  increases the convective flow fields become more and more stronger. As cavity volume increases with aspect ratio and more volume of cooling air is involved in cooling the heat source leading to better cooling effect. Fig. 5.48-5.59 shows the effect of aspect ratio at different rotational angle. In all the cases, it can be observed that  $Nu_{av}$  increases with increasing aspect ratio for all rotational angles, leading to better heat transfer. Fig. 5.60-5.67 shows a comparative analysis of aiding and opposing flow conditions. There it can be seen that, the aiding flow condition always dominates the opposing flow condition in terms of  $Nu_{av}$ , which indicates better heat transfer at all rotational angle.  $\Phi=0^\circ$  gives better heat transfer than the opposing flow conditions. The aiding flow condition provides stronger convective currents which can be easily visible in fig. 5.33-5.47, as the natural convection aids the shear driven flow. As a result the maximum value of the isotherms is lower in case of aiding flow condition, indicating lower temperature. But in opposing condition the natural convection opposes the shear driven flow, providing weak convective currents. The  $Nu_{av}$  is also sensitive to rotational angle, fig. 5.60-5.67 (**Op** for opposing flow condition and **Ad** for Aiding flow condition). At  $Re=400$  it can be seen that, Nusselt number decreases as the rotational angle,  $\Phi$  increases from  $0^\circ$  in case of opposing flow condition. But at aiding flow condition Nusselt number increases until  $\Phi=30^\circ$  and then its starts decreasing.  $Nu_{av}$  increases marginally at  $\Phi=30^\circ$  from  $\Phi=45^\circ$  but at  $\Phi=60^\circ$ ,  $Nu_{av}$  drops significantly for all the aspect ratios, fig. 5.60-5.63. The flow fields also changes accordingly. At  $Re=600$ , the maximum heat transfer has been obtained at  $\Phi=45^\circ$ , in terms of average Nusselt number, fig. 5.64-5.67.  $Nu_{av}$  increases marginally at  $\Phi=45^\circ$  from  $\Phi=30^\circ$  but drops significantly at  $\Phi=60^\circ$ , indicating poor heat transfer at  $\Phi=60^\circ$ .

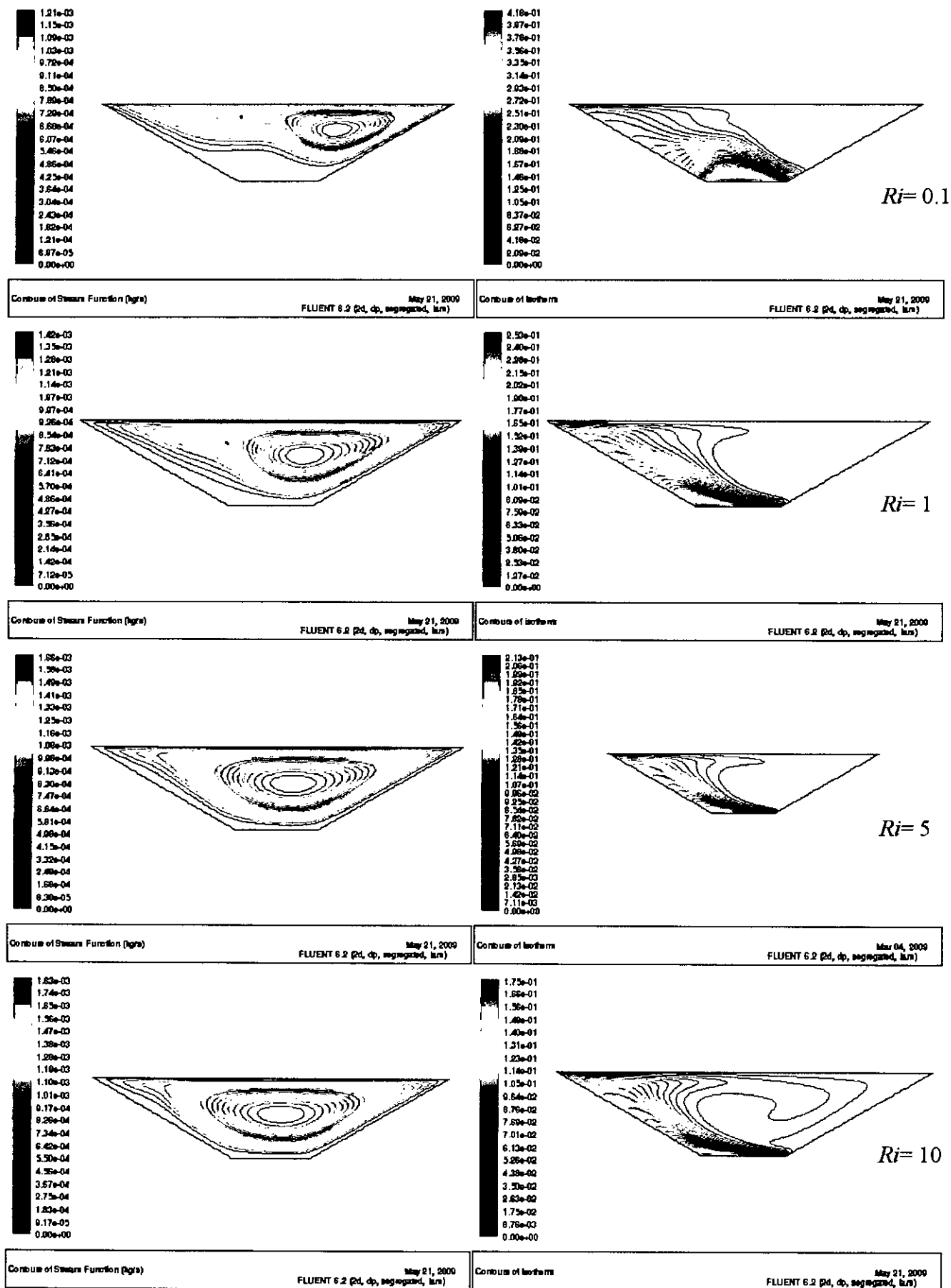


Figure 5.1: Contours of Streamlines and isotherms at  $Re=400$ ,  $A=1.0$  and  $\gamma=30^\circ$

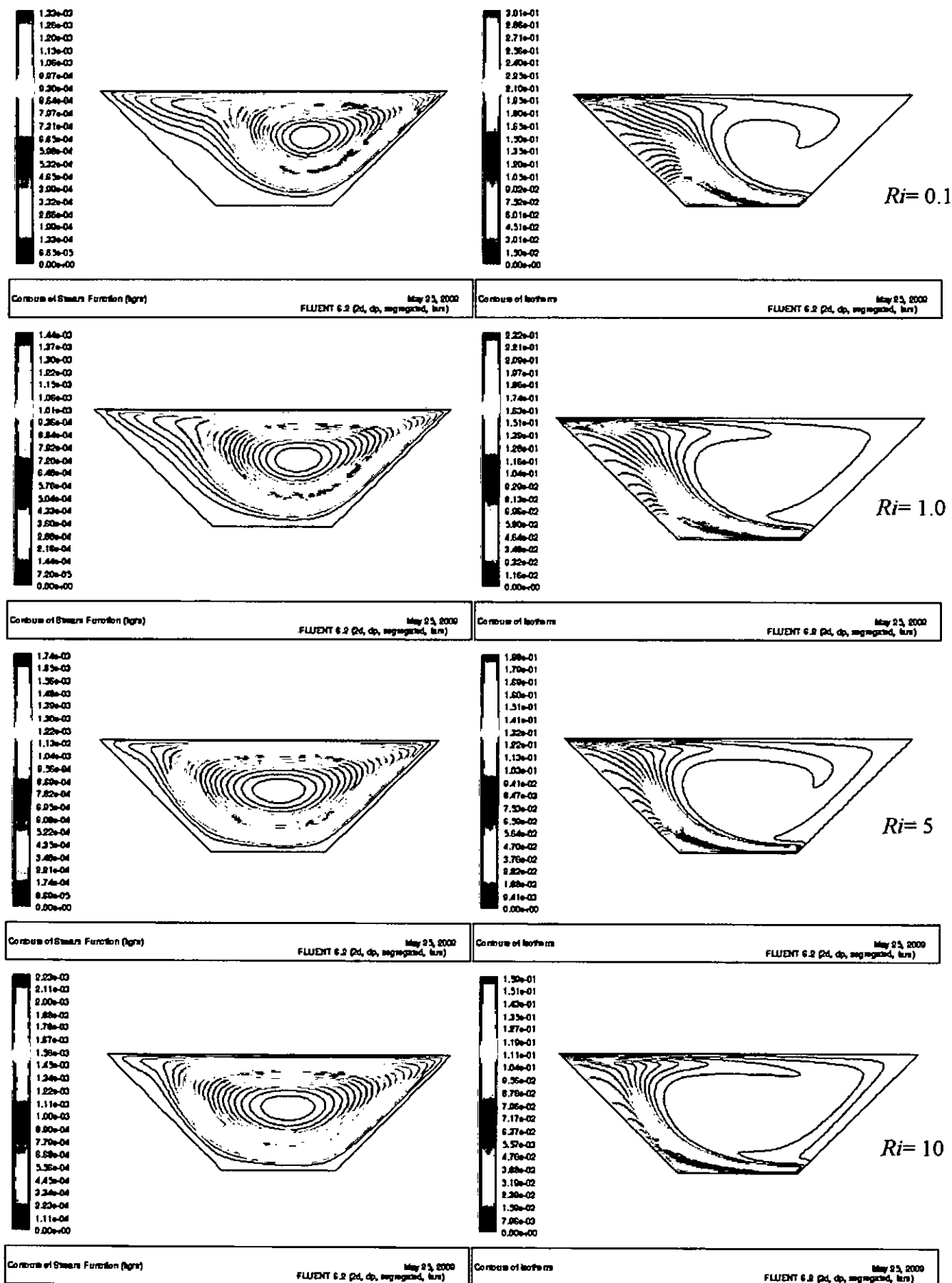


Figure 5.2: Contours of Streamlines and isotherms at  $Re=400$ ,  $A=1.0$  and  $\gamma=45^\circ$

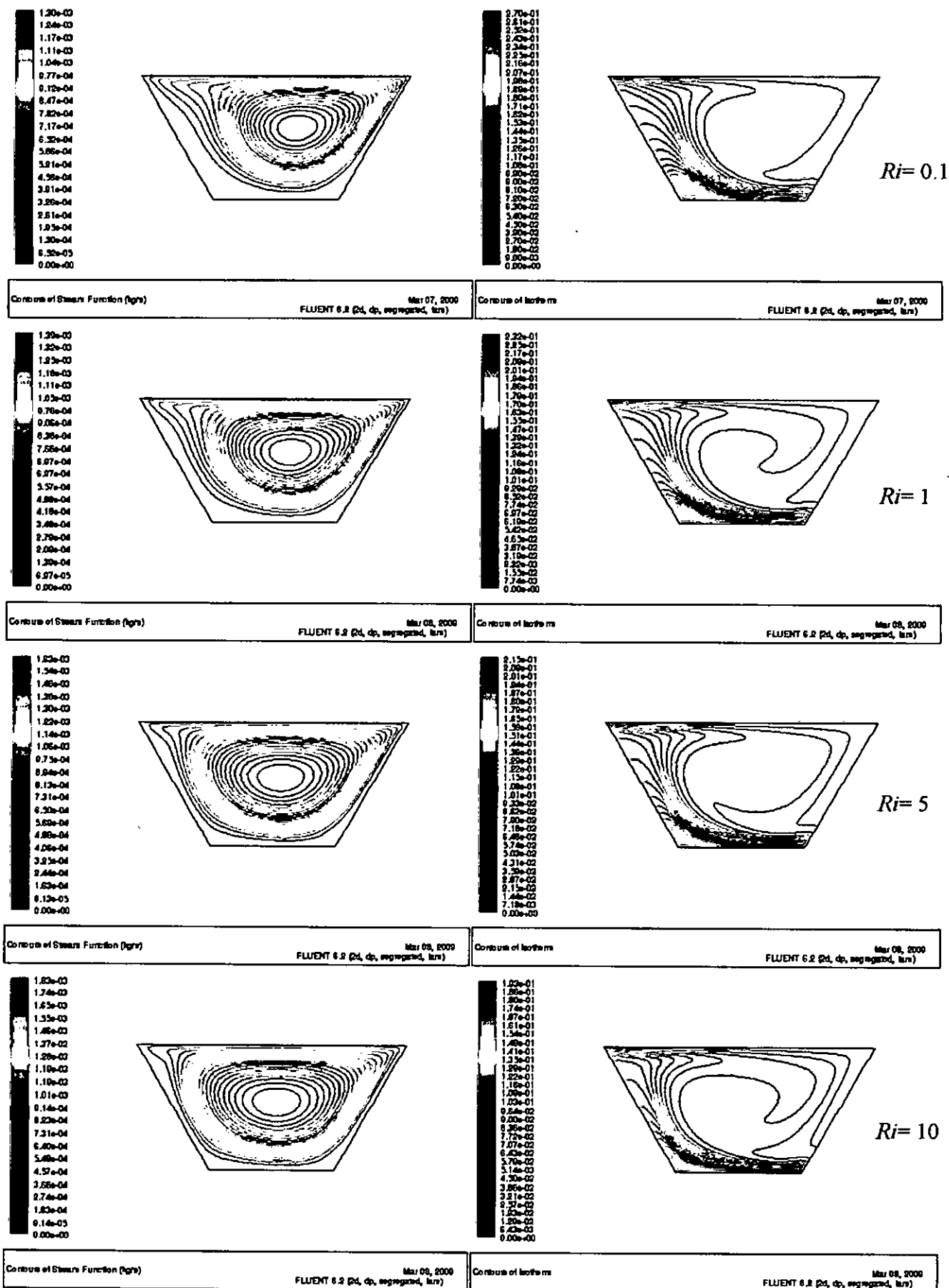


Figure 5.3: Contours of Streamlines and isotherms at  $Re=400$ ,  $A=1.0$  and  $\gamma=60^\circ$

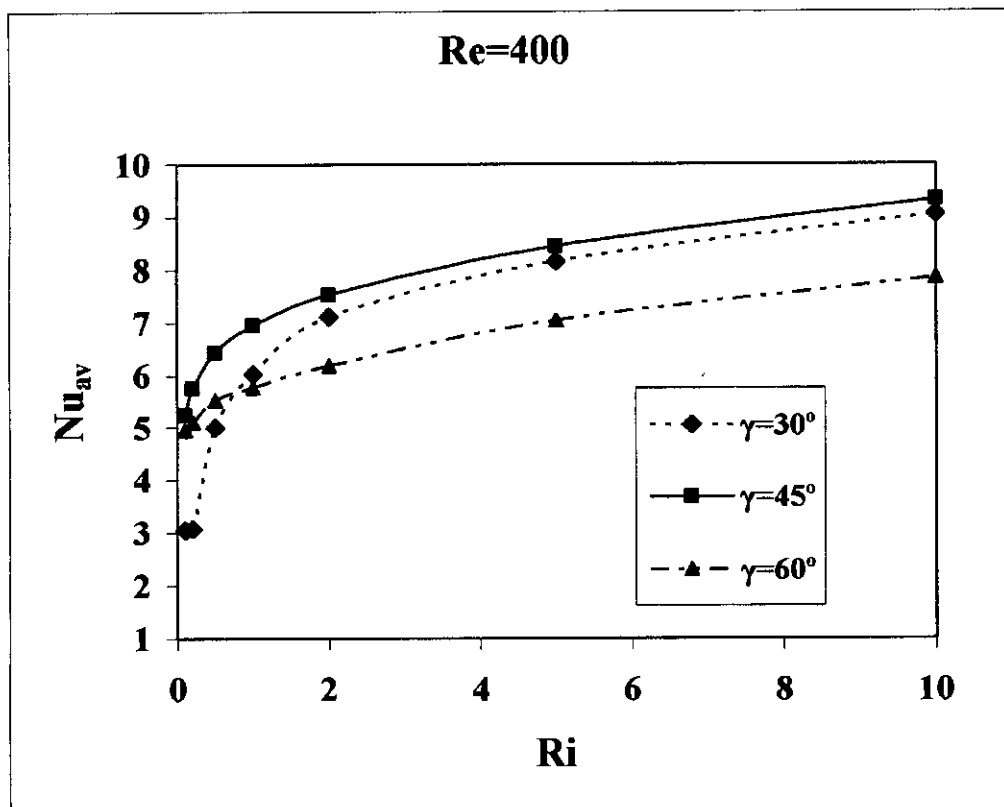


Figure 5.4: Average Nusselt number,  $Nu_{av}$  vs Richardson number at  $Re=400$ ,  $A=1$

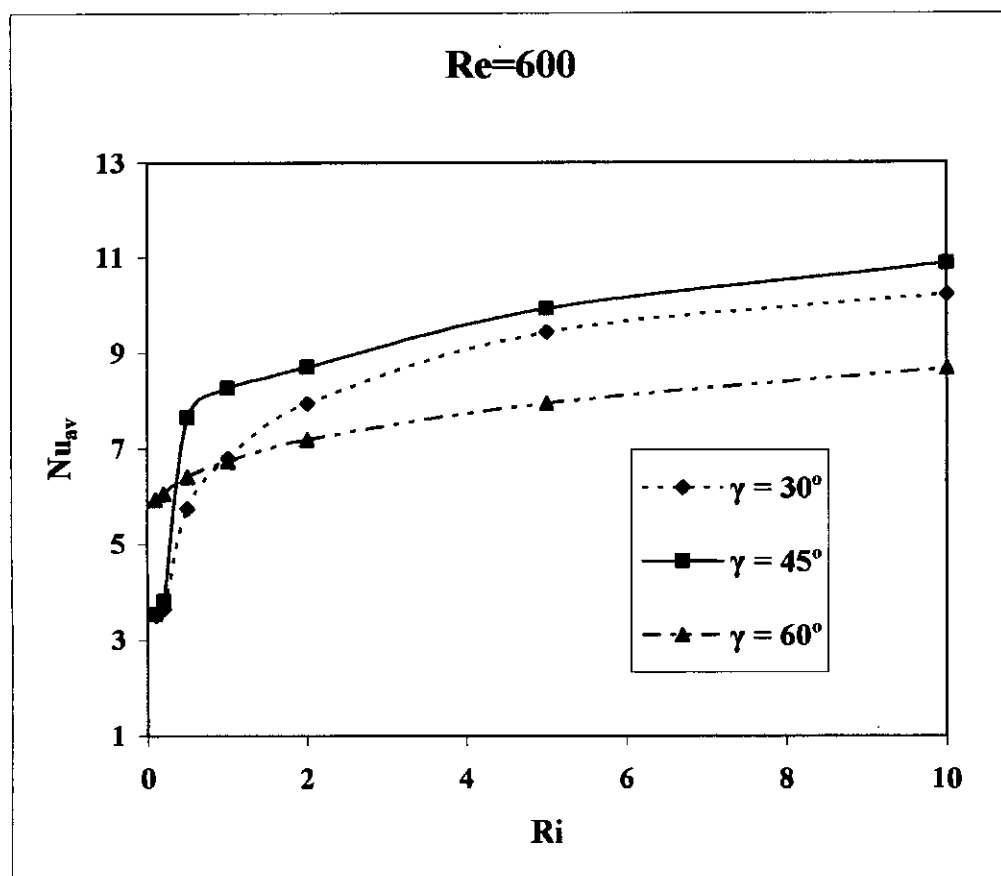
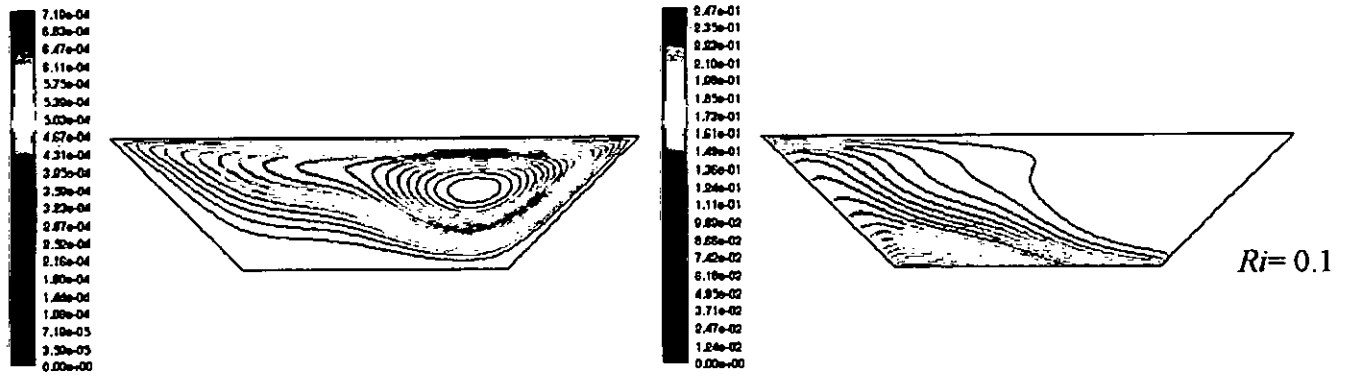
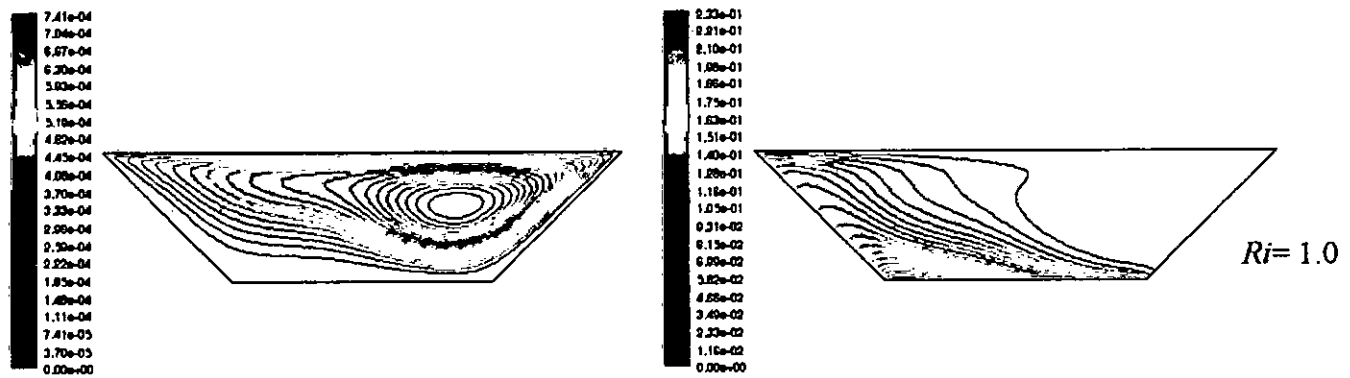


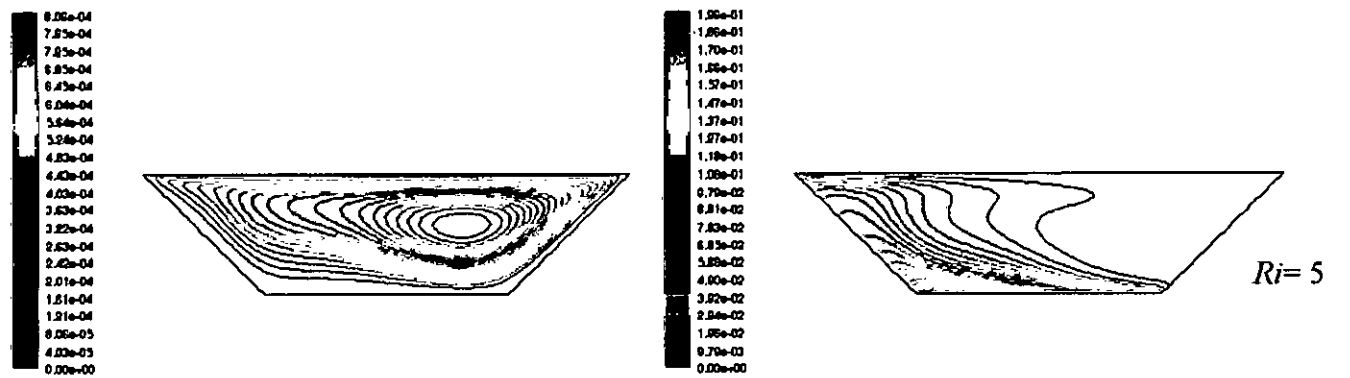
Figure 5.5: Average Nusselt number,  $Nu_{av}$  vs Richardson number at  $Re=600$ ,  $A=1$



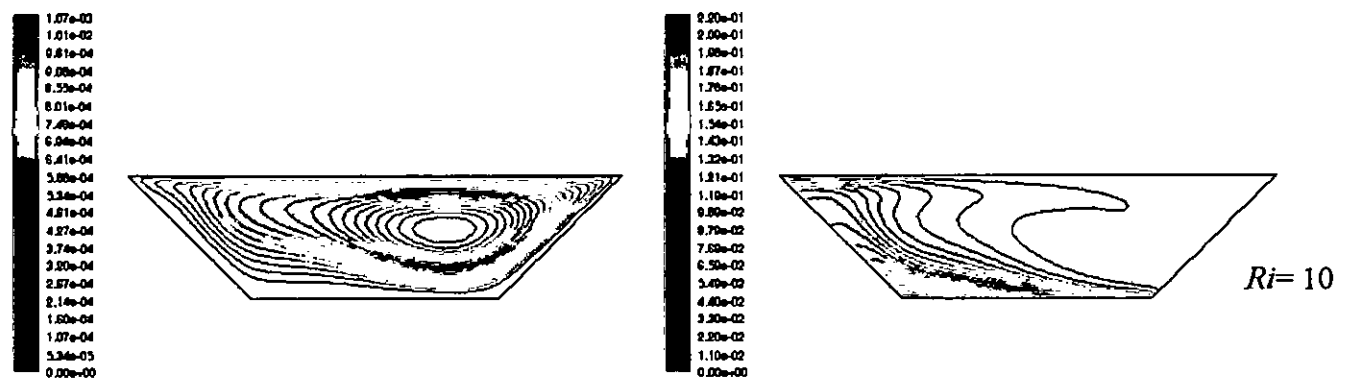
Contours of Stream Function (left) Mar 13, 2009 FLUENT 6.2 (2d, dp, segregated, lsm)      Contours of Isotherms Mar 13, 2009 FLUENT 6.2 (2d, dp, segregated, lsm)



Contours of Stream Function (left) Mar 13, 2009 FLUENT 6.2 (2d, dp, segregated, lsm)      Contours of Isotherms Mar 13, 2009 FLUENT 6.2 (2d, dp, segregated, lsm)

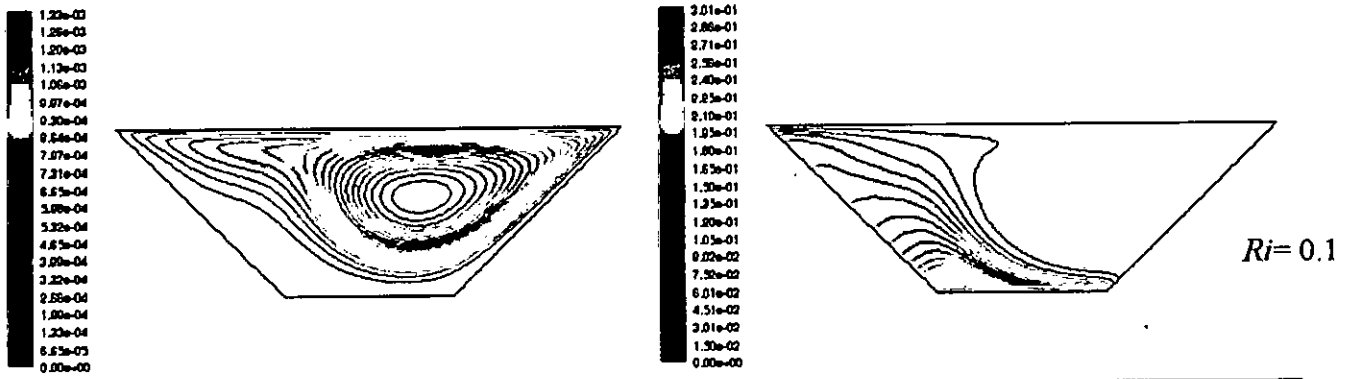


Contours of Stream Function (left) Mar 13, 2009 FLUENT 6.2 (2d, dp, segregated, lsm)      Contours of Isotherms Mar 13, 2009 FLUENT 6.2 (2d, dp, segregated, lsm)

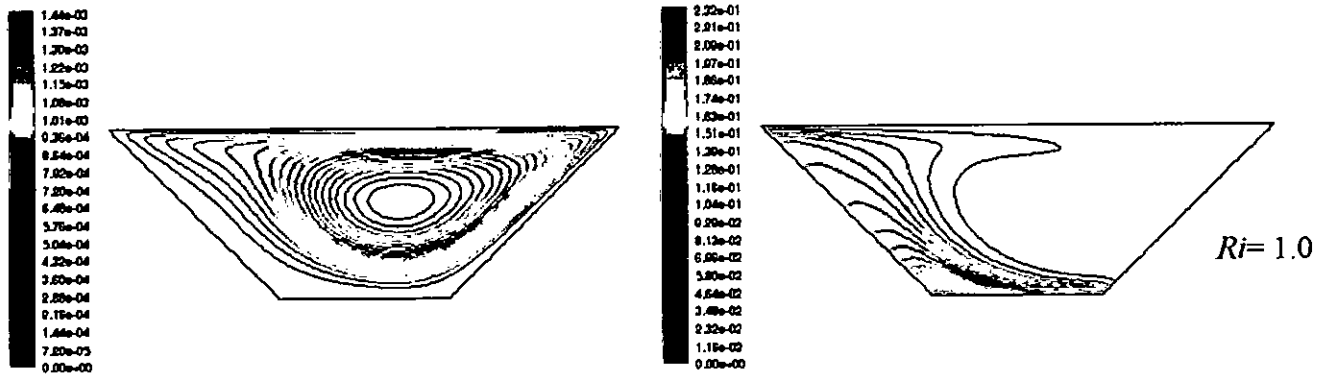


Contours of Stream Function (left) Mar 13, 2009 FLUENT 6.2 (2d, dp, segregated, lsm)      Contours of Isotherms Mar 13, 2009 FLUENT 6.2 (2d, dp, segregated, lsm)

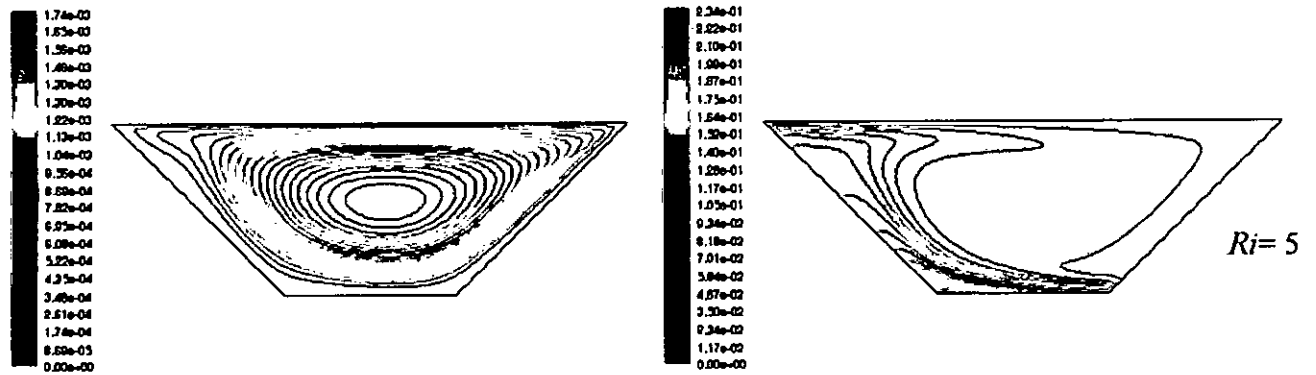
Figure 5.6: Contours of Streamlines and isotherms at  $Re=400$ ,  $A=0.5$  and  $\Phi=0^\circ$



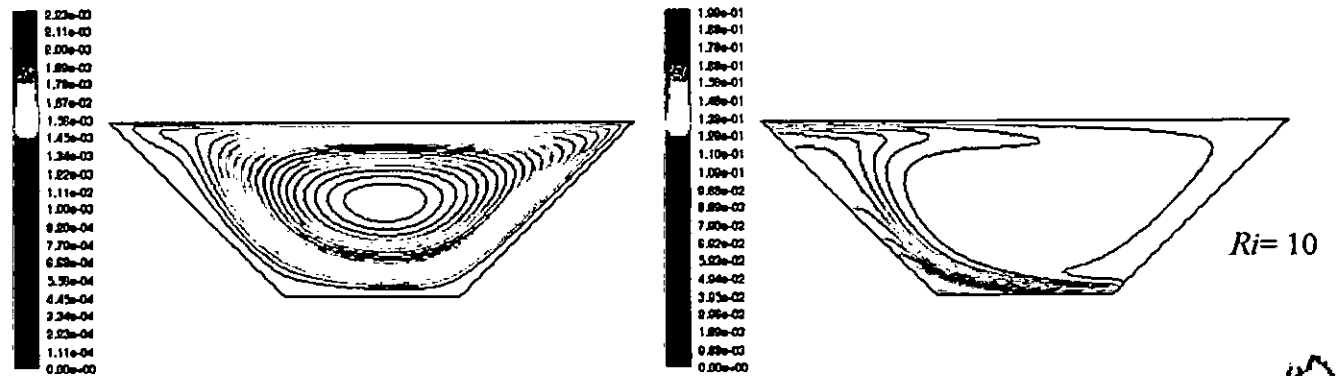
Contours of Stream Function (left) Mar 13, 2000 FLUENT 6.2 (2d, dp, segregated, km)      Contours of Isotherms Mar 13, 2000 FLUENT 6.2 (2d, dp, segregated, km)



Contours of Stream Function (left) Mar 13, 2000 FLUENT 6.2 (2d, dp, segregated, km)      Contours of Isotherms Mar 13, 2000 FLUENT 6.2 (2d, dp, segregated, km)



Contours of Stream Function (left) Mar 13, 2000 FLUENT 6.2 (2d, dp, segregated, km)      Contours of Isotherms Mar 13, 2000 FLUENT 6.2 (2d, dp, segregated, km)



Contours of Stream Function (left) Mar 13, 2000 FLUENT 6.2 (2d, dp, segregated, km)      Contours of Isotherms Mar 13, 2000 FLUENT 6.2 (2d, dp, segregated, km)

Figure 5.7: Contours of Streamlines and isotherms at  $Re=400$ ,  $A=1.0$  and  $\Phi=0^\circ$



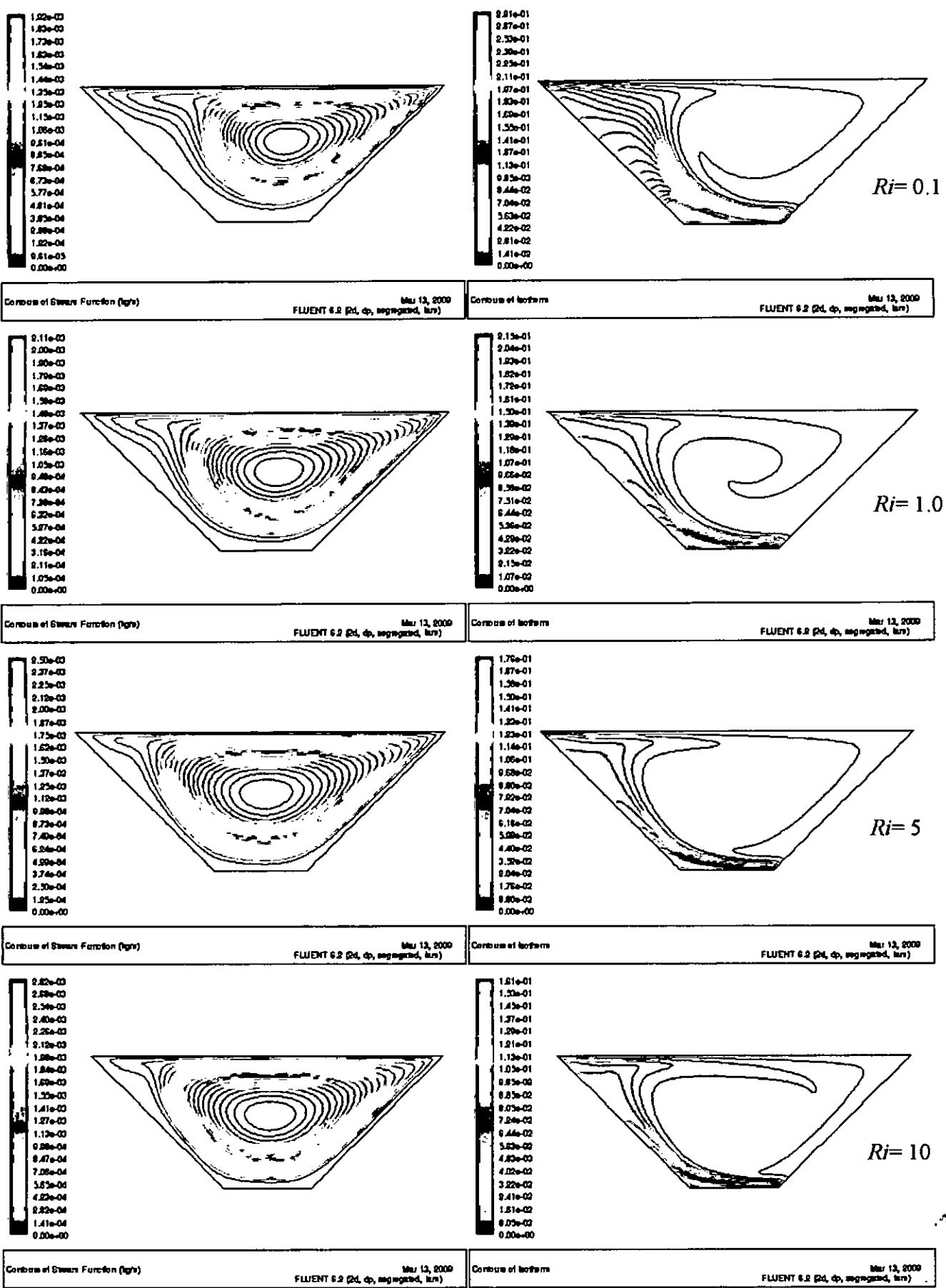


Figure 5.8: Contours of Streamlines and isotherms at  $Re=400$ ,  $A=1.5$  and  $\Phi=0^\circ$

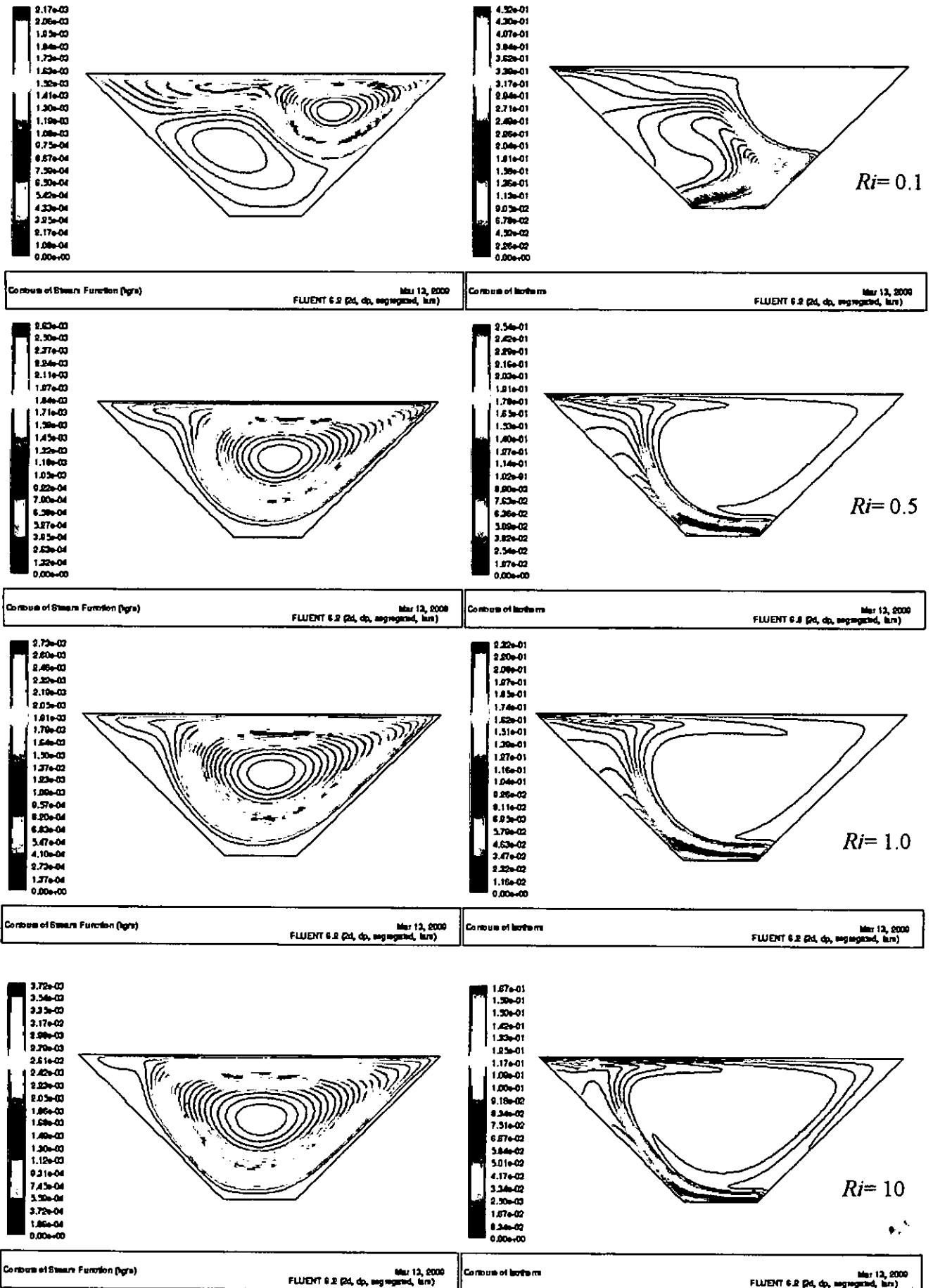


Figure 5.9: Contours of Streamlines and isotherms at  $Re=400$ ,  $A=2.0$  and  $\Phi=0^\circ$

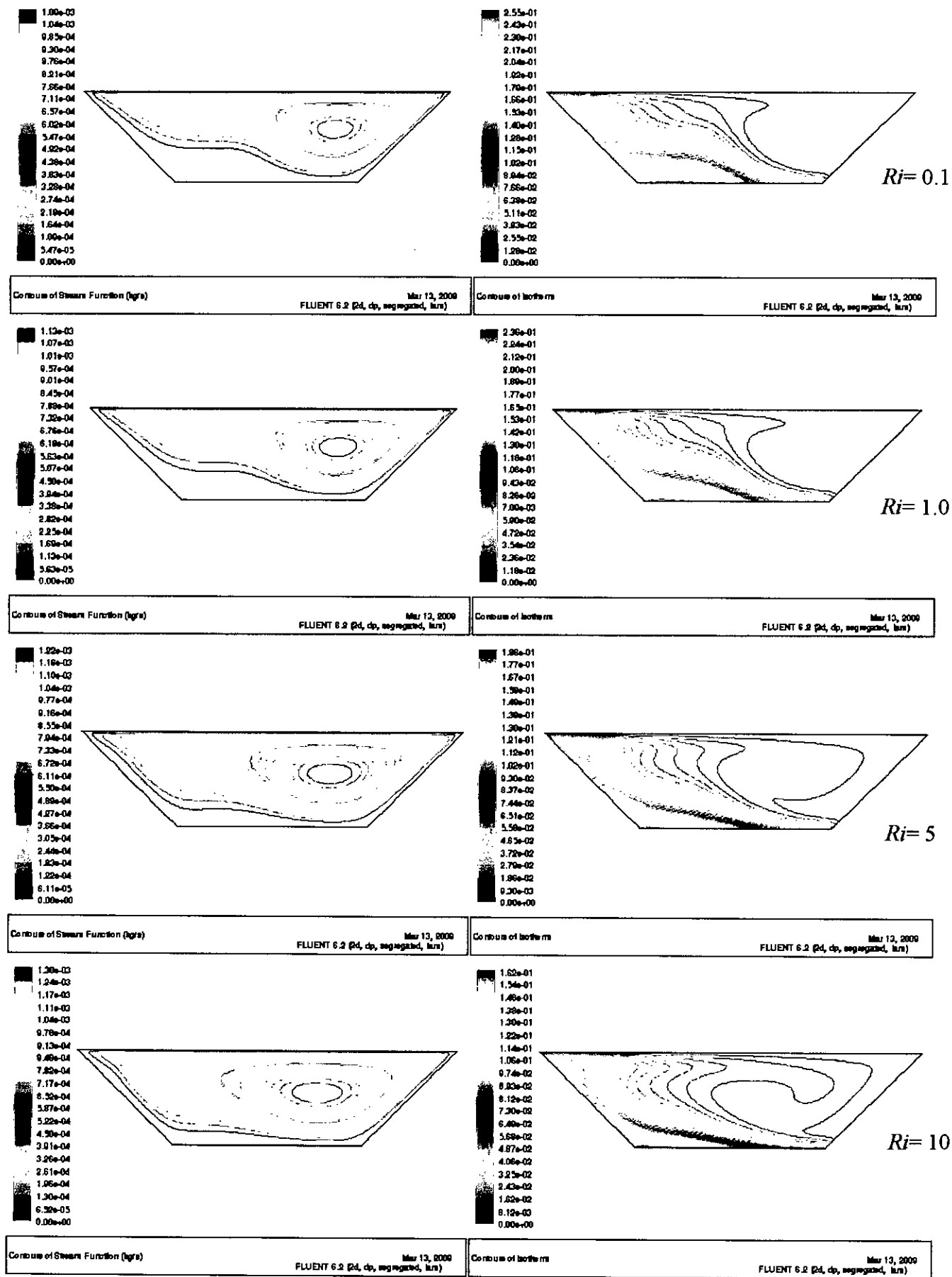


Figure 5.10: Contours of Streamlines and isotherms at  $Re=600$ ,  $A=0.5$  and  $\Phi=0^\circ$

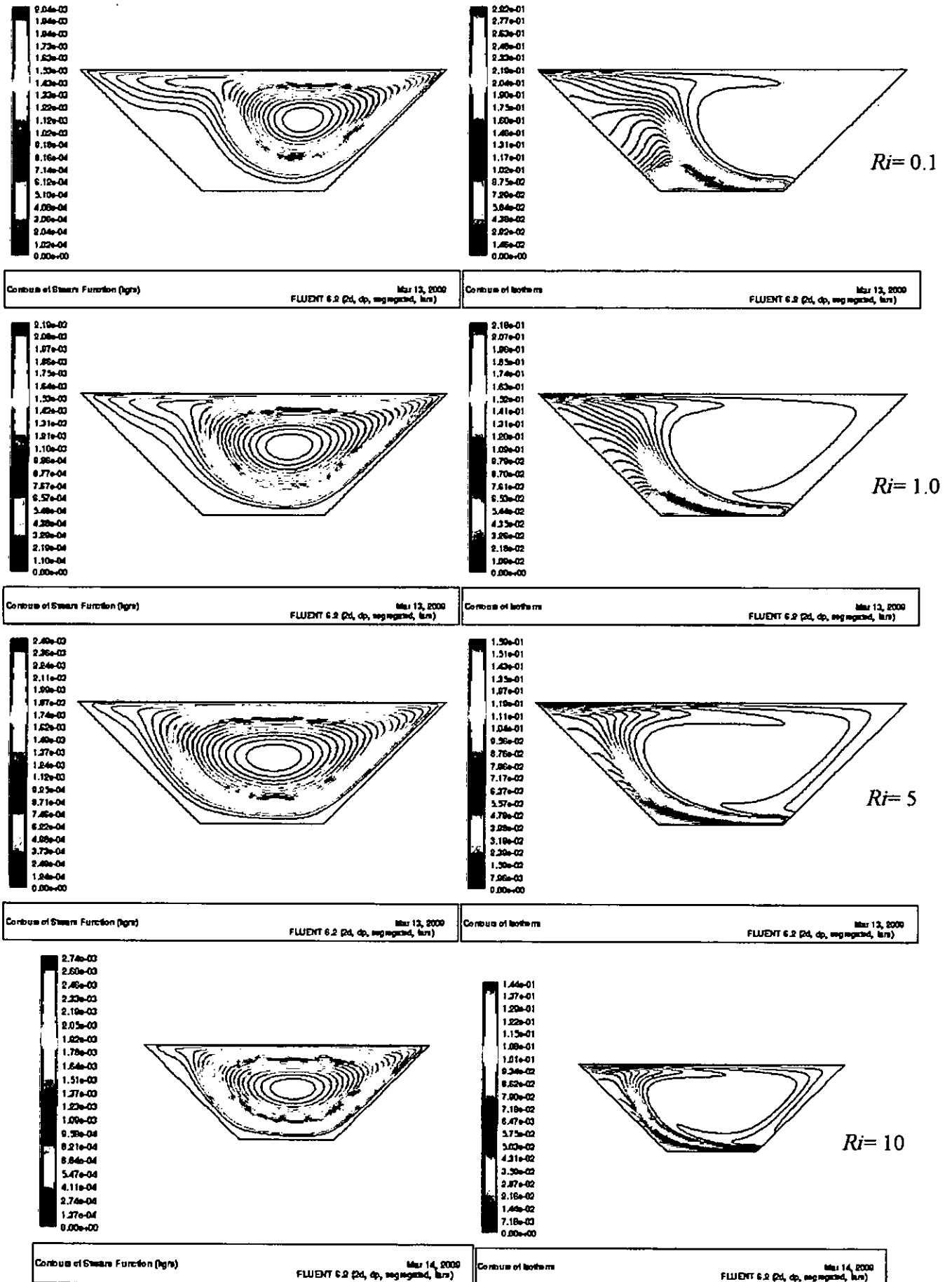


Figure 5.11: Contours of Streamlines and isotherms at  $Re=600$ ,  $A=1$  and  $\Phi=0^\circ$

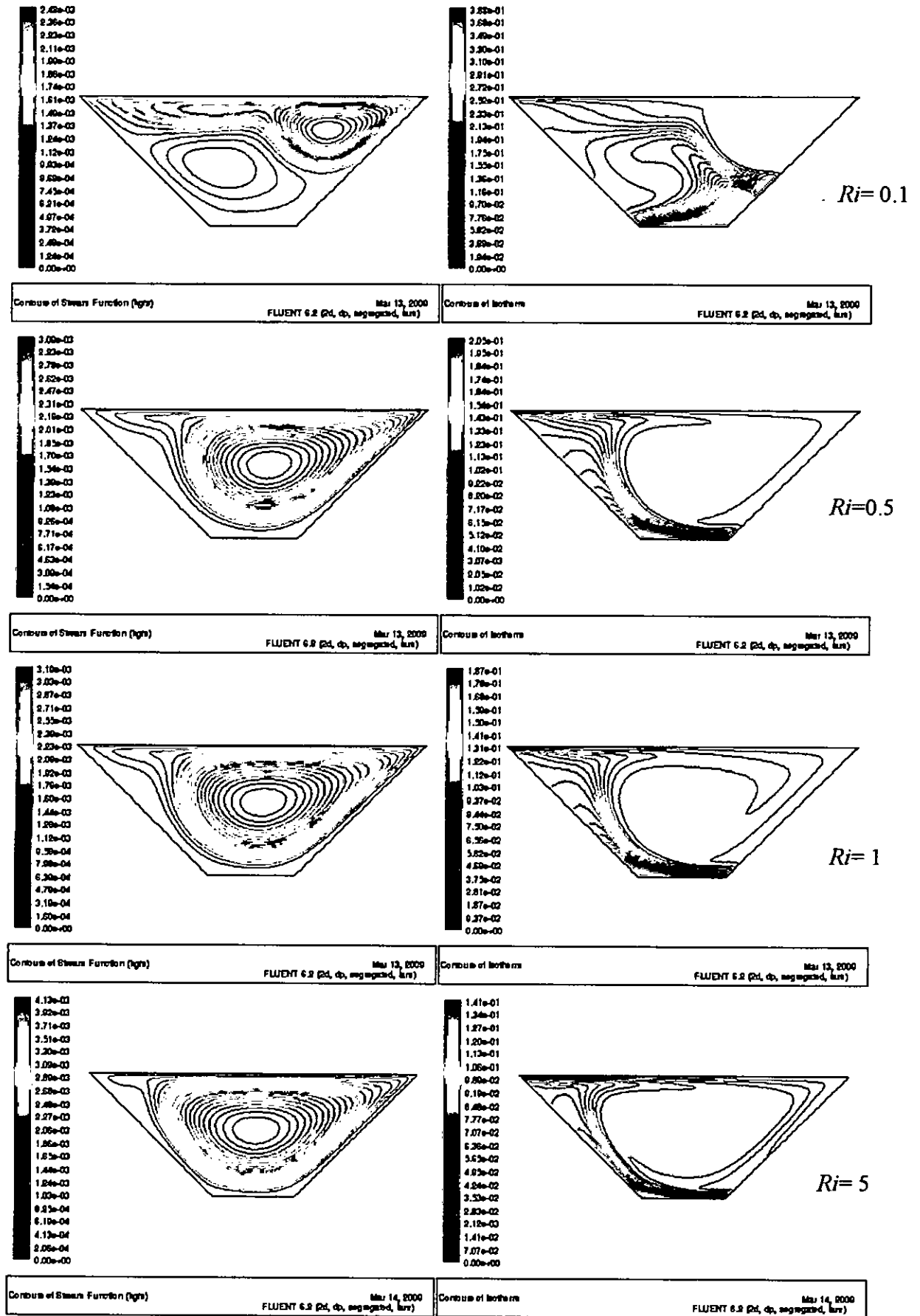
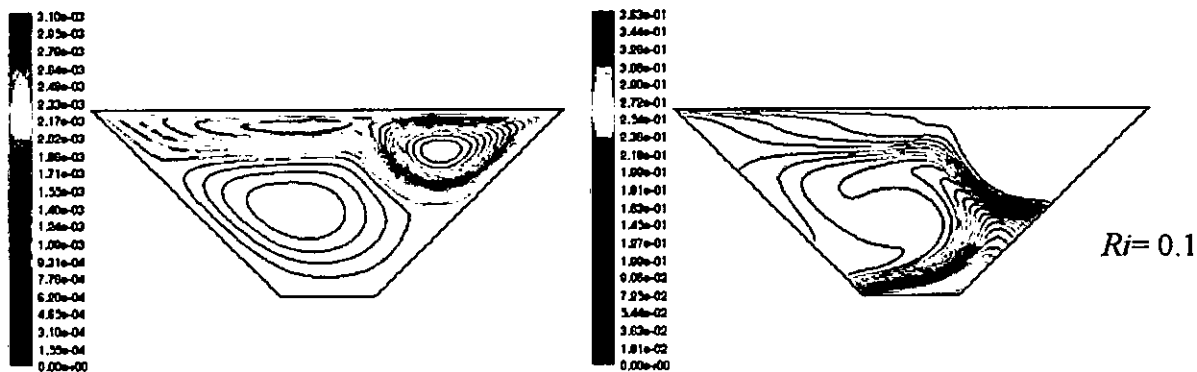
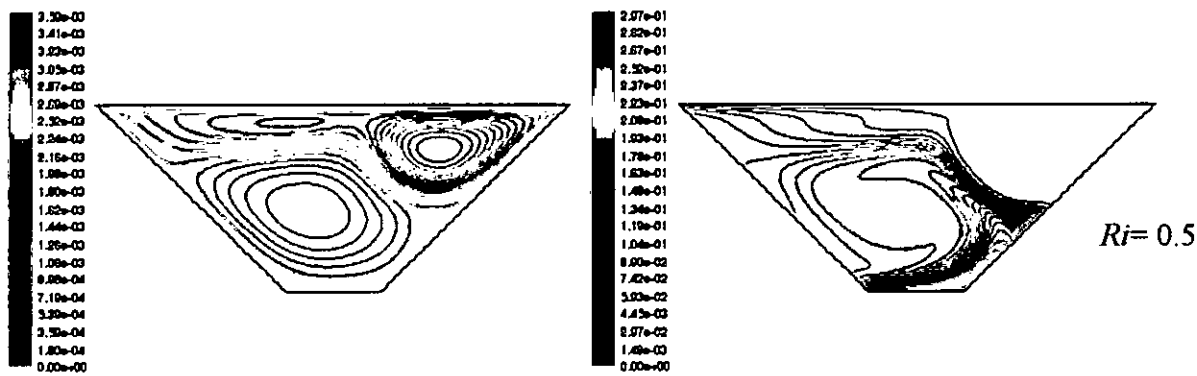


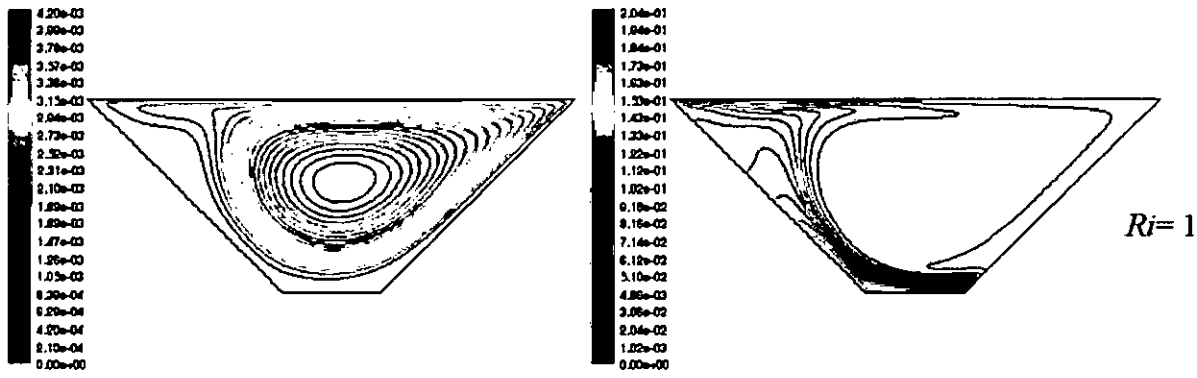
Figure 5.12: Contours of Streamlines and isotherms at  $Re=600$ ,  $A=1.5$  and  $\Phi=0^\circ$



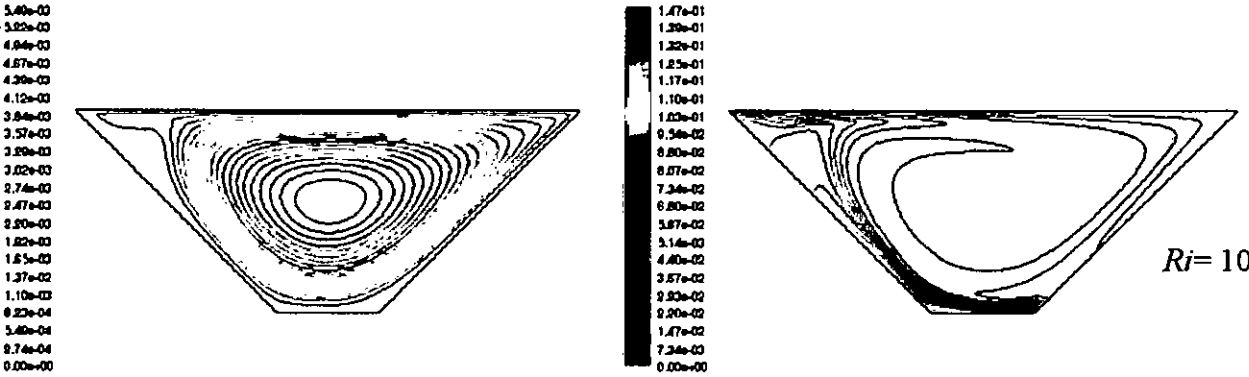
Contours of Stream Function (kg/s) Mar 14, 2000 FLUENT 6.2 (2d, dp, segregated, km)      Contours of Isotherms Mar 14, 2000 FLUENT 6.2 (2d, dp, segregated, km)



Contours of Stream Function (kg/s) Mar 14, 2000 FLUENT 6.2 (2d, dp, segregated, km)      Contours of Isotherms Mar 14, 2000 FLUENT 6.2 (2d, dp, segregated, km)



Contours of Stream Function (kg/s) Mar 14, 2000 FLUENT 6.2 (2d, dp, segregated, km)      Contours of Isotherms Mar 14, 2000 FLUENT 6.2 (2d, dp, segregated, km)



Contours of Stream Function (kg/s) Mar 14, 2000 FLUENT 6.2 (2d, dp, segregated, km)      Contours of Isotherms Mar 14, 2000 FLUENT 6.2 (2d, dp, segregated, km)

Figure 5.13: Contours of Streamlines and isotherms at  $Re=600$ ,  $A=2.0$  and  $\Phi=0^\circ$

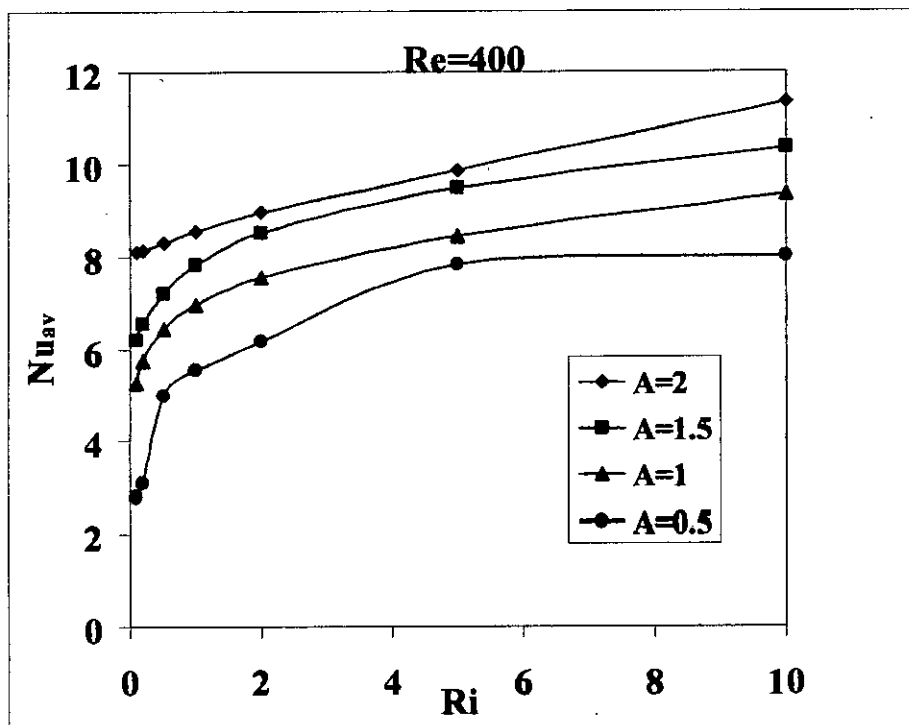


Figure 5.14: Variation of  $Nu_{av}$  with  $Ri$  at  $Re=400$  and  $\Phi=0^\circ$

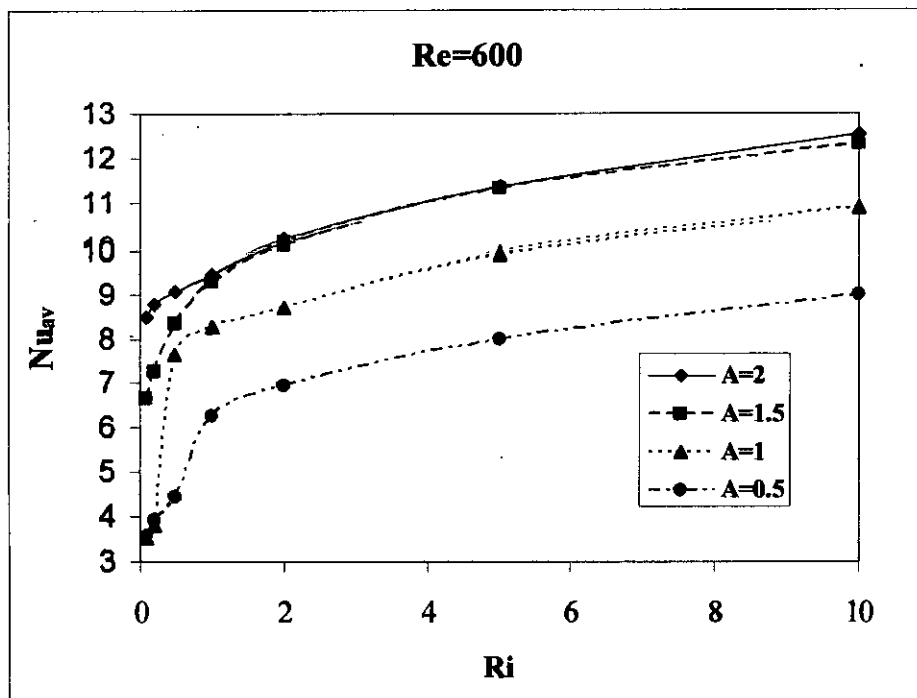


Figure 5.15: Variation of  $Nu_{av}$  with  $Ri$  at  $Re=600$  and  $\Phi=0^\circ$

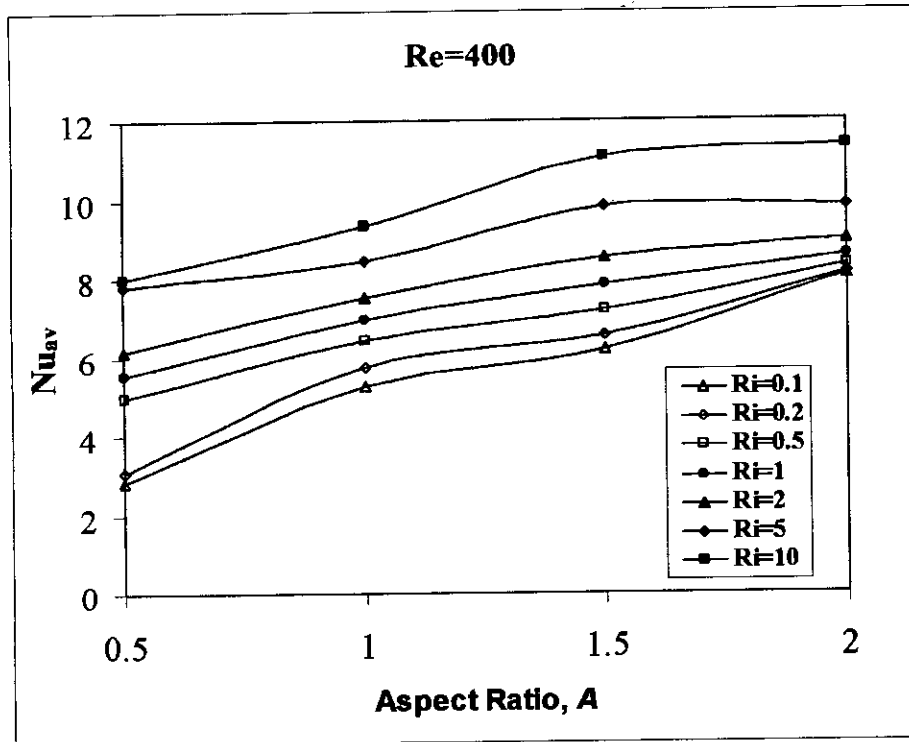


Figure 5.16: Variation of  $Nu_{av}$  with A at  $Re=400$  and  $\Phi=0^\circ$

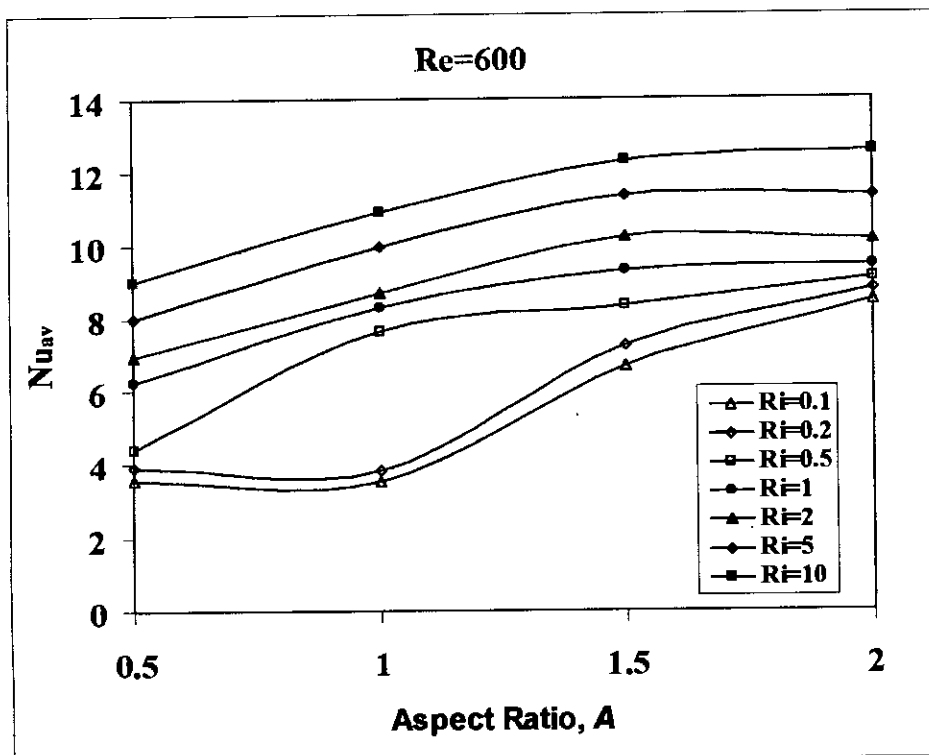


Figure 5.17: Variation of  $Nu_{av}$  with A at  $Re=600$  and  $\Phi=0^\circ$



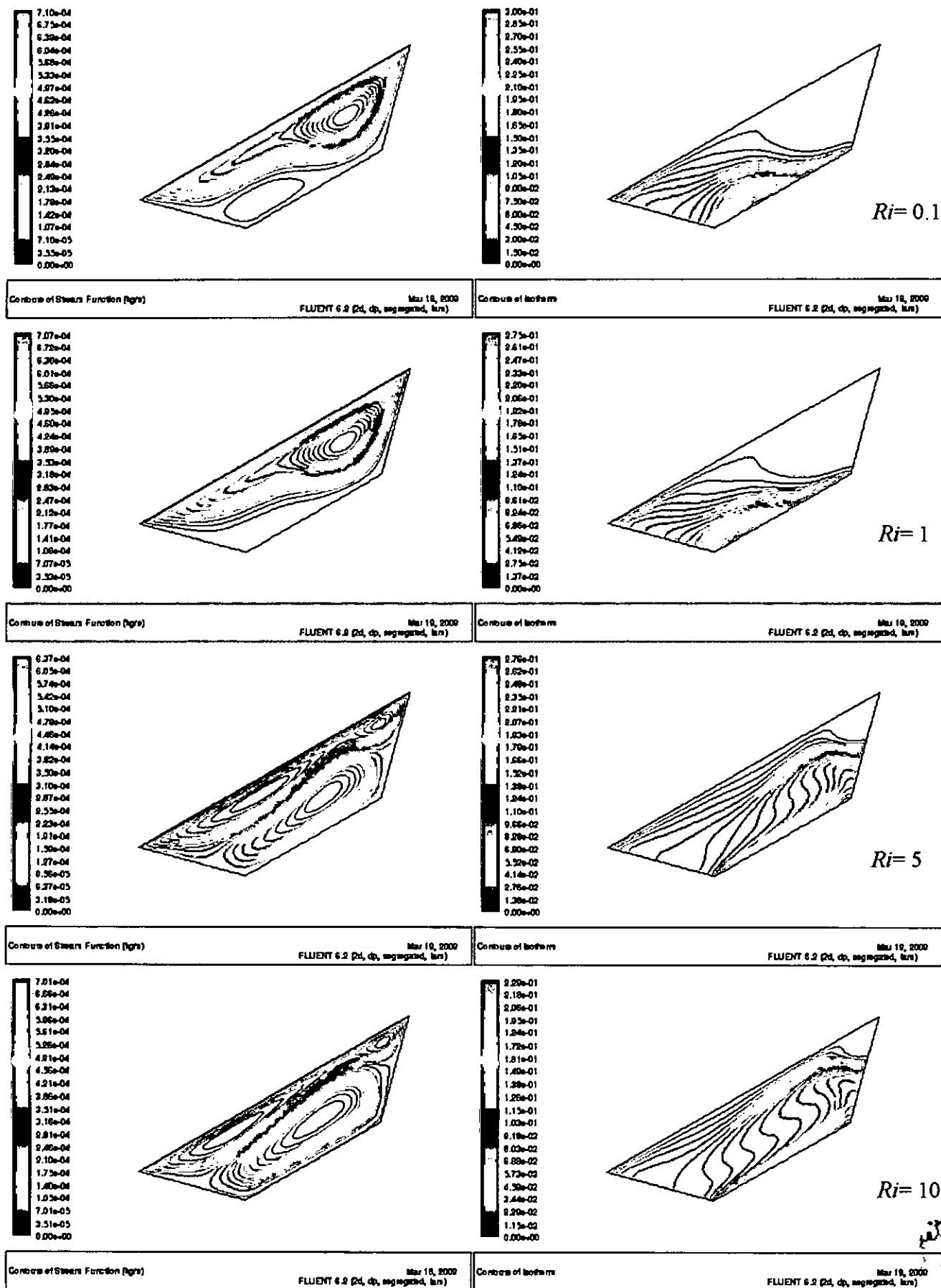


Figure 5.18: Contours of Streamlines and isotherms at  $Re=400$ ,  $A=0.5$  and  $\Phi=30^\circ$ , Opposing Flow

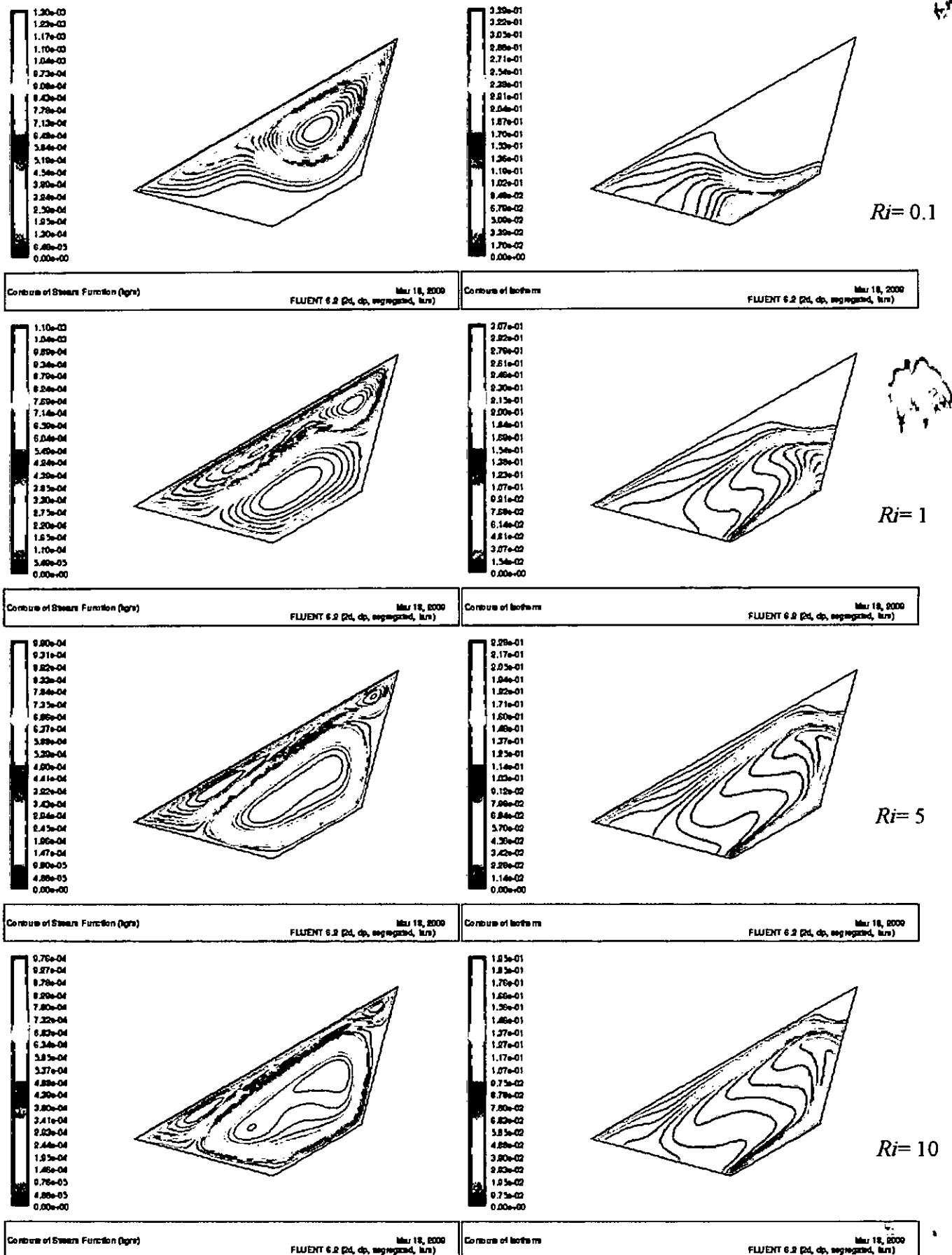
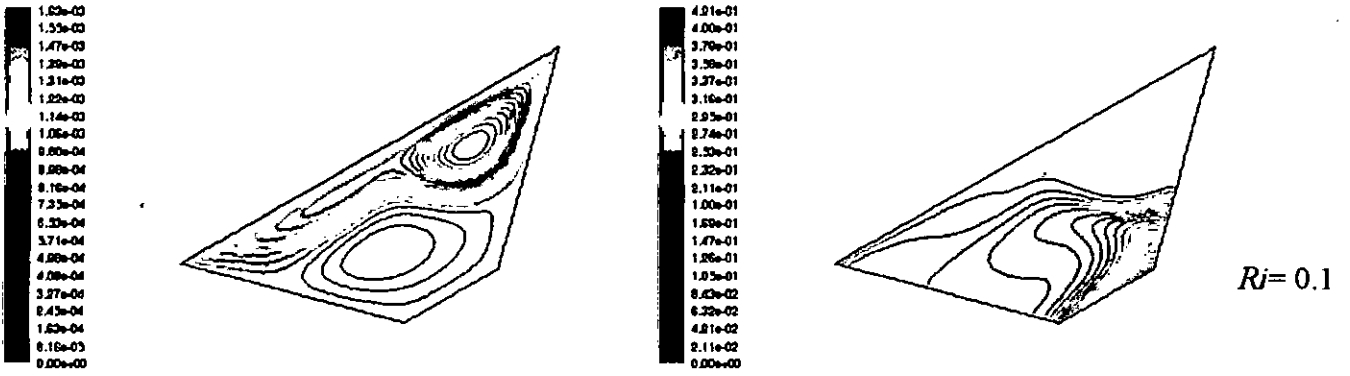
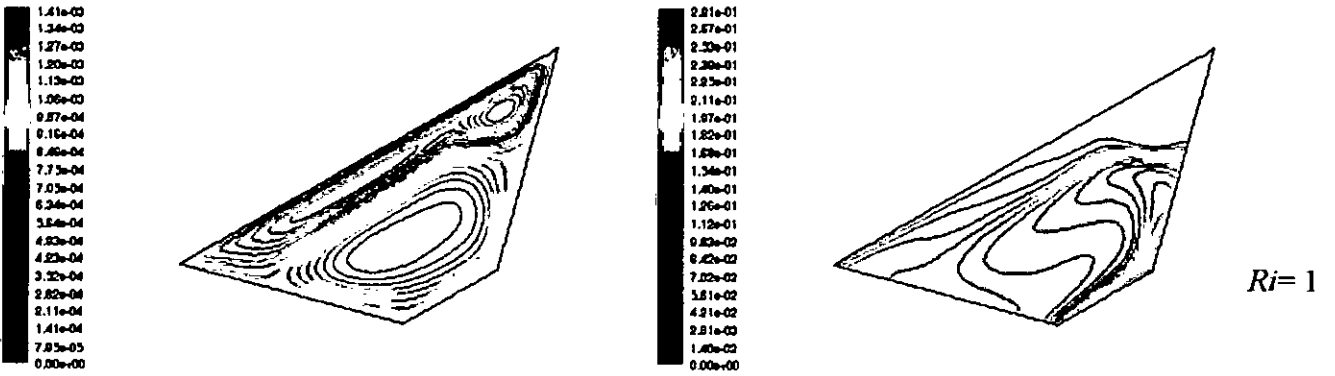


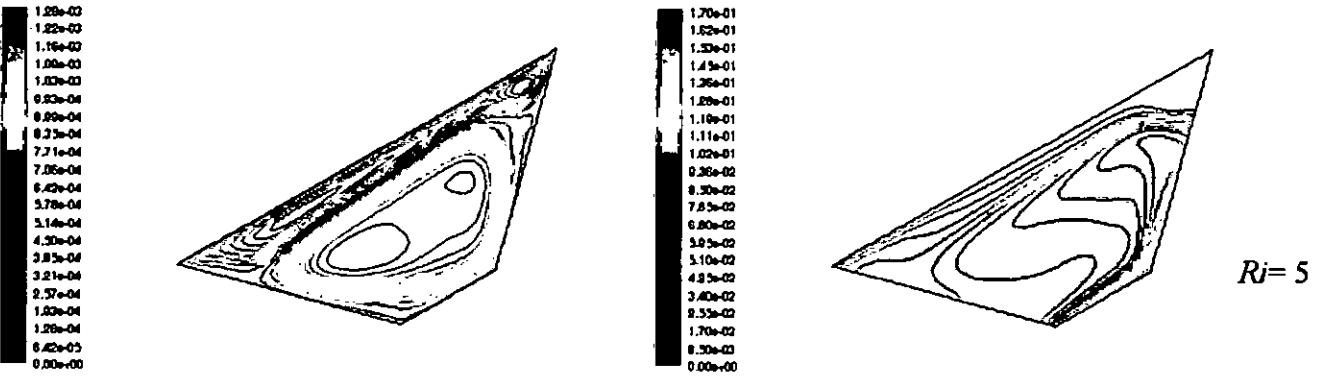
Figure 5.19: Contours of Streamlines and isotherms at  $Re=400$ ,  $A=1$  and  $\Phi=30^\circ$ , Opposing Flow



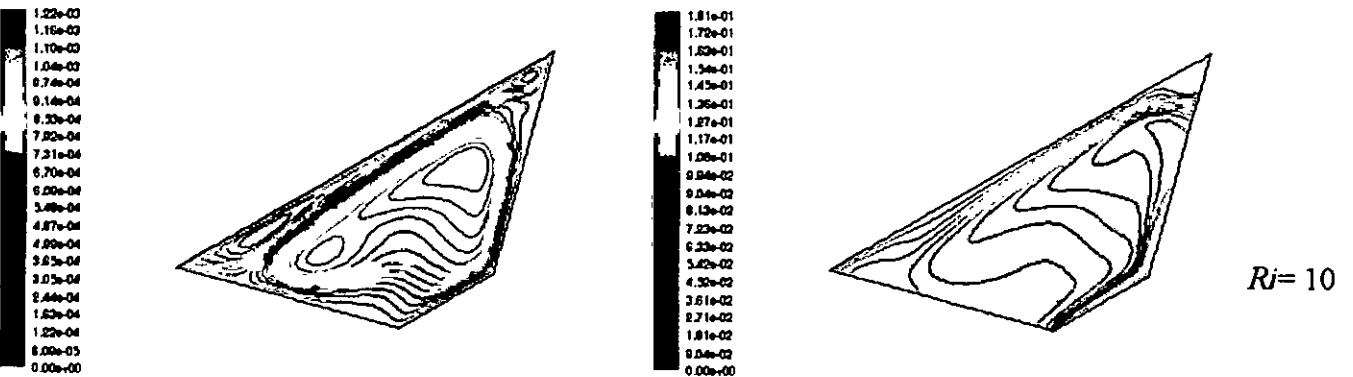
Contours of Stream Function (kg/s) Mar 18, 2000 FLUENT 6.2 (2d, dp, segregated, km)      Contours of Isotherms Mar 18, 2000 FLUENT 6.2 (2d, dp, segregated, km)



Contours of Stream Function (kg/s) Mar 18, 2000 FLUENT 6.2 (2d, dp, segregated, km)      Contours of Isotherms Mar 18, 2000 FLUENT 6.2 (2d, dp, segregated, km)

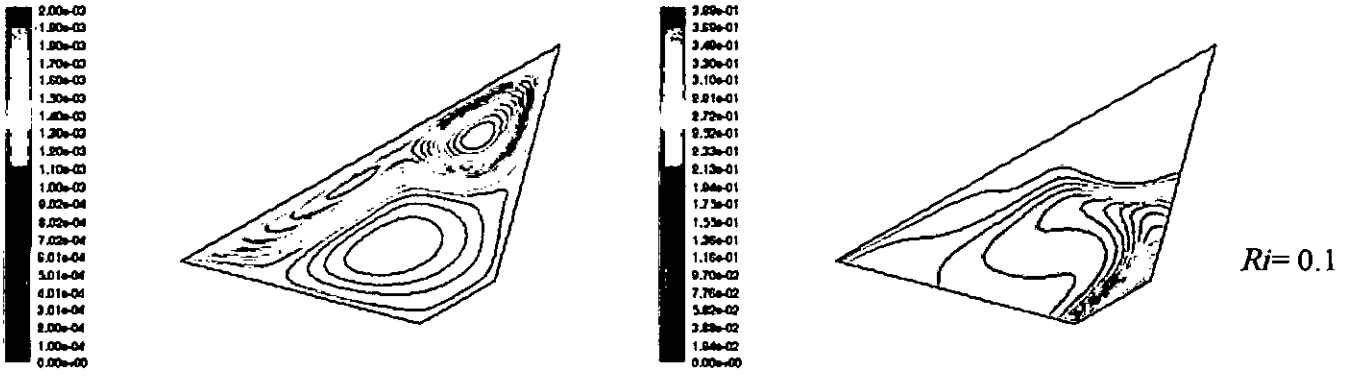


Contours of Stream Function (kg/s) Mar 18, 2000 FLUENT 6.2 (2d, dp, segregated, km)      Contours of Isotherms Mar 18, 2000 FLUENT 6.2 (2d, dp, segregated, km)

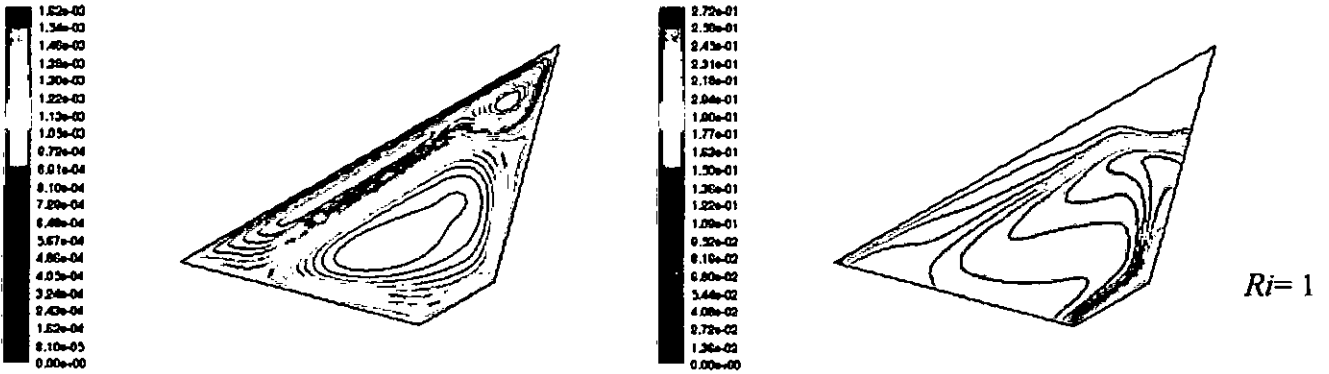


Contours of Stream Function (kg/s) Mar 18, 2000 FLUENT 6.2 (2d, dp, segregated, km)      Contours of Isotherms Mar 18, 2000 FLUENT 6.2 (2d, dp, segregated, km)

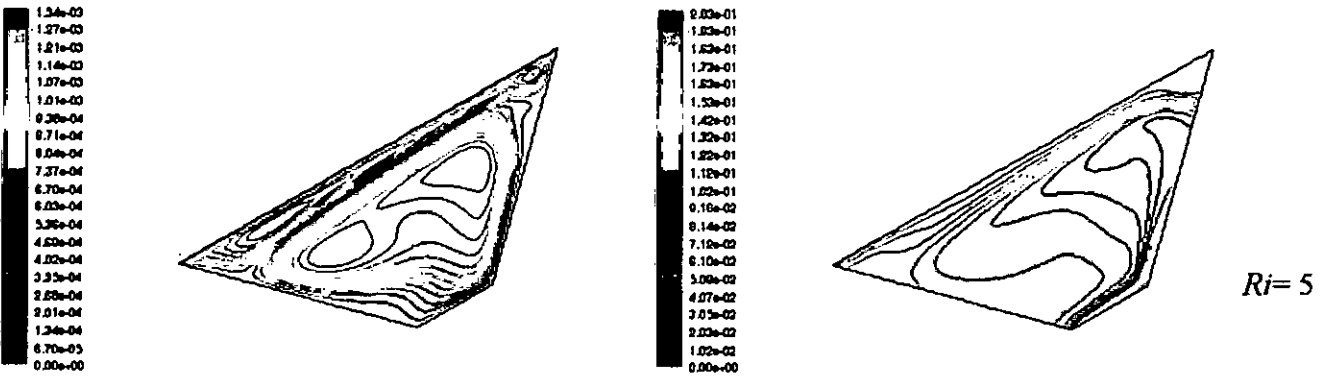
Figure 5.20: Contours of Streamlines and isotherms at  $Re=400$ ,  $A=1.5$  and  $\Phi=30^\circ$ , Opposing Flow



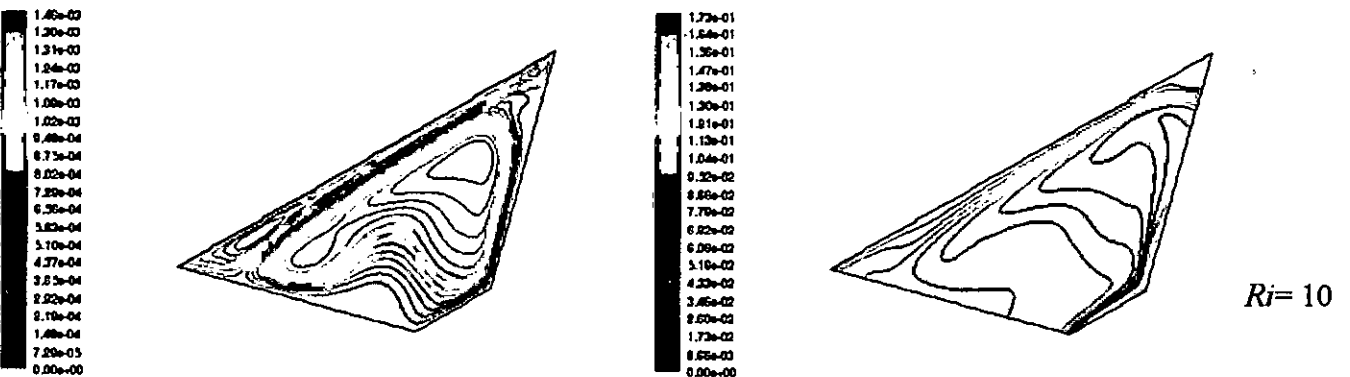
Contours of Stream Function (left) Contours of Isotherms  
Mar 10, 2000 FLUENT 6.2 (2d, dp, segregated, km) Mar 10, 2000 FLUENT 6.2 (2d, dp, segregated, km)



Contours of Stream Function (left) Contours of Isotherms  
Mar 10, 2000 FLUENT 6.2 (2d, dp, segregated, km) Mar 10, 2000 FLUENT 6.2 (2d, dp, segregated, km)



Contours of Stream Function (left) Contours of Isotherms  
Mar 10, 2000 FLUENT 6.2 (2d, dp, segregated, km) Mar 10, 2000 FLUENT 6.2 (2d, dp, segregated, km)



Contours of Stream Function (left) Contours of Isotherms  
Mar 10, 2000 FLUENT 6.2 (2d, dp, segregated, km) Mar 10, 2000 FLUENT 6.2 (2d, dp, segregated, km)

Figure 5.21: Contours of Streamlines and isotherms at  $Re=400$ ,  $A=2$  and  $\Phi=30^\circ$ , Opposing Flow

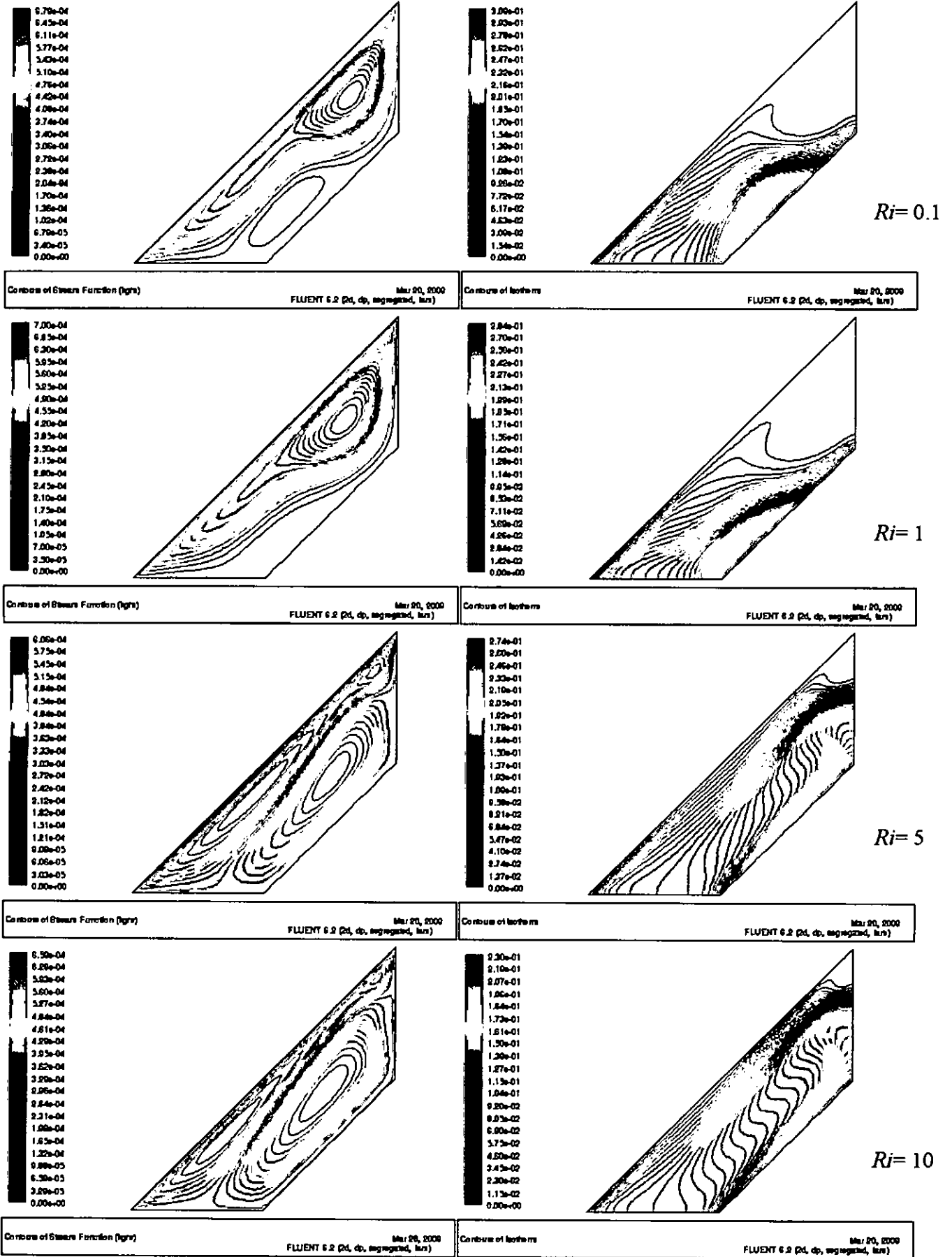
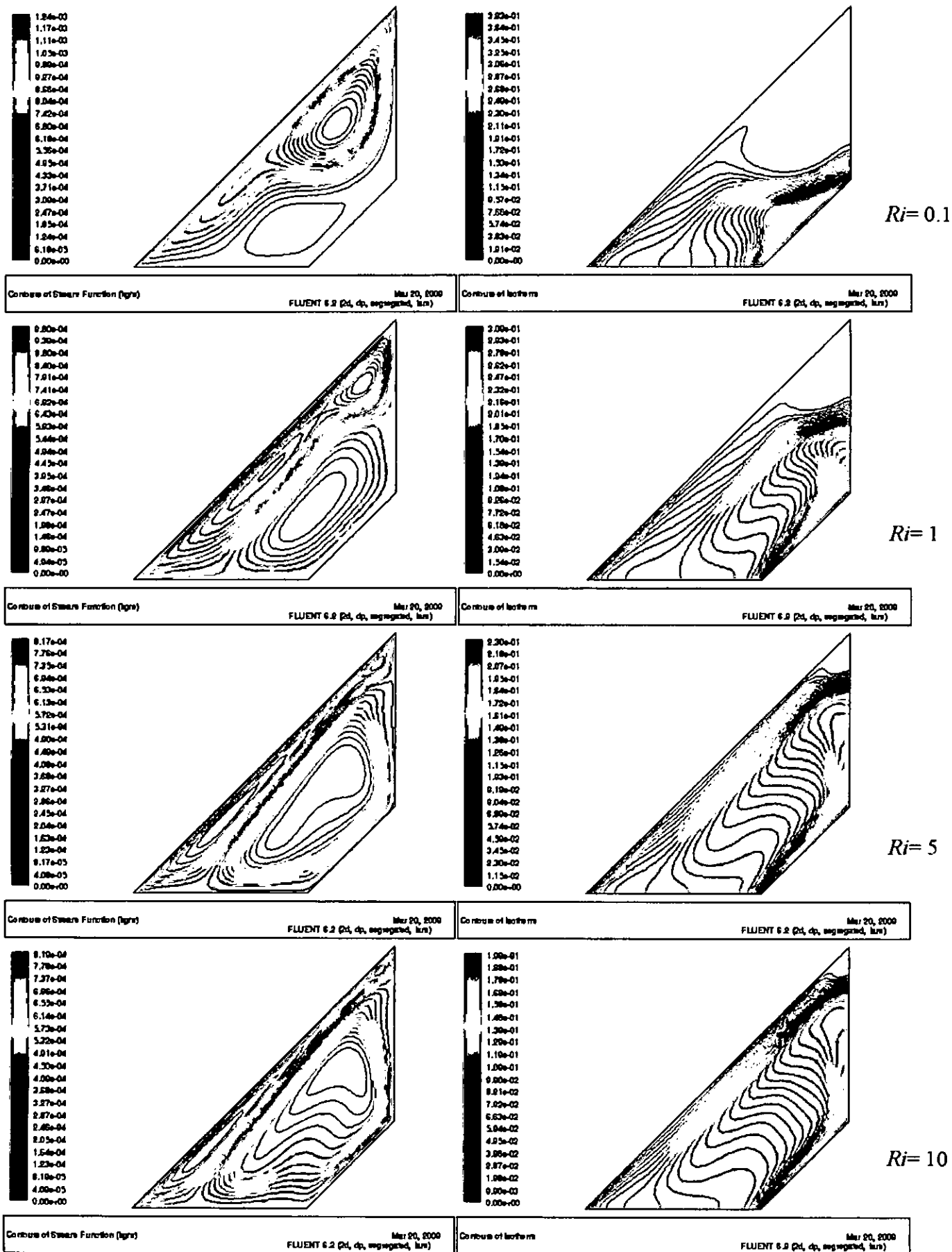


Figure 5.22: Contours of Streamlines and isotherms at  $Re=400$ ,  $A=0.5$  and  $\Phi=45^\circ$ , Opposing Flow



Ri=0.1

Ri=1

Ri=5

Ri=10

Figure 5.23: Contours of Streamlines and isotherms at Re=400, A=1 and  $\Phi=45^\circ$ , Opposing Flow

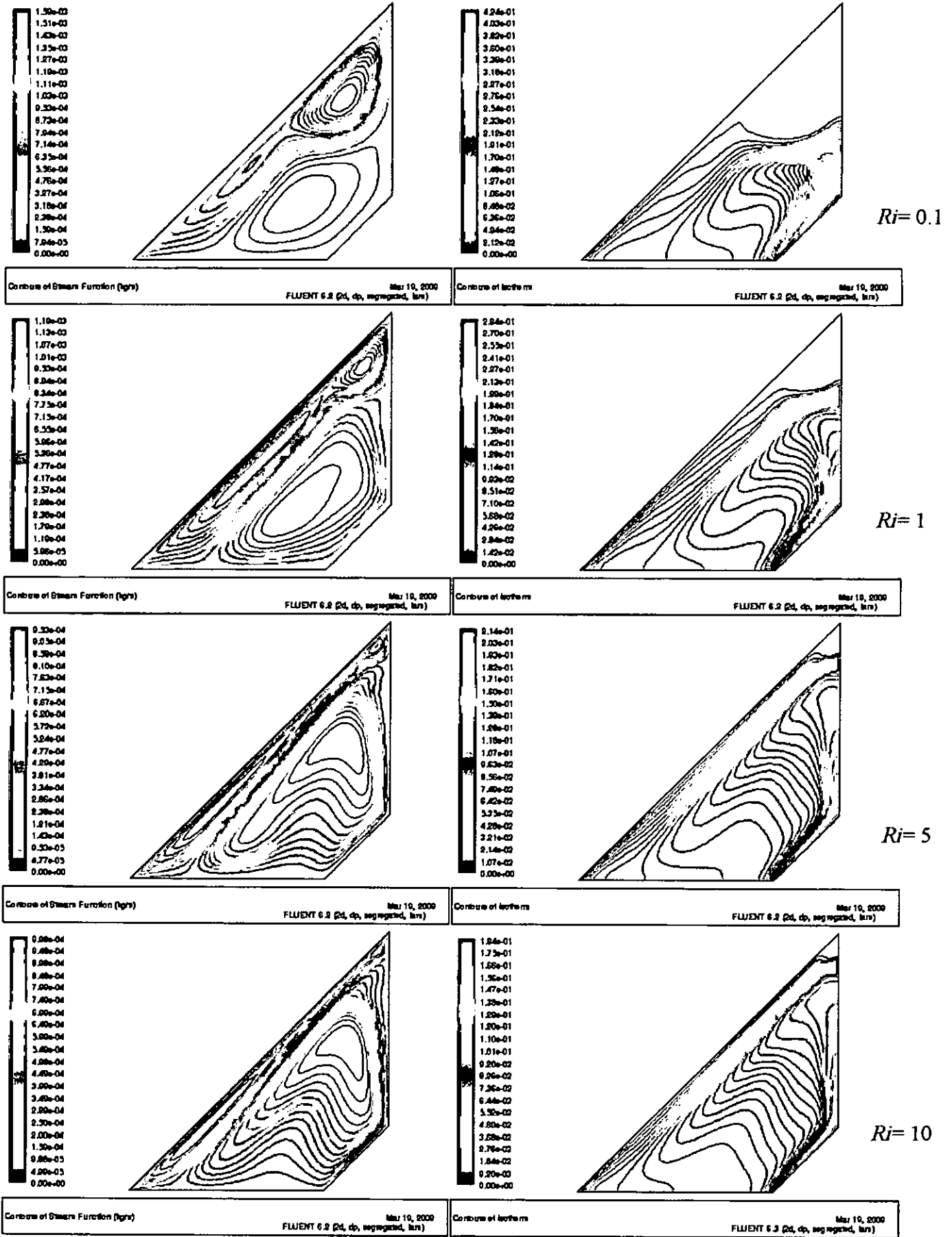
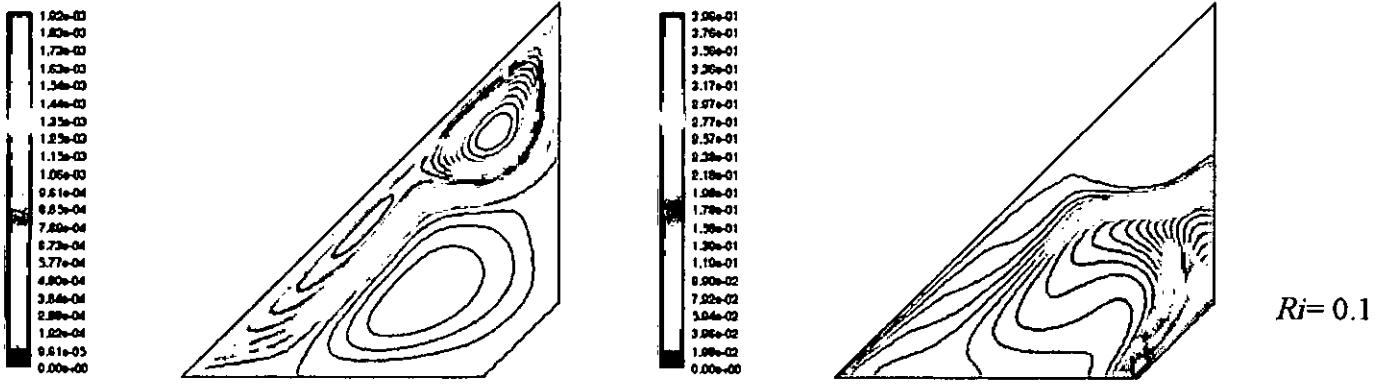
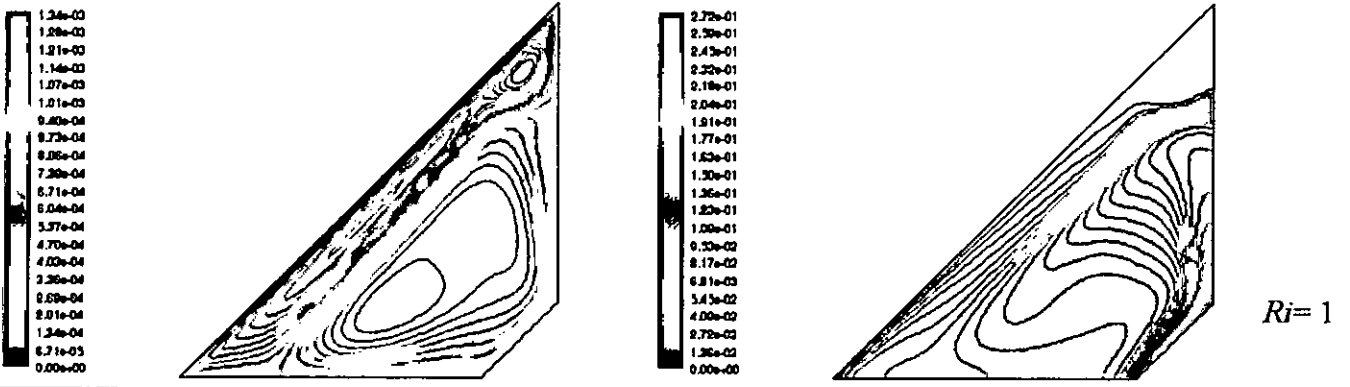


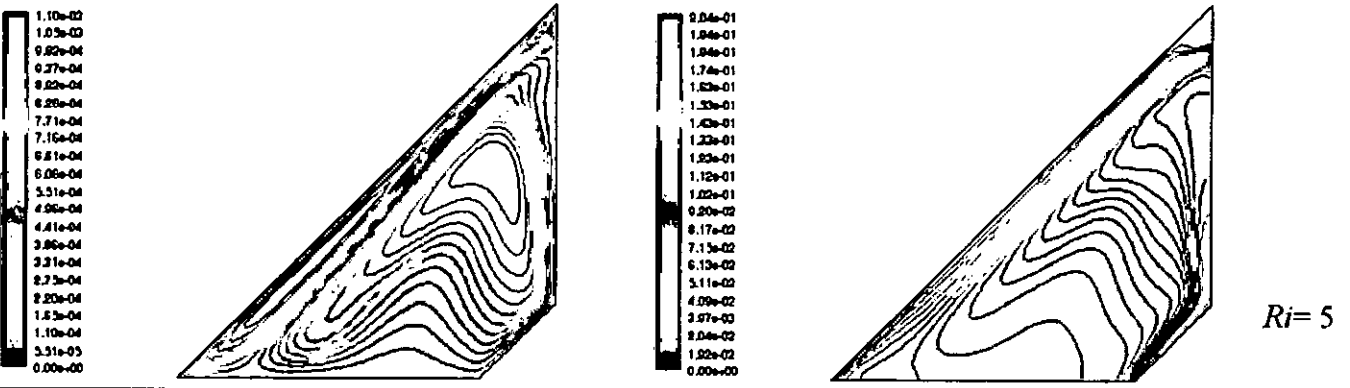
Figure 5.24: Contours of Streamlines and isotherms at Re=400, A=1.5 and  $\Phi=45^\circ$ , Opposing Flow



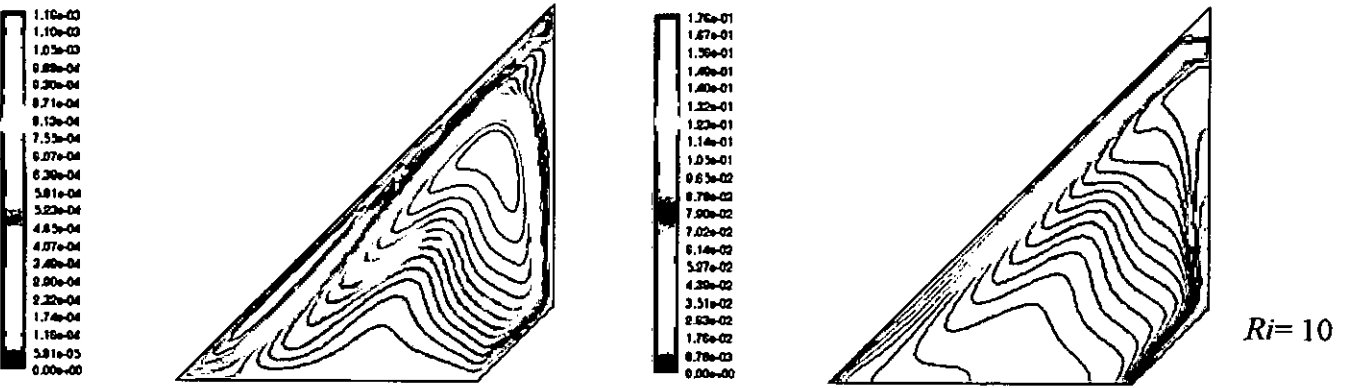
Contours of Stream Function (Psi) Mar 10, 2000 FLUENT 6.2 (2d, dp, segregated, lsr)      Contours of Isotherms Mar 10, 2000 FLUENT 6.2 (2d, dp, segregated, lsr)



Contours of Stream Function (Psi) Mar 10, 2000 FLUENT 6.2 (2d, dp, segregated, lsr)      Contours of Isotherms Mar 10, 2000 FLUENT 6.2 (2d, dp, segregated, lsr)



Contours of Stream Function (Psi) Mar 10, 2000 FLUENT 6.2 (2d, dp, segregated, lsr)      Contours of Isotherms Mar 10, 2000 FLUENT 6.2 (2d, dp, segregated, lsr)



Contours of Stream Function (Psi) Mar 10, 2000 FLUENT 6.2 (2d, dp, segregated, lsr)      Contours of Isotherms Mar 10, 2000 FLUENT 6.2 (2d, dp, segregated, lsr)

Figure 5.25: Contours of Streamlines and isotherms at  $Re=400$ ,  $A=2$  and  $\Phi=45^\circ$ , Opposing Flow



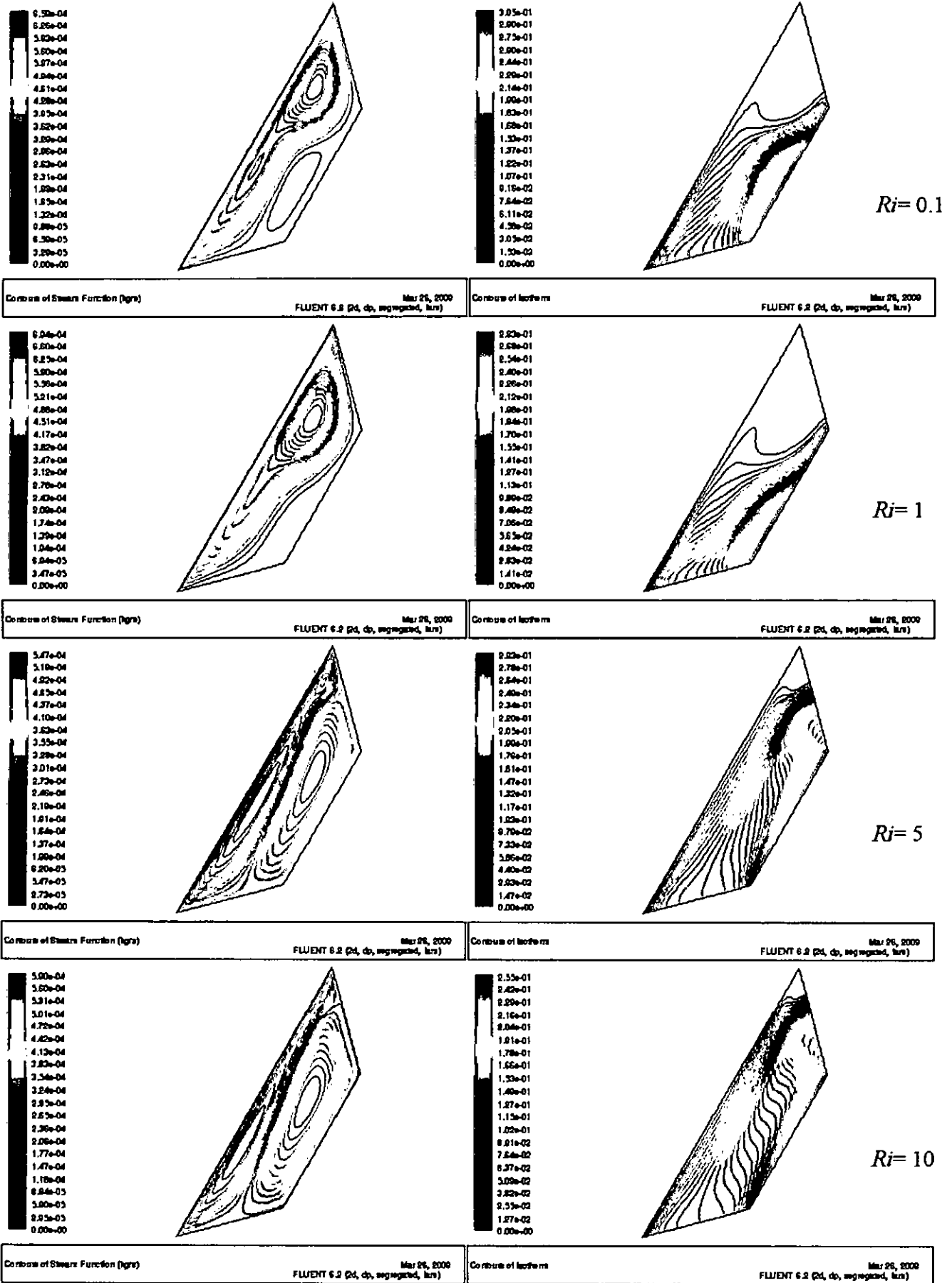


Figure 5.26: Contours of Streamlines and isotherms at  $Re=400$ ,  $A=0.5$  and  $\Phi=60^\circ$ , Opposing Flow

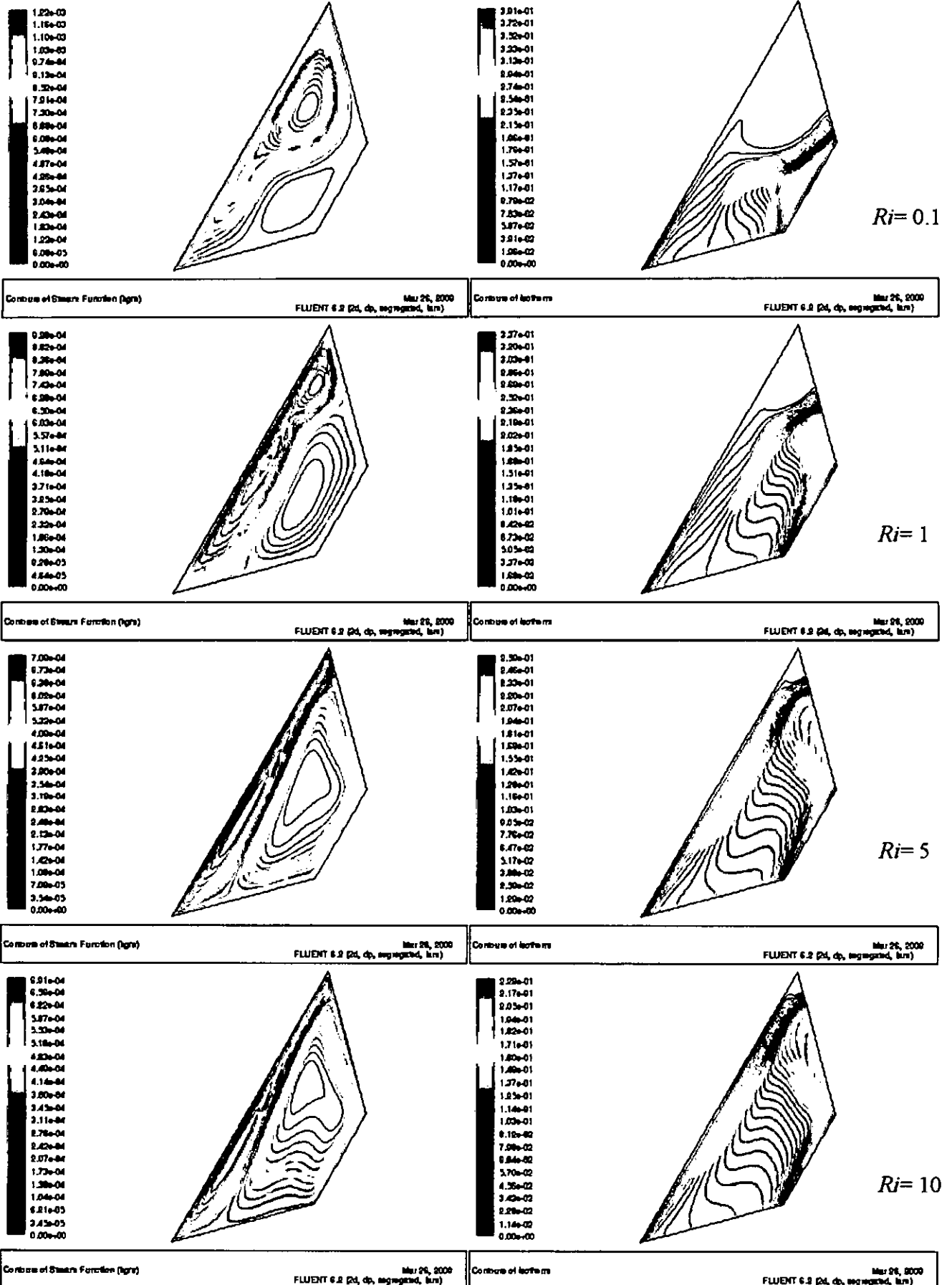


Figure 5.27: Contours of Streamlines and isotherms at  $Re=400$ ,  $A=1$  and  $\Phi=60^\circ$ , Opposing Flow

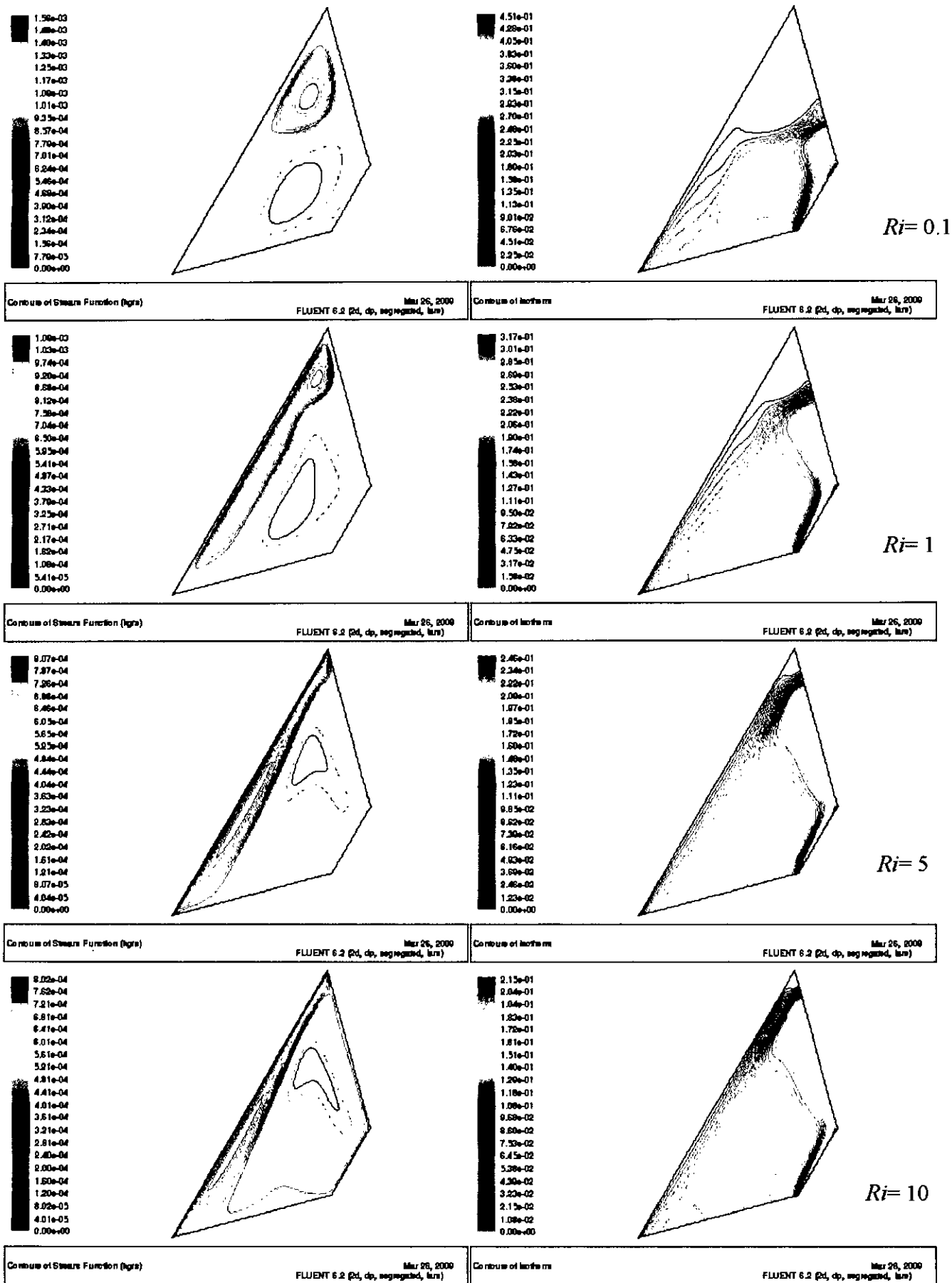
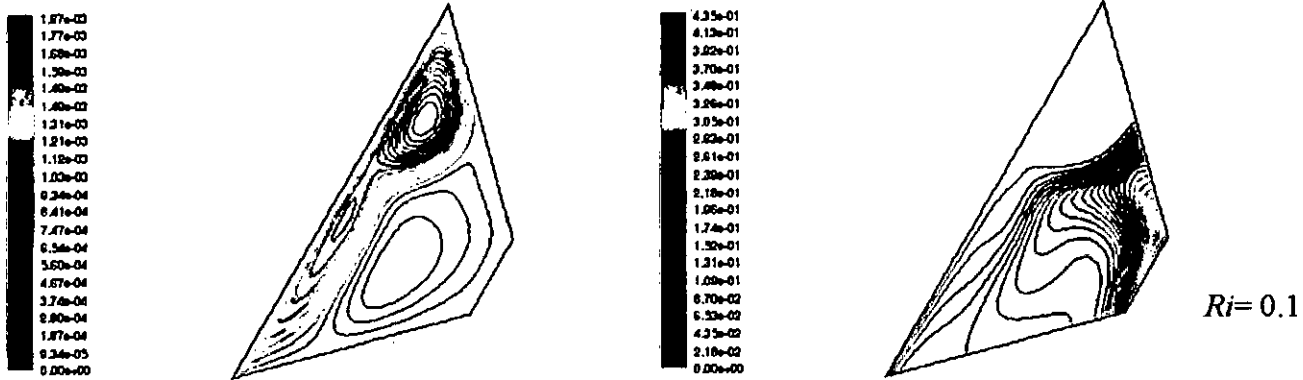
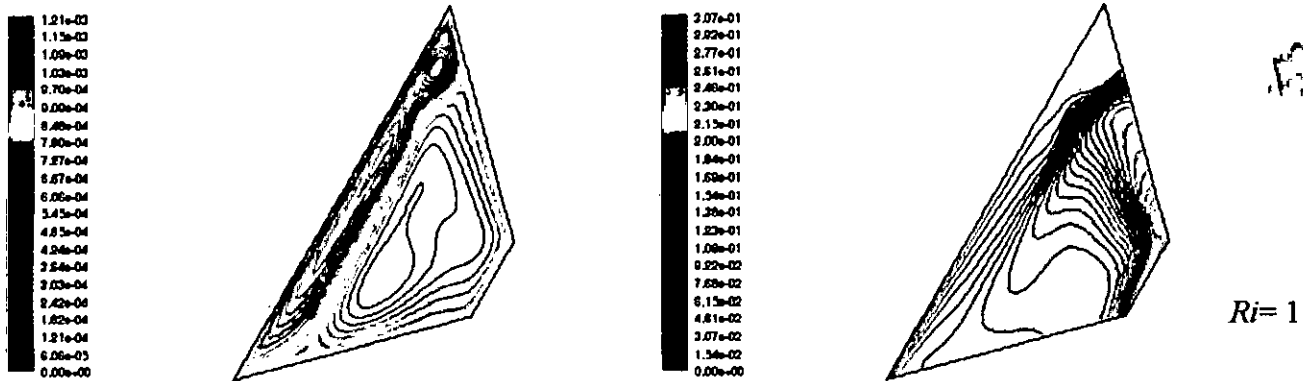


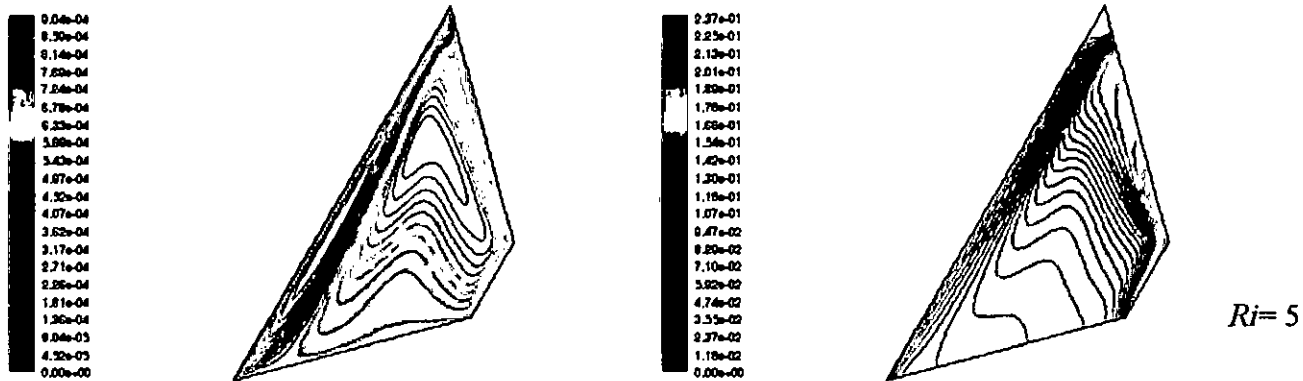
Figure 5.28: Contours of Streamlines and isotherms at  $Re=400$ ,  $A=1.5$  and  $\Phi=60^\circ$ , Opposing Flow



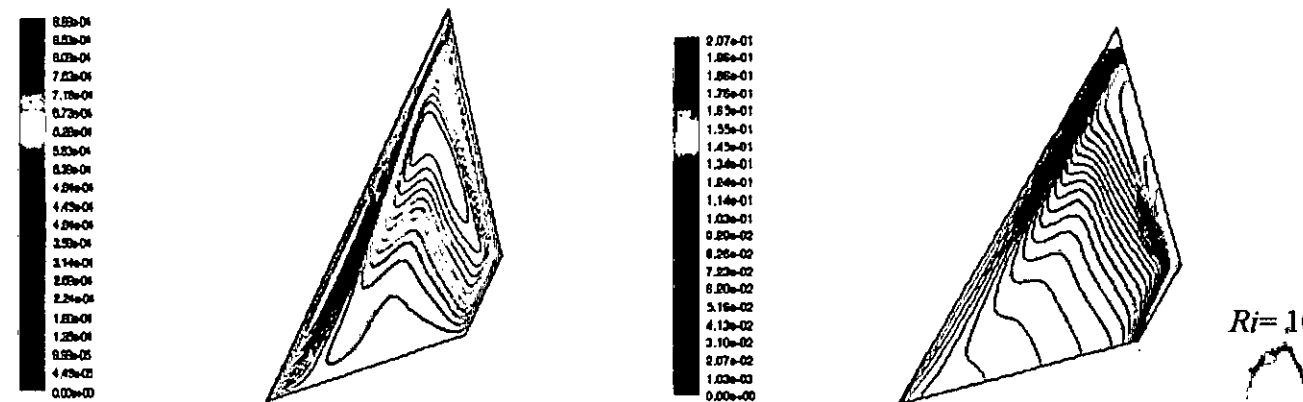
Contours of Stream Function (kg/s) Contours of Isotherms  
 Mar 06, 2000 Mar 06, 2000  
 FLUENT 6.2 (2d, dp, segregated, km) FLUENT 6.2 (2d, dp, segregated, km)



Contours of Stream Function (kg/s) Contours of Isotherms  
 Mar 06, 2000 Mar 06, 2000  
 FLUENT 6.2 (2d, dp, segregated, km) FLUENT 6.2 (2d, dp, segregated, km)

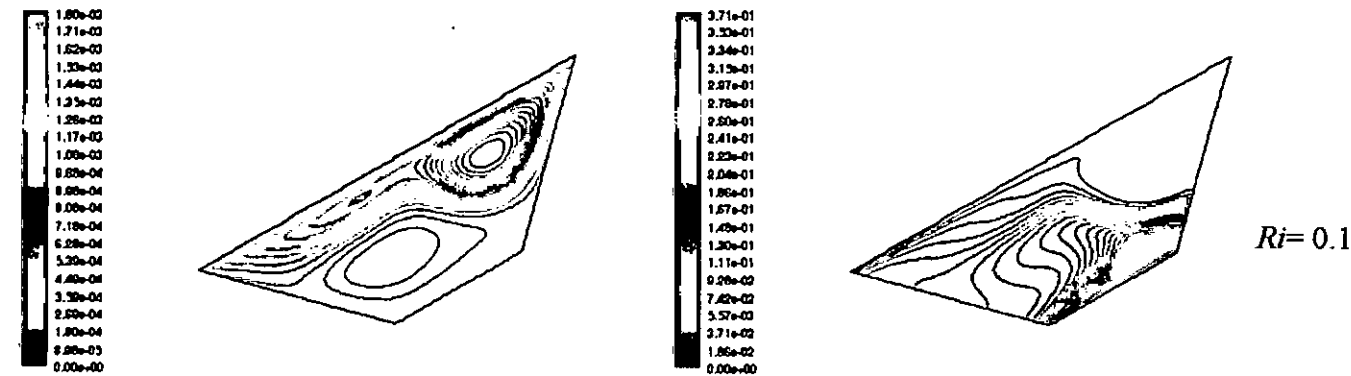


Contours of Stream Function (kg/s) Contours of Isotherms  
 Mar 06, 2000 Mar 06, 2000  
 FLUENT 6.2 (2d, dp, segregated, km) FLUENT 6.2 (2d, dp, segregated, km)

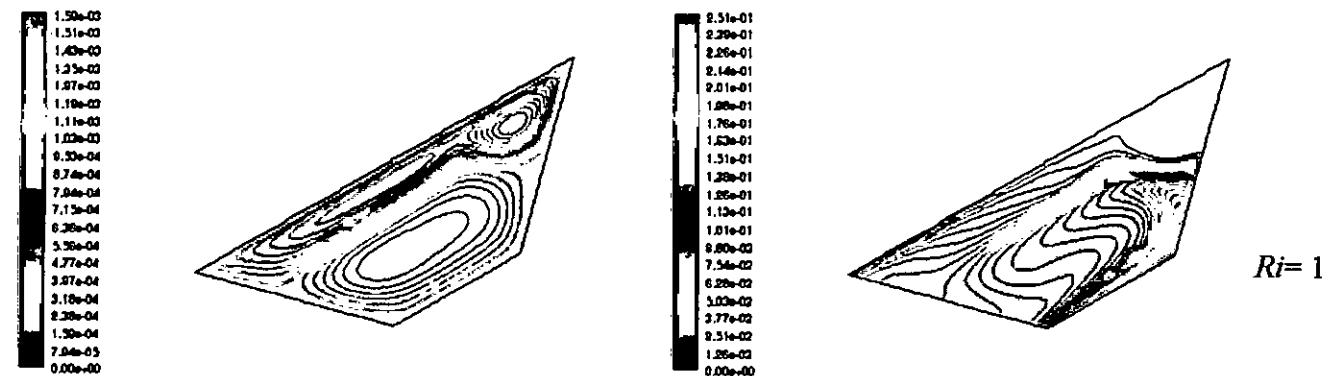


Contours of Stream Function (kg/s) Contours of Isotherms  
 Apr 02, 2000 Mar 06, 2000  
 FLUENT 6.2 (2d, dp, segregated, km) FLUENT 6.2 (2d, dp, segregated, km)

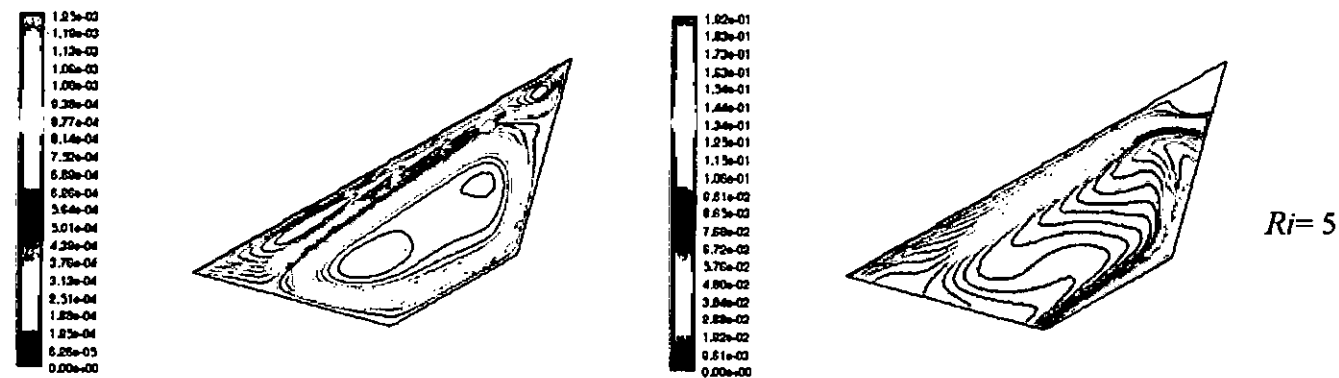
Figure 5.29: Contours of Streamlines and isotherms at  $Re=400$ ,  $A=2$  and  $\Phi=60^\circ$ , Opposing Flow



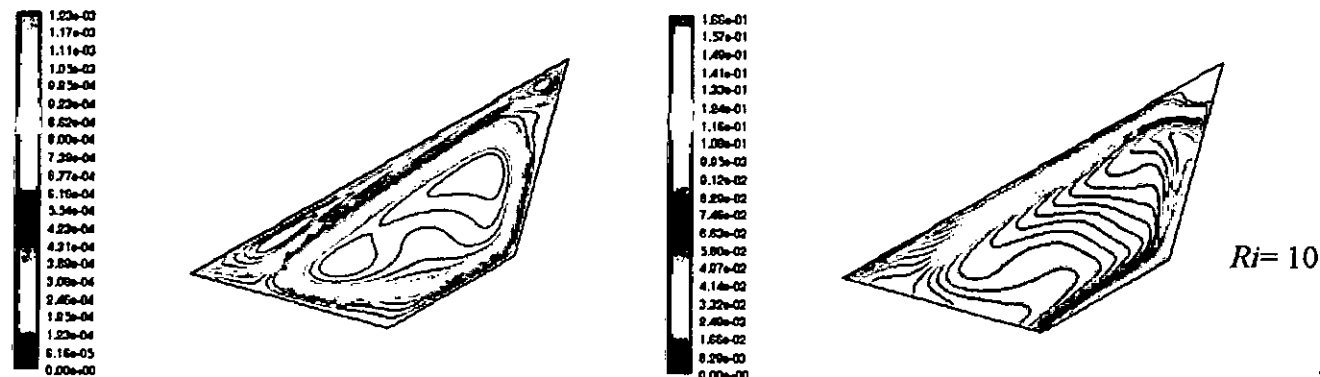
Contours of Stream Function (left) Mar 21, 2000 FLUENT 6.2 (2d, dp, segregated, lsm)      Contours of Isotherms Mar 21, 2000 FLUENT 6.2 (2d, dp, segregated, lsm)



Contours of Stream Function (left) Mar 21, 2000 FLUENT 6.2 (2d, dp, segregated, lsm)      Contours of Isotherms Mar 21, 2000 FLUENT 6.2 (2d, dp, segregated, lsm)



Contours of Stream Function (left) Mar 21, 2000 FLUENT 6.2 (2d, dp, segregated, lsm)      Contours of Isotherms Mar 21, 2000 FLUENT 6.2 (2d, dp, segregated, lsm)



Contours of Stream Function (left) Mar 21, 2000 FLUENT 6.2 (2d, dp, segregated, lsm)      Contours of Isotherms Mar 21, 2000 FLUENT 6.2 (2d, dp, segregated, lsm)

Figure 5.30: Contours of Streamlines and isotherms at  $Re=600$ ,  $A=1$  and  $\Phi=30^\circ$ , Opposing Flow

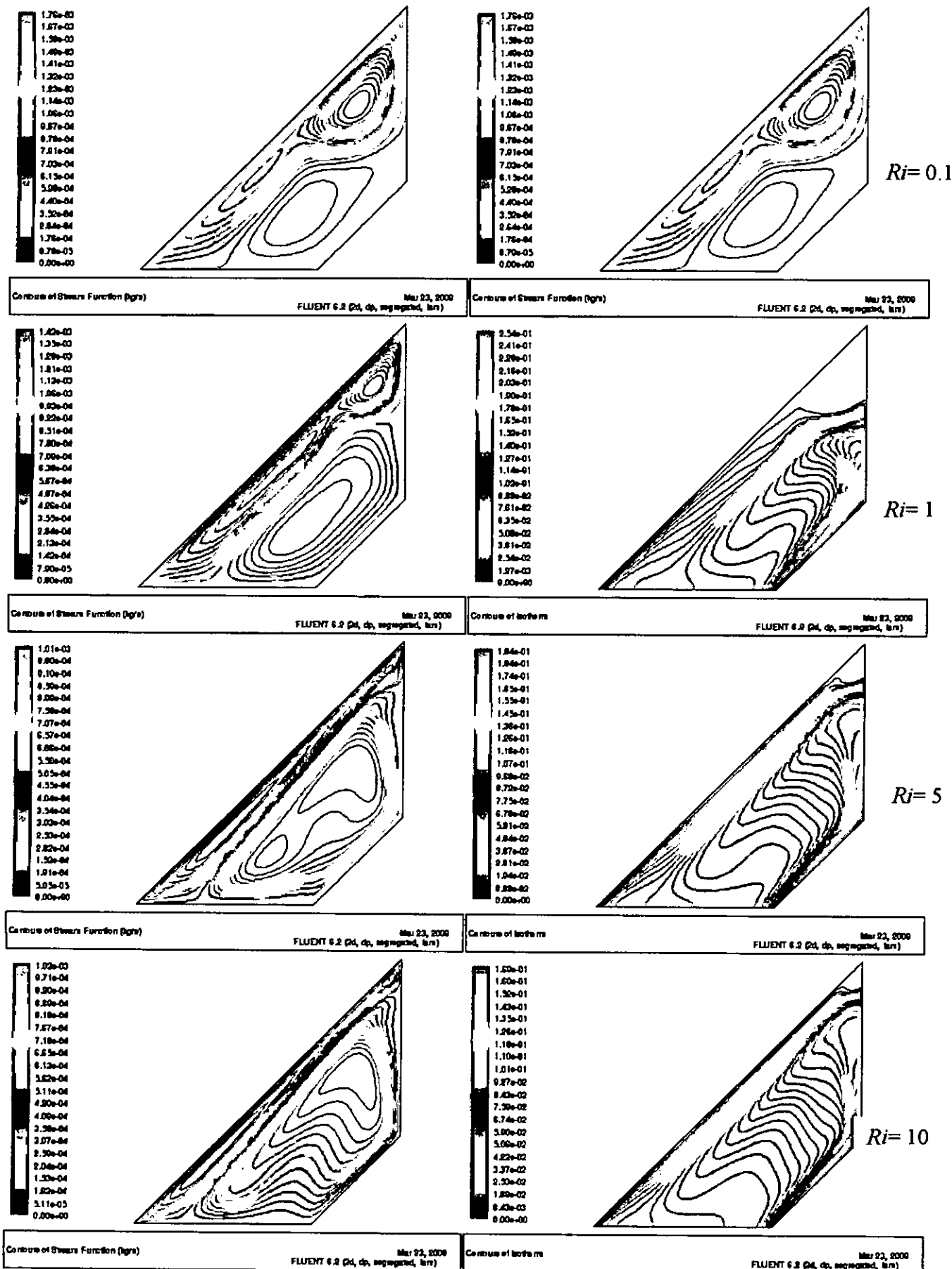


Figure 5.31: Contours of Streamlines and isotherms at  $Re=600$ ,  $A=1$  and  $\Phi=45^\circ$ , Opposing Flow

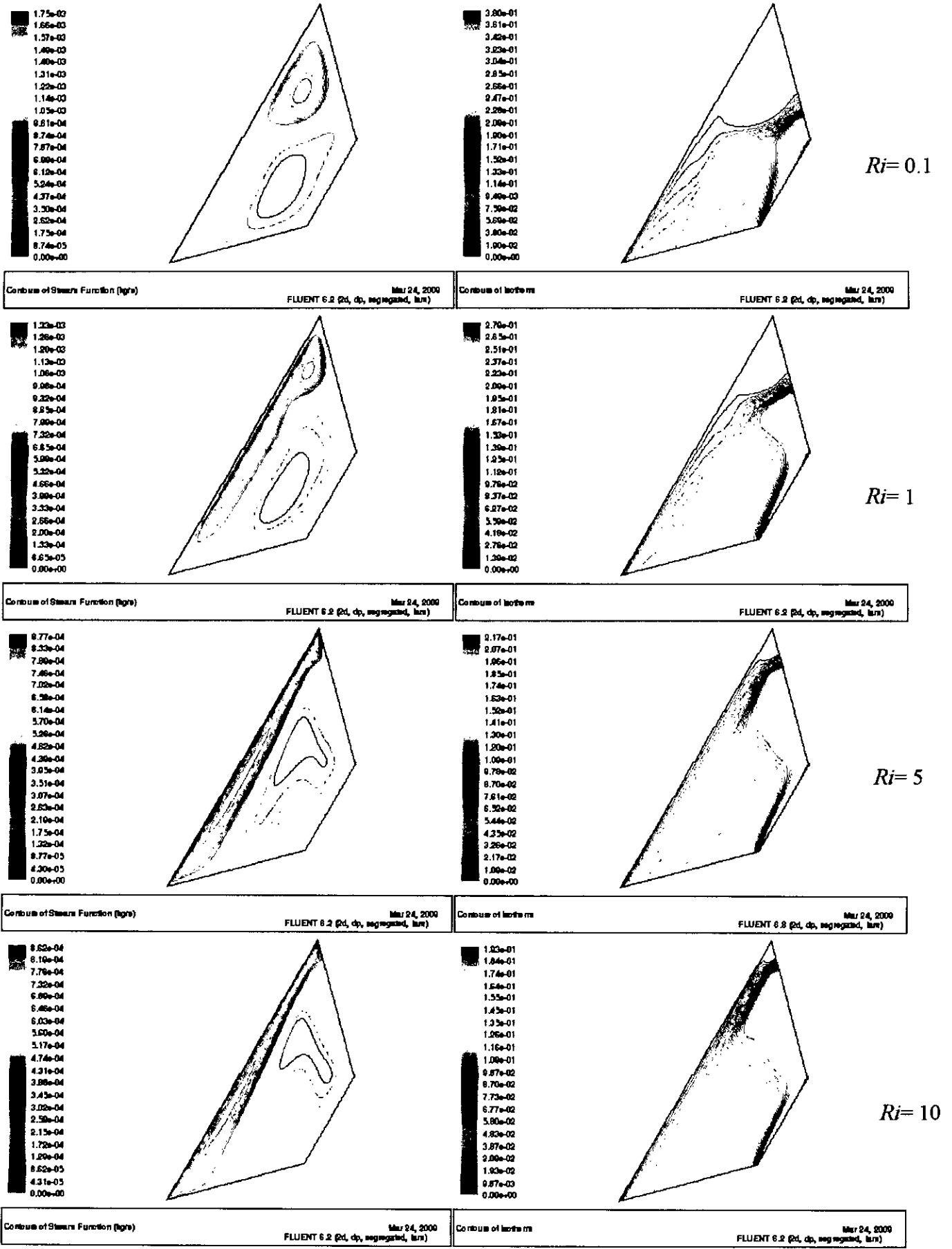


Figure 5.32: Contours of Streamlines and isotherms at Re=600, A=1 and  $\Phi=60^\circ$ , Opposing Flow

107288

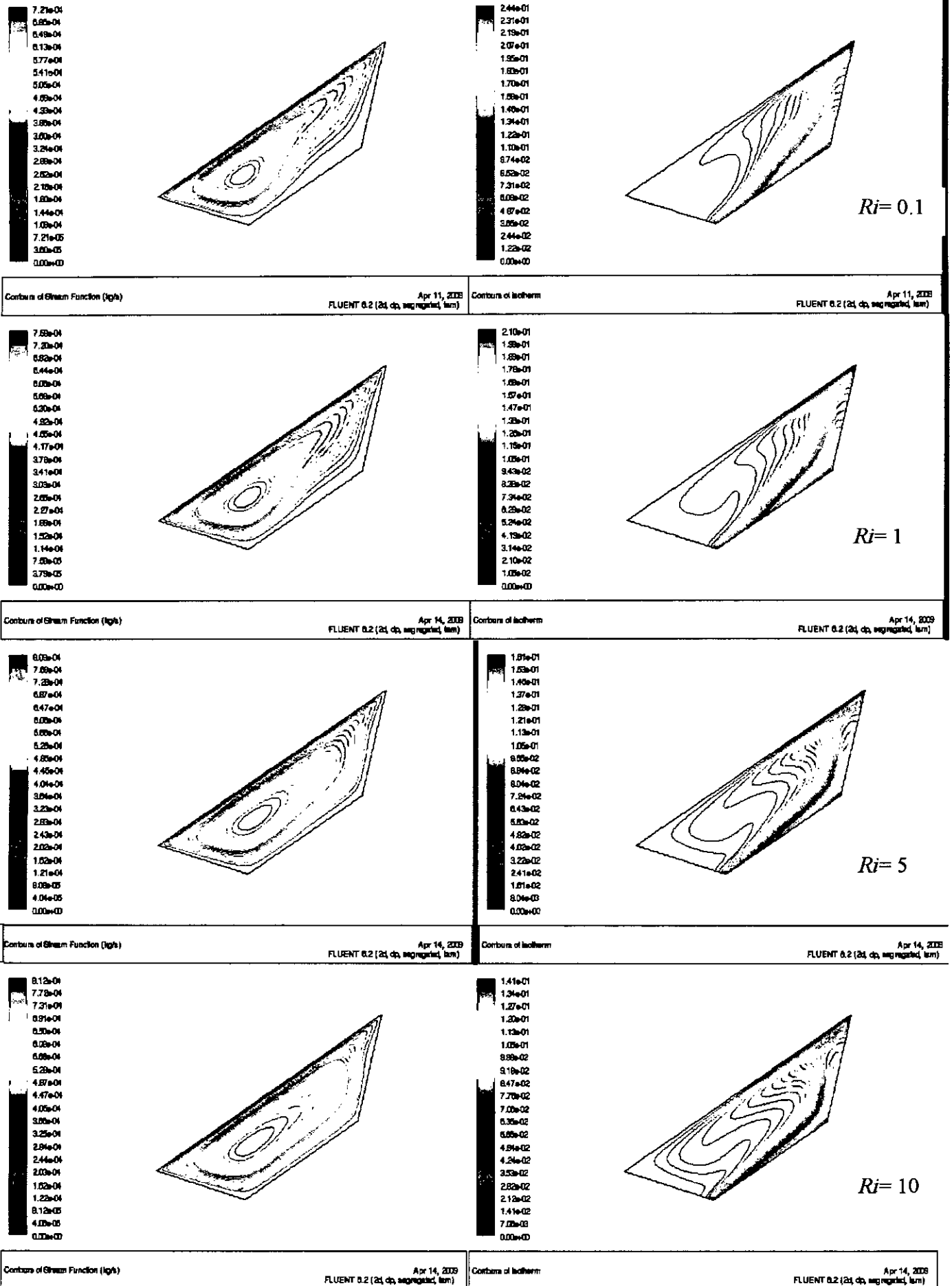


Figure 5.33: Contours of Streamlines and isotherms at  $Re=400$ ,  $A=0.5$  and  $\Phi=30^\circ$ , Aiding Flow



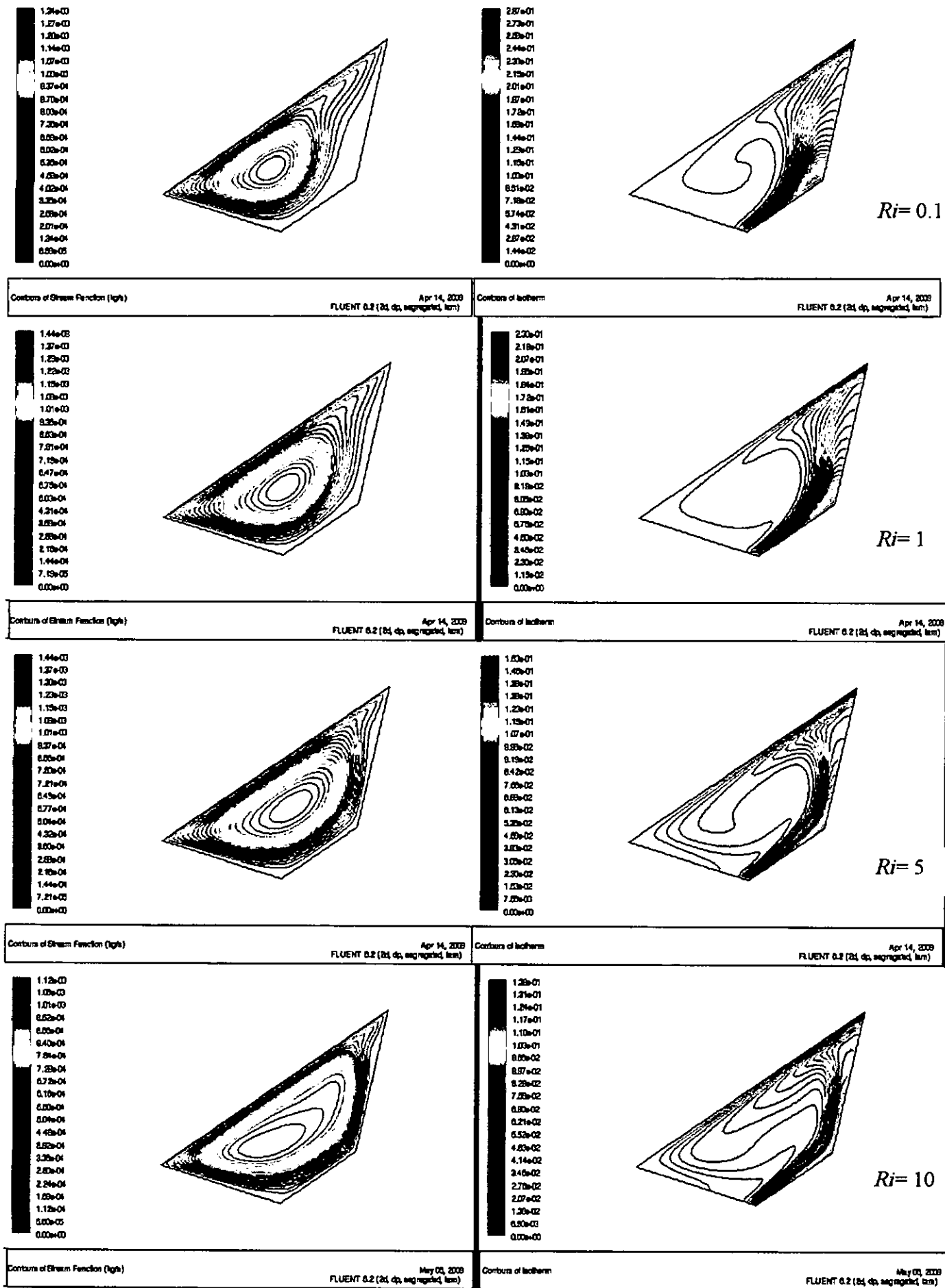


Figure 5.34: Contours of Streamlines and isotherms at  $Re=400$ ,  $A=1$  and  $\Phi=30^\circ$ , Aiding Flow

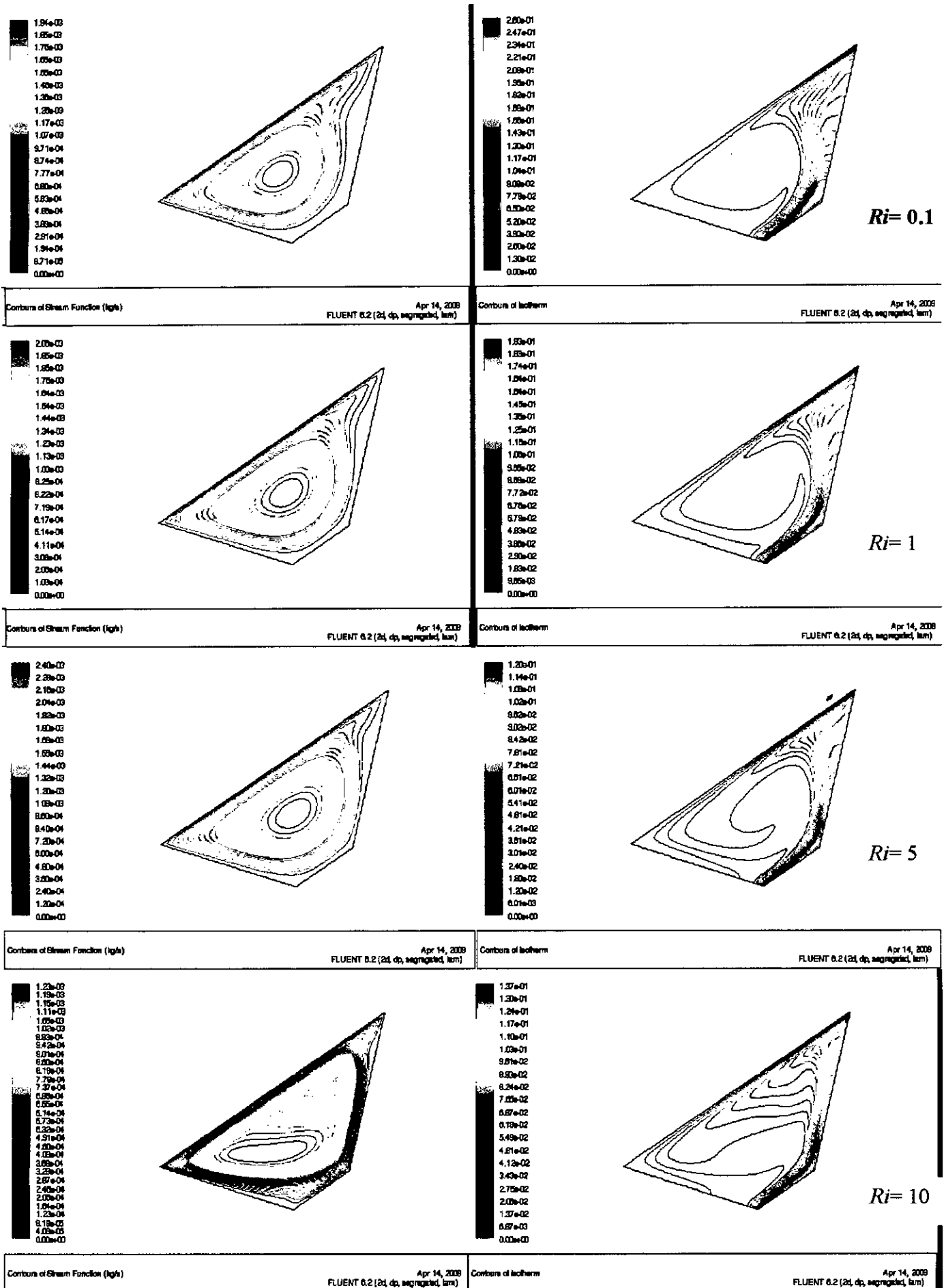


Figure 5.35: Contours of Streamlines and isotherms at  $Re=400$ ,  $A=1.5$  and  $\Phi=30^\circ$ , Aiding Flow

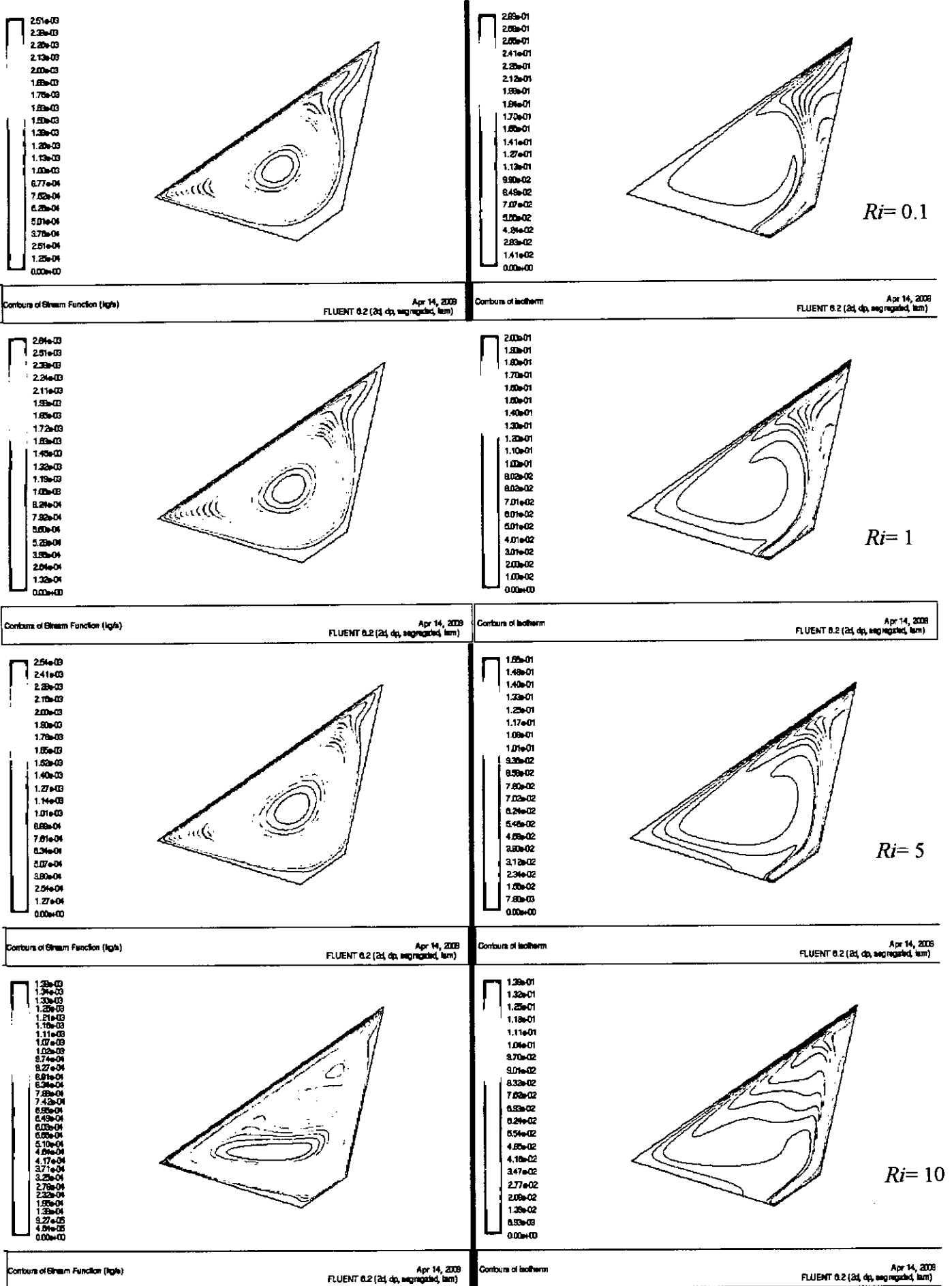
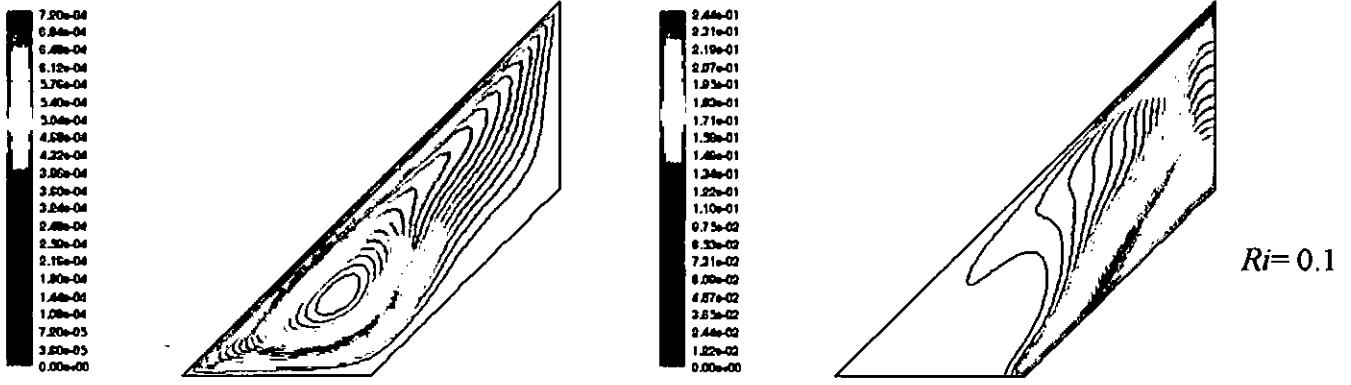
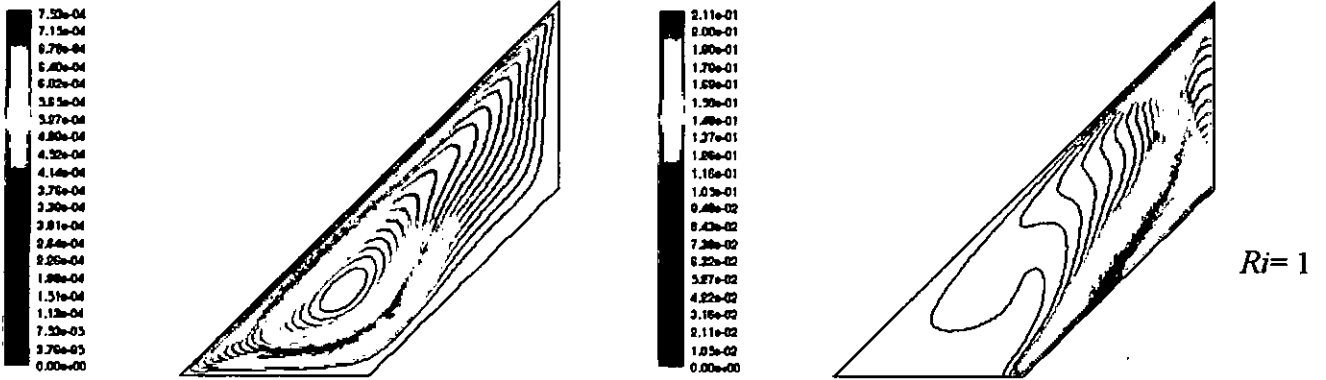


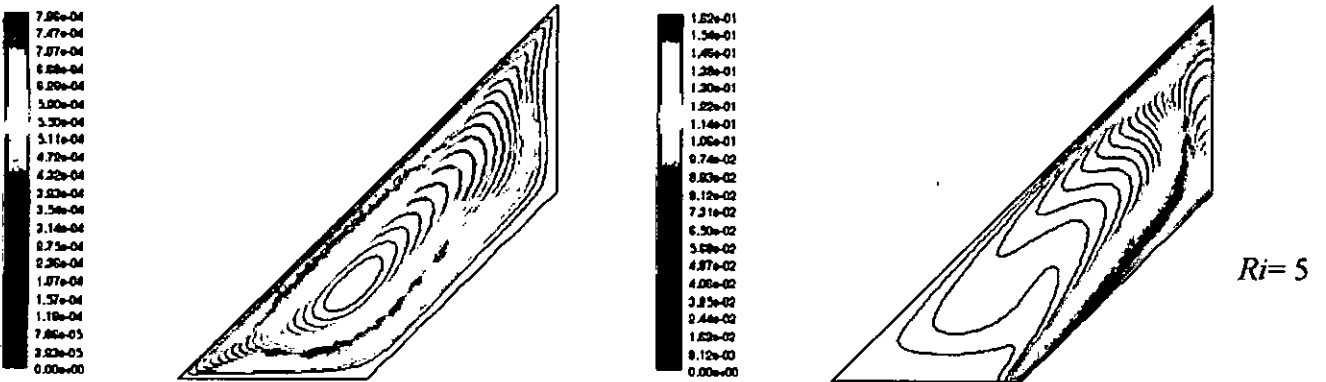
Figure 5.36: Contours of Streamlines and isotherms at  $Re=400$ ,  $A=2$  and  $\Phi=30^\circ$ , Aiding Flow



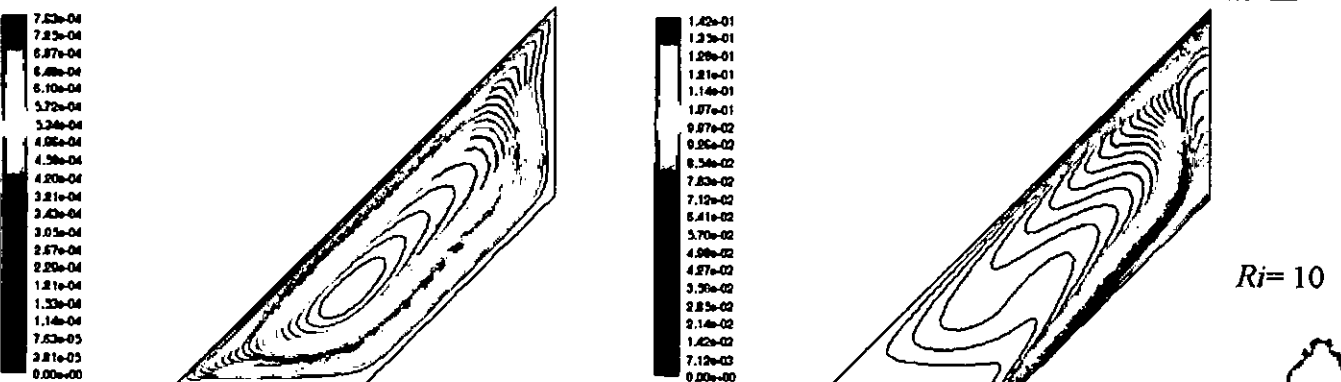
Contours of Stream Function (kg/s) FLUENT 6.2 (2d, dp, segregated, lsm) Apr 14, 2000  
Contours of Isotherms FLUENT 6.2 (2d, dp, segregated, lsm) Apr 14, 2000



Contours of Stream Function (kg/s) FLUENT 6.2 (2d, dp, segregated, lsm) Apr 14, 2000  
Contours of Isotherms FLUENT 6.2 (2d, dp, segregated, lsm) Apr 14, 2000

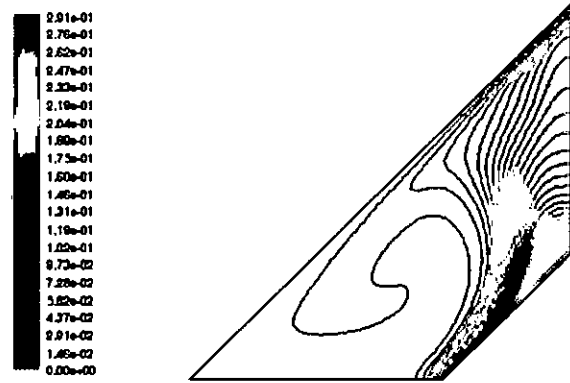
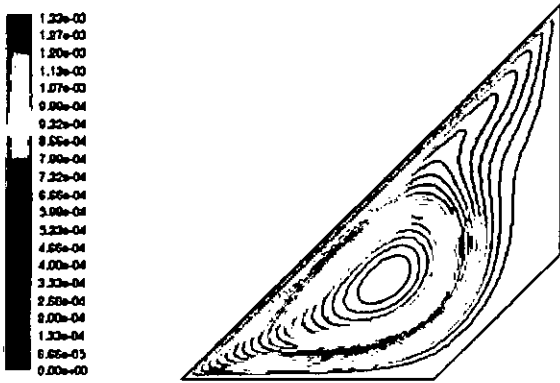


Contours of Stream Function (kg/s) FLUENT 6.2 (2d, dp, segregated, lsm) Apr 14, 2000  
Contours of Isotherms FLUENT 6.2 (2d, dp, segregated, lsm) Apr 14, 2000



Contours of Stream Function (kg/s) FLUENT 6.2 (2d, dp, segregated, lsm) Apr 14, 2000  
Contours of Isotherms FLUENT 6.2 (2d, dp, segregated, lsm) Apr 14, 2000

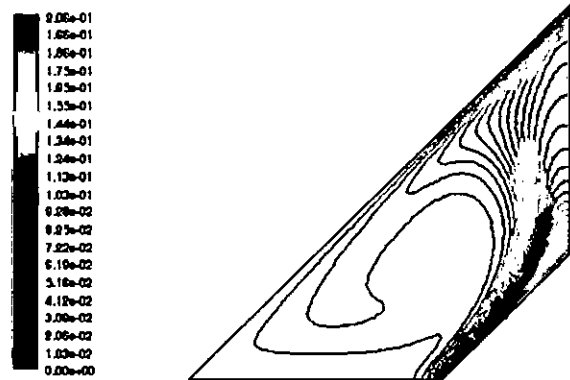
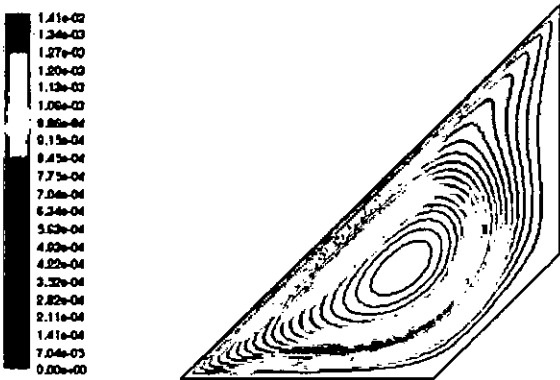
Figure 5.37: Contours of Streamlines and isotherms at  $Re=400$ ,  $A=0.5$  and  $\Phi=45^\circ$ , Aiding Flow



$Ri=0.1$

Contours of Stream Function (kg/s) Apr 14, 2000 FLUENT 6.2 (2d, dp, segregated, ltr)

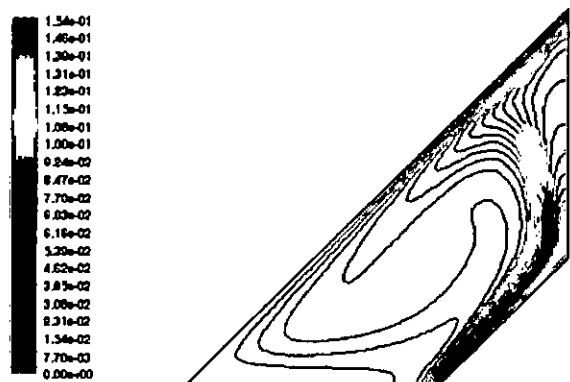
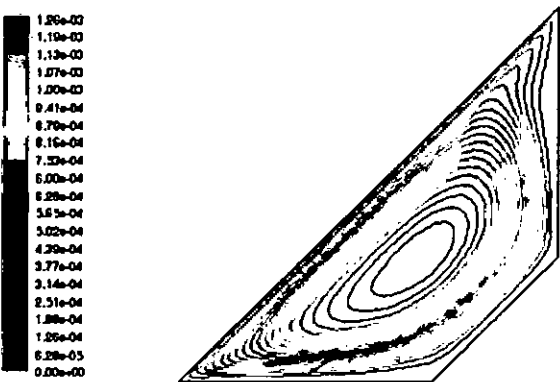
Contours of Isotherms Apr 14, 2000 FLUENT 6.2 (2d, dp, segregated, ltr)



$Ri=1$

Contours of Stream Function (kg/s) Apr 14, 2000 FLUENT 6.2 (2d, dp, segregated, ltr)

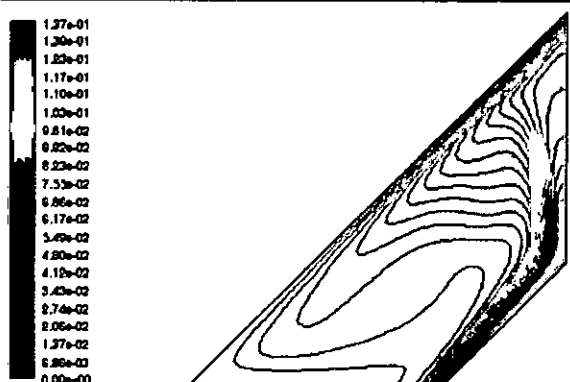
Contours of Isotherms Apr 14, 2000 FLUENT 6.2 (2d, dp, segregated, ltr)



$Ri=5$

Contours of Stream Function (kg/s) Apr 14, 2000 FLUENT 6.2 (2d, dp, segregated, ltr)

Contours of Isotherms Apr 14, 2000 FLUENT 6.2 (2d, dp, segregated, ltr)

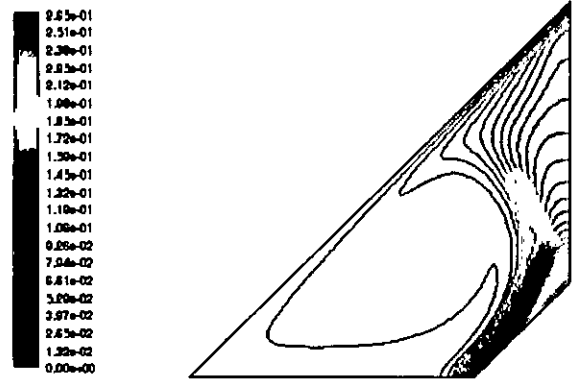
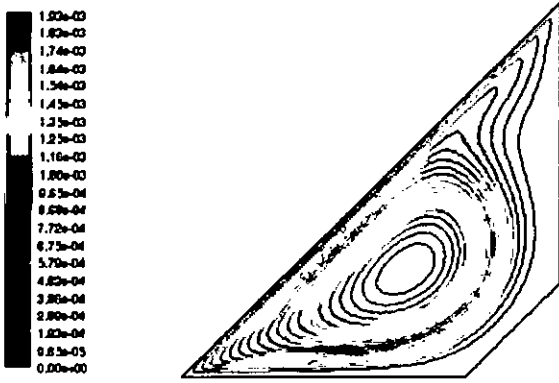


$Ri=10$

Contours of Stream Function (kg/s) Apr 14, 2000 FLUENT 6.2 (2d, dp, segregated, ltr)

Contours of Isotherms Apr 14, 2000 FLUENT 6.2 (2d, dp, segregated, ltr)

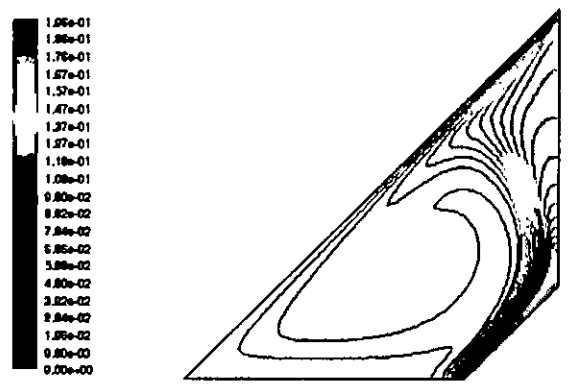
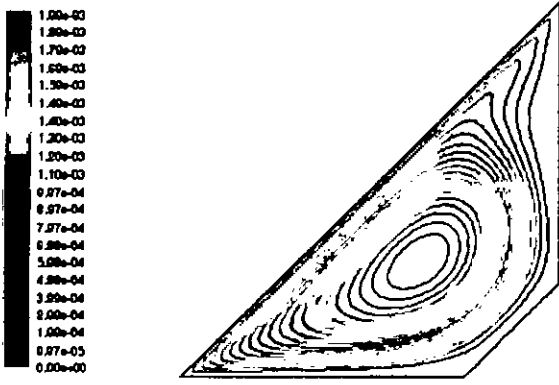
Figure 5.38: Contours of Streamlines and isotherms at  $Re=400$ ,  $A=1$  and  $\Phi=45^\circ$ , Aiding Flow



$Ri = 0.1$

Contours of Stream Function (Psi) FLUENT 6.2 (2d, dp, segregated, ltr) Apr 14, 2000

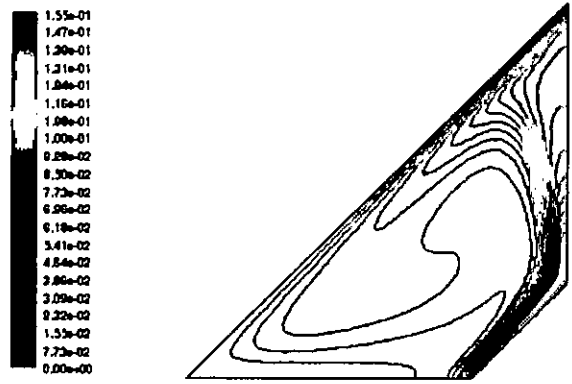
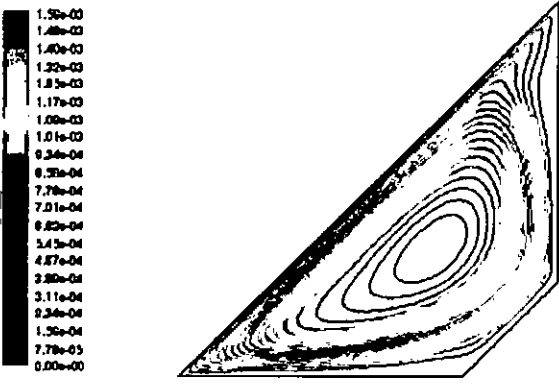
Contours of Isotherms FLUENT 6.2 (2d, dp, segregated, ltr) Apr 14, 2000



$Ri = 1$

Contours of Stream Function (Psi) FLUENT 6.2 (2d, dp, segregated, ltr) Apr 14, 2000

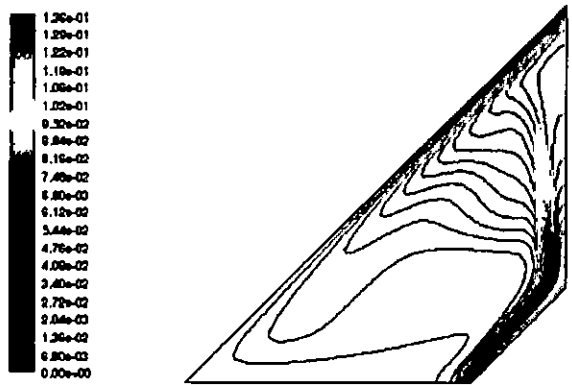
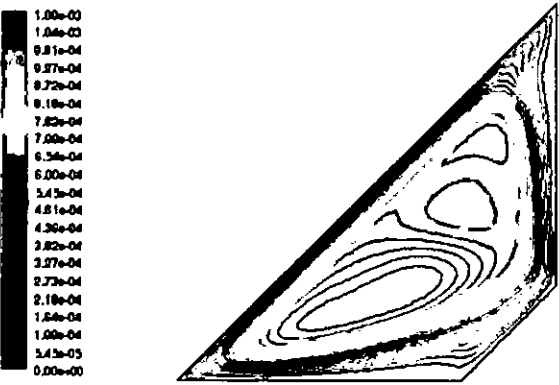
Contours of Isotherms FLUENT 6.2 (2d, dp, segregated, ltr) Apr 14, 2000



$Ri = 5$

Contours of Stream Function (Psi) FLUENT 6.2 (2d, dp, segregated, ltr) Apr 15, 2000

Contours of Isotherms FLUENT 6.2 (2d, dp, segregated, ltr) Apr 15, 2000



$Ri = 10$

Contours of Stream Function (Psi) FLUENT 6.2 (2d, dp, segregated, ltr) Apr 14, 2000

Contours of Isotherms FLUENT 6.2 (2d, dp, segregated, ltr) Apr 14, 2000

Figure 5.39: Contours of Streamlines and isotherms at  $Re=400$ ,  $A=1.5$  and  $\Phi=45^\circ$ , Aiding Flow

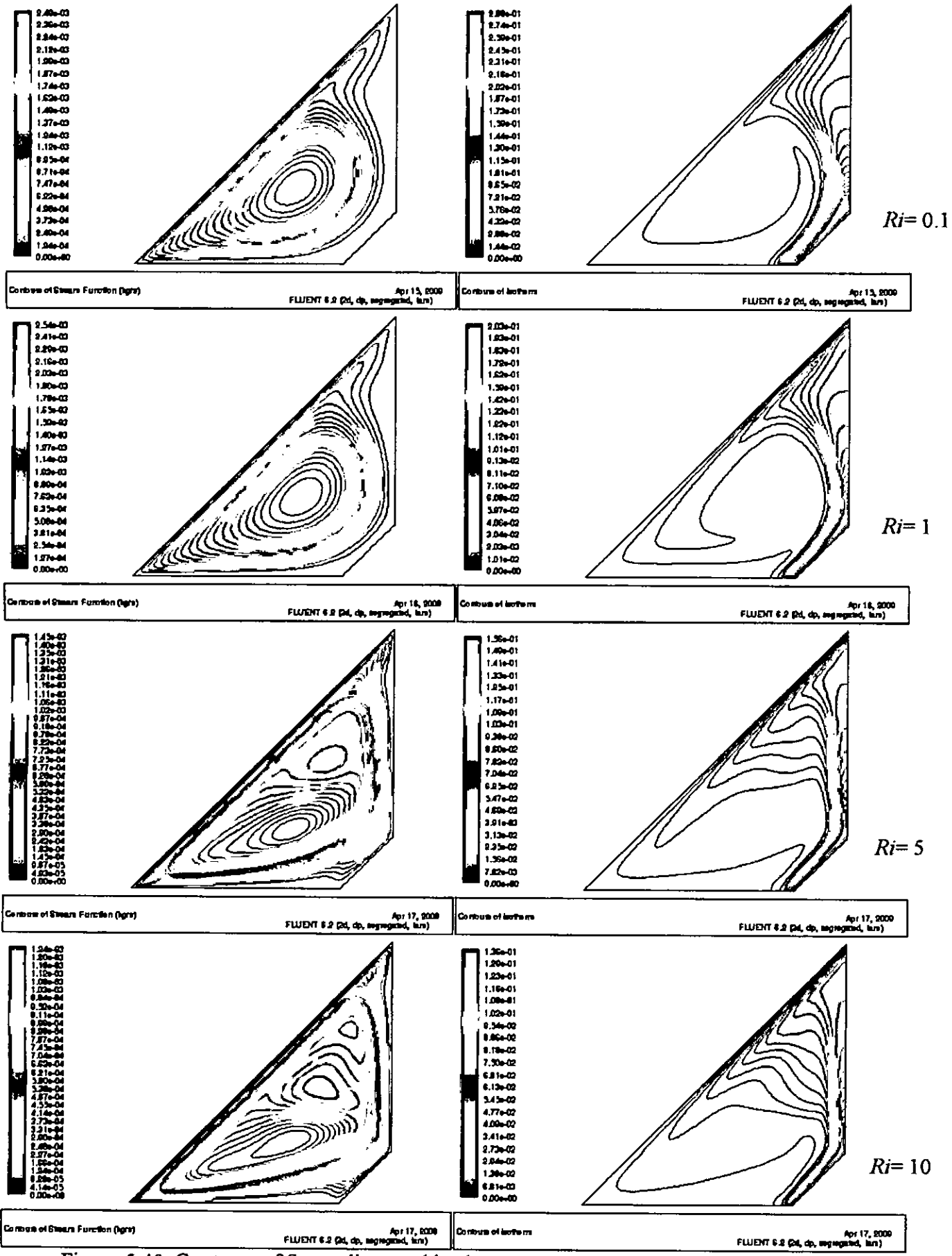


Figure 5.40: Contours of Streamlines and isotherms at  $Re=400$ ,  $A=2$  and  $\Phi=45^\circ$ , Aiding Flow

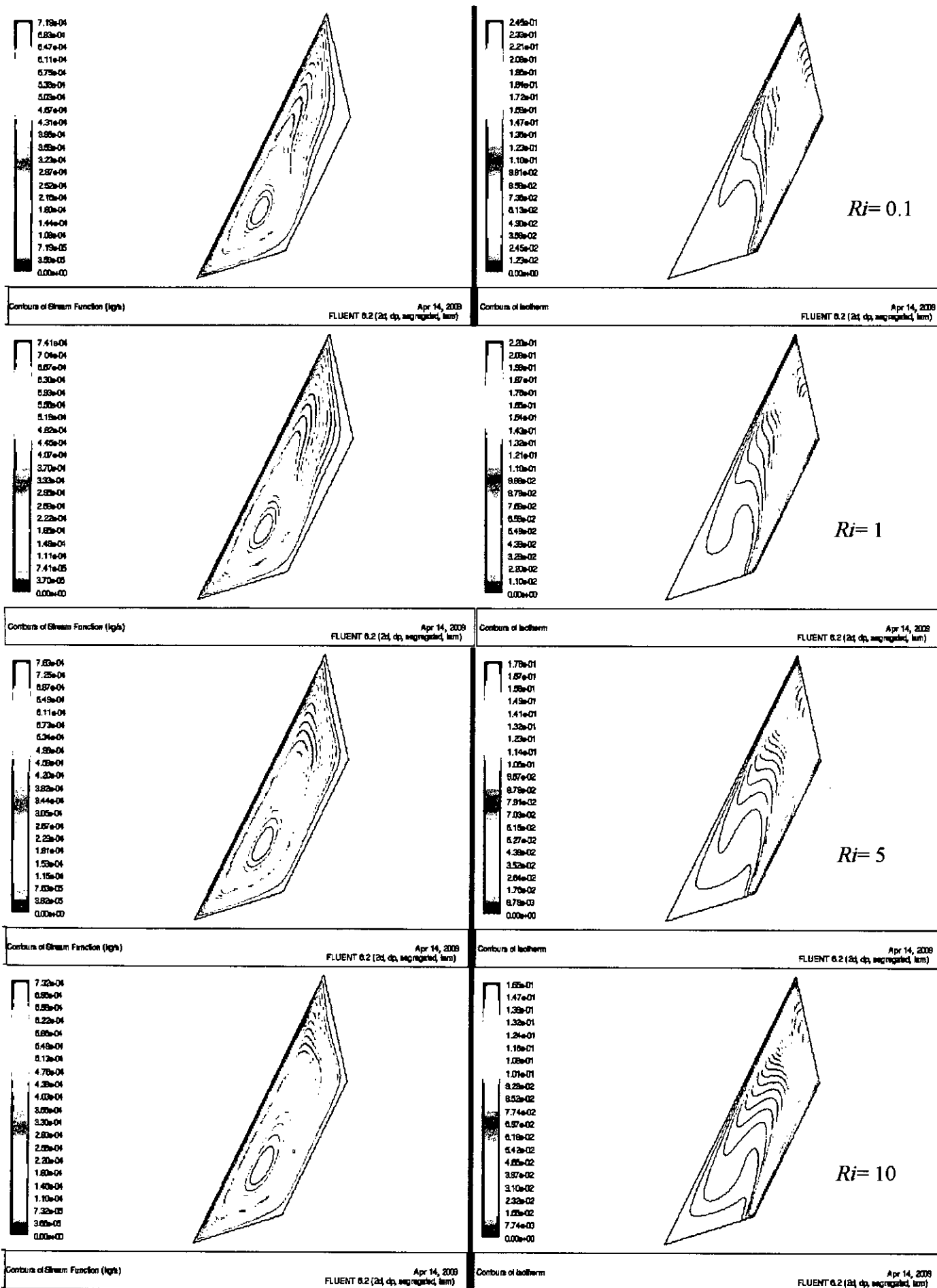


Figure 5.41: Contours of Streamlines and isotherms at  $Re=400$ ,  $A=0.5$  and  $\Phi=60^\circ$ , Aiding Flow



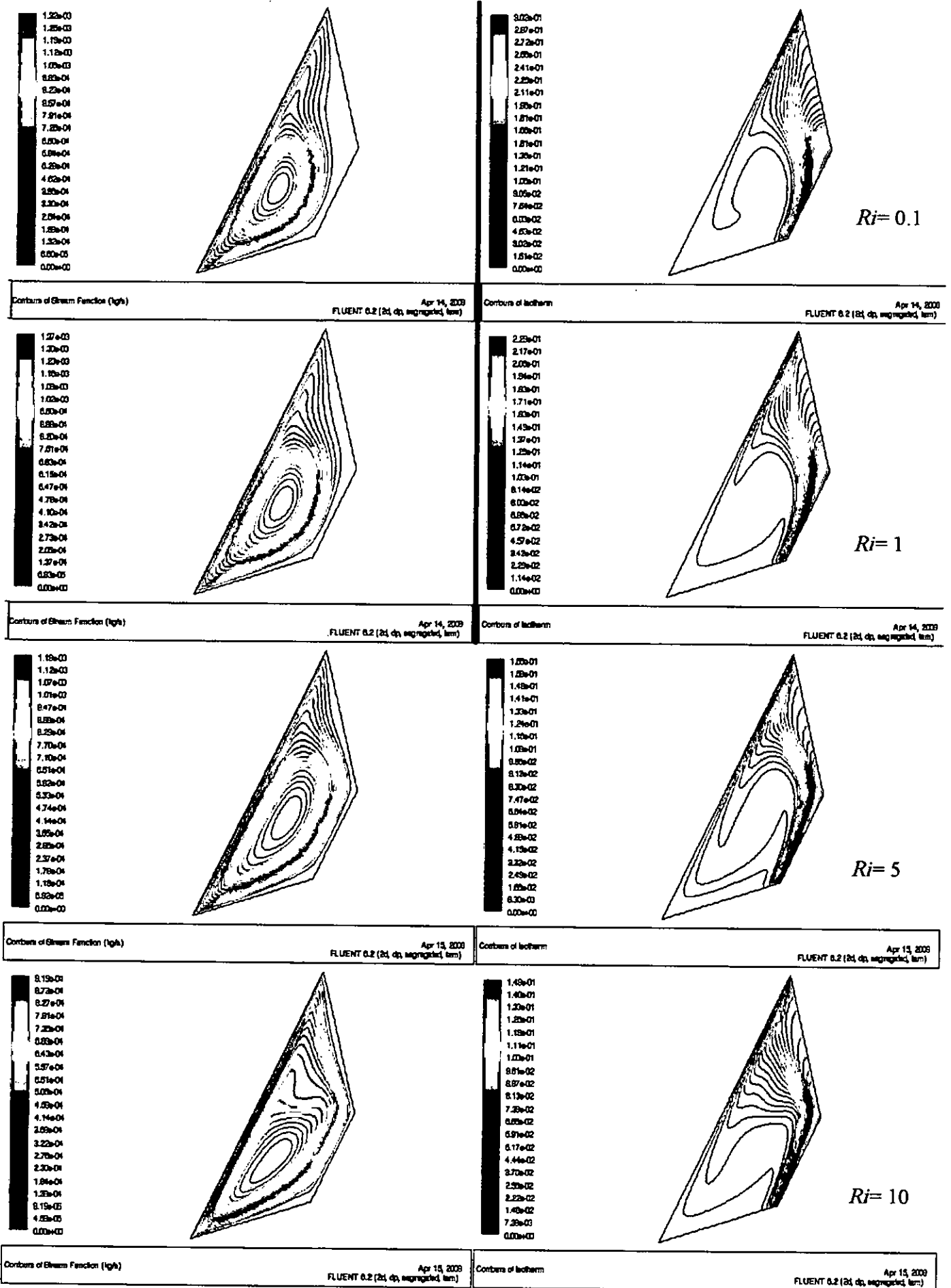


Figure 5.42: Contours of Streamlines and isotherms at  $Re=400$ ,  $A=1$  and  $\Phi=60^\circ$ , Aiding Flow

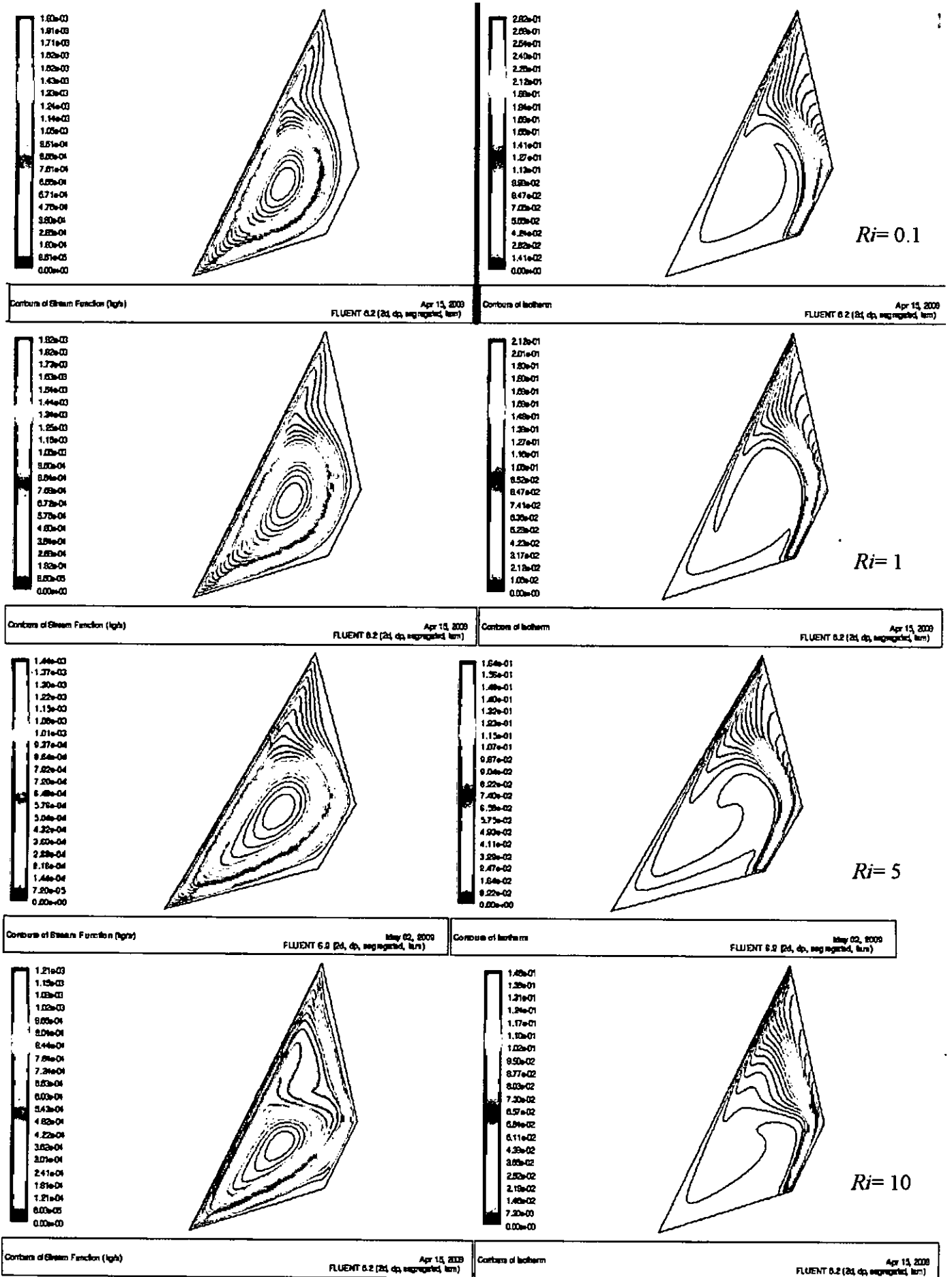


Figure 5.43: Contours of Streamlines and isotherms at  $Re=400$ ,  $A=1.5$  and  $\Phi=60^\circ$ , Aiding Flow

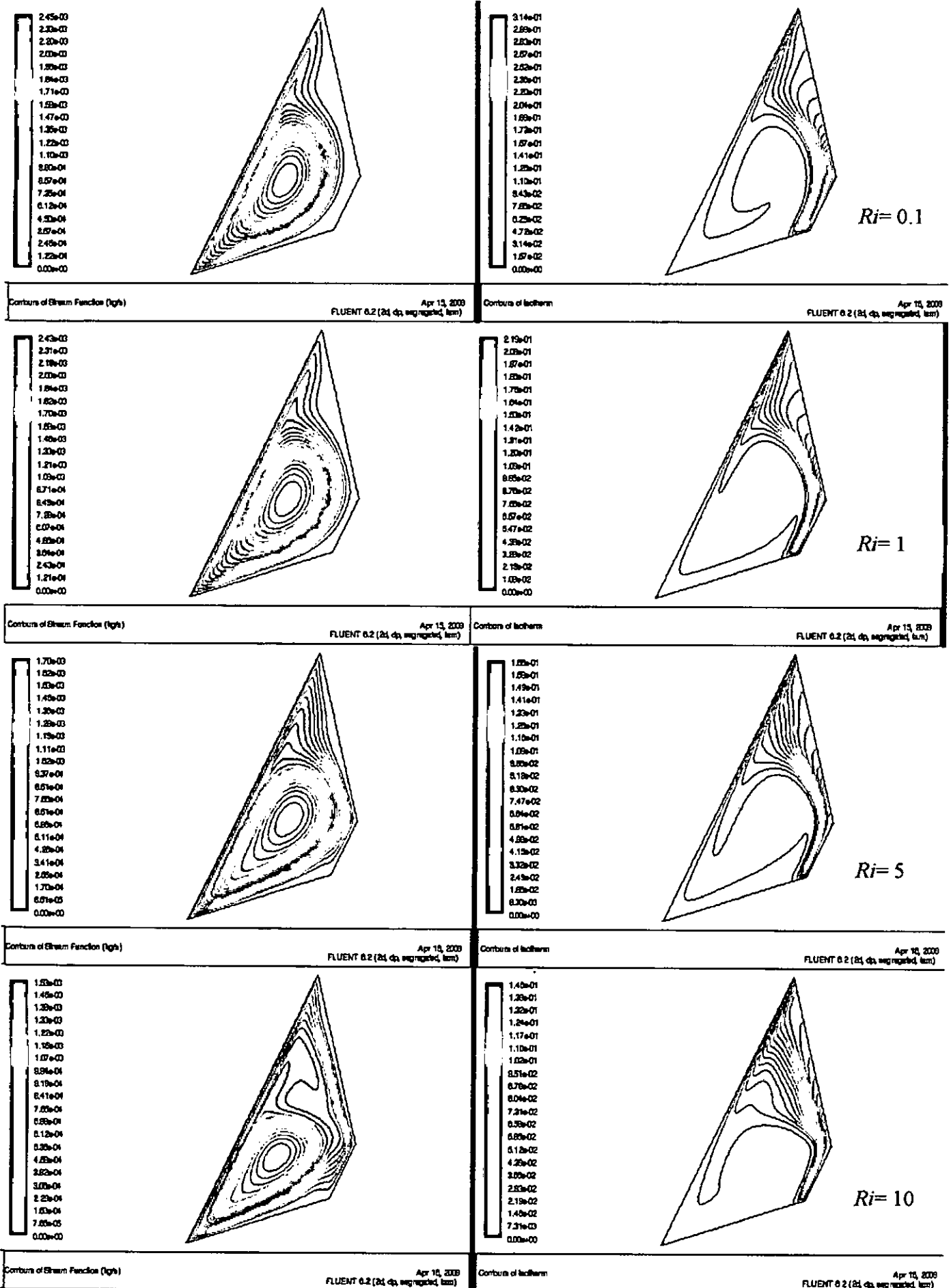


Figure 5.44: Contours of Streamlines and isotherms at  $Re=400$ ,  $A=2$  and  $\Phi=60^\circ$ , Aiding Flow

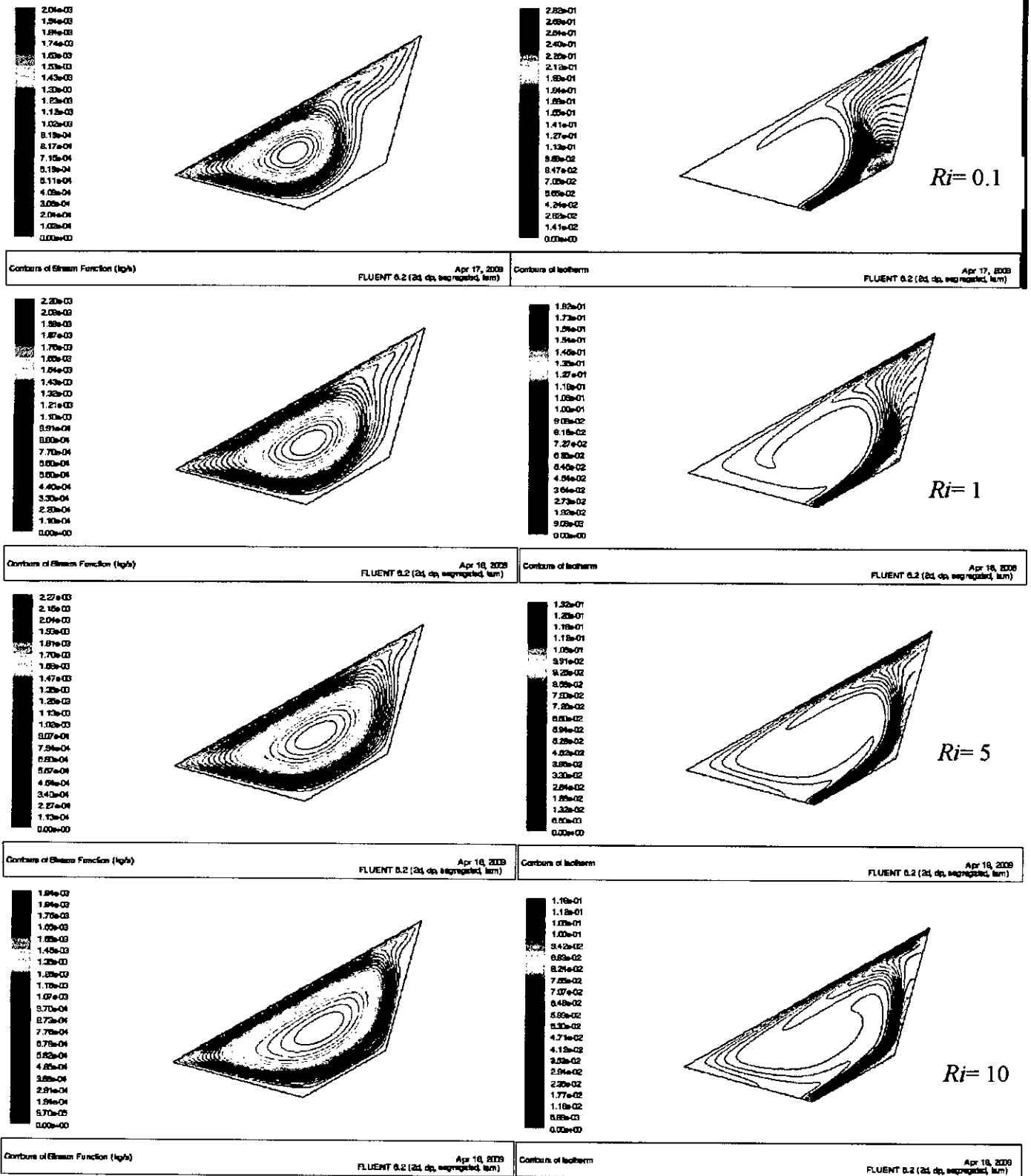
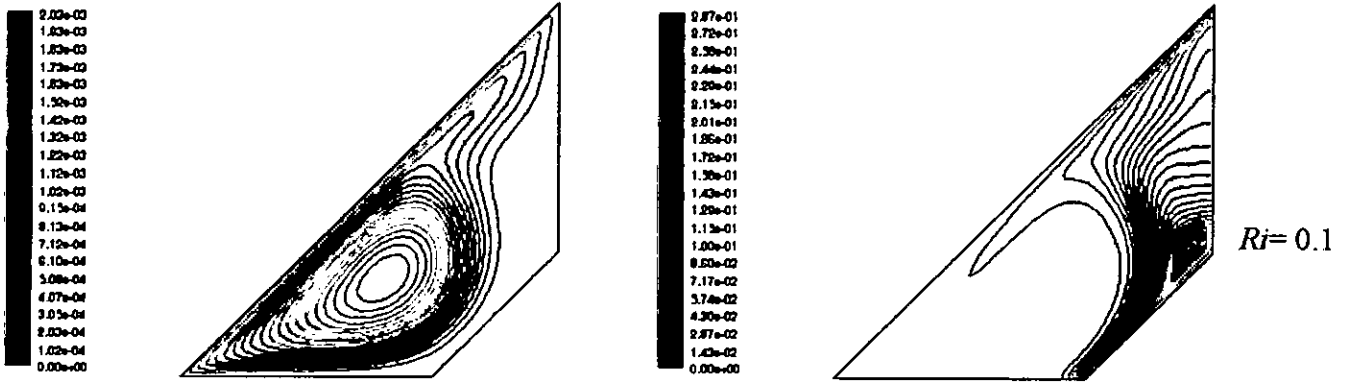
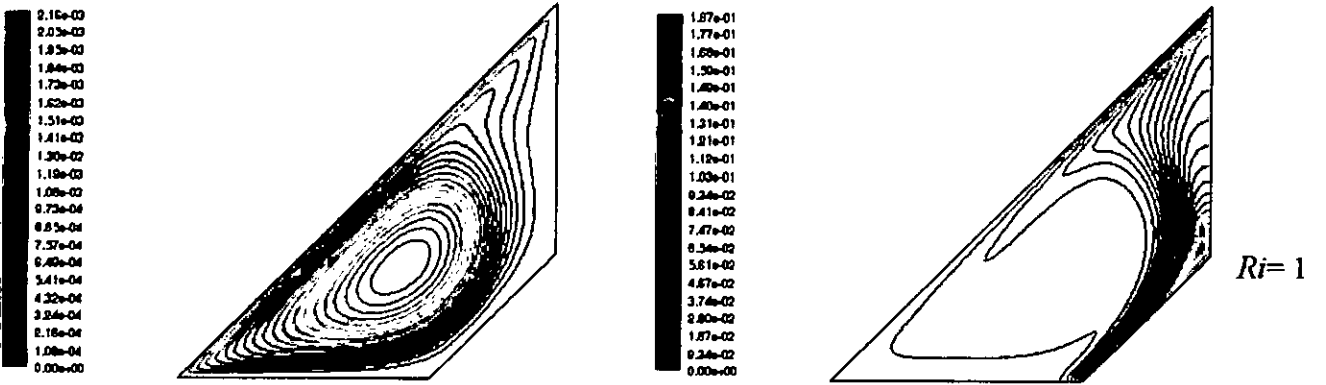


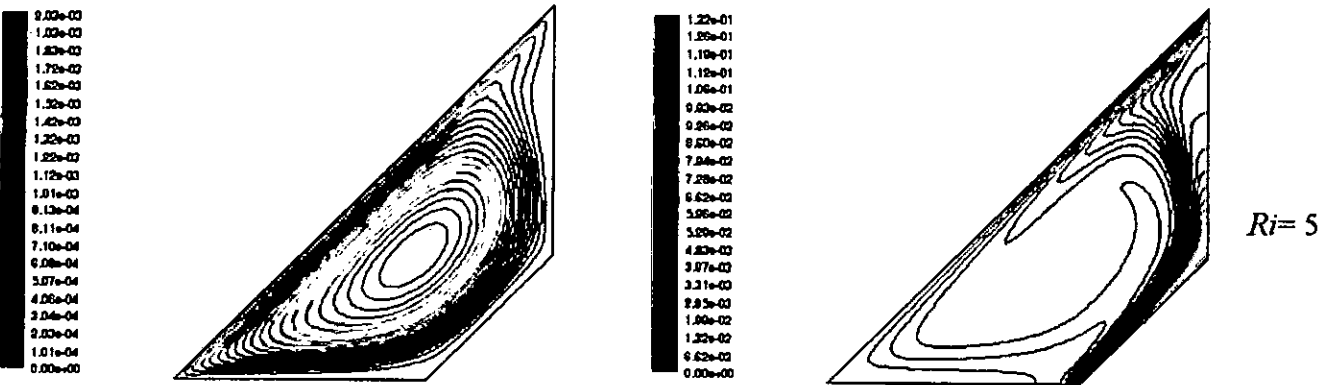
Figure 5.45: Contours of Streamlines and isotherms at  $Re=600$ ,  $A=1$  and  $\Phi=30^\circ$ , Aiding Flow



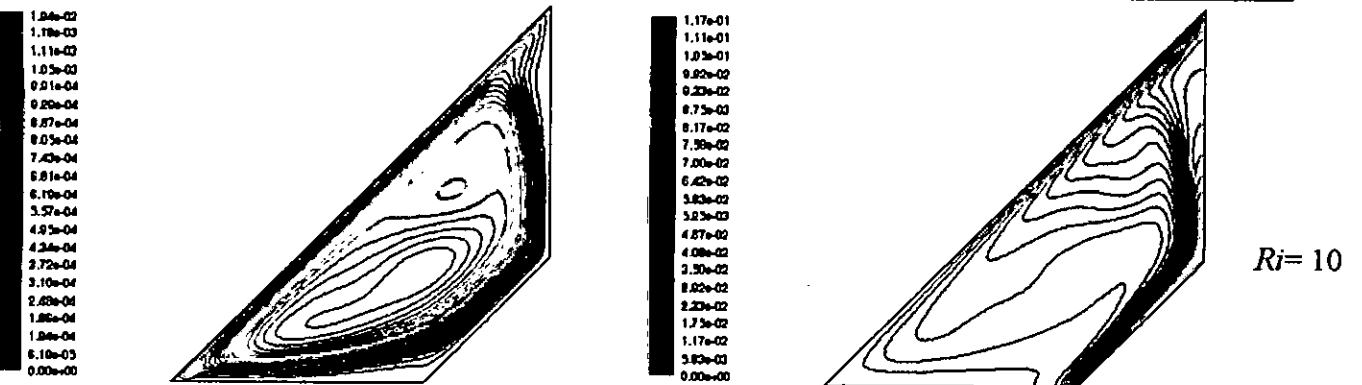
Contours of Stream Function (l/sr) Apr 24, 2000 FLUENT 6.2 (2d, dp, segregated, lsm)      Contours of Isotherms Apr 24, 2000 FLUENT 6.2 (2d, dp, segregated, lsm)



Contours of Stream Function (l/sr) Apr 18, 2000 FLUENT 6.2 (2d, dp, segregated, lsm)      Contours of Isotherms Apr 18, 2000 FLUENT 6.2 (2d, dp, segregated, lsm)



Contours of Stream Function (l/sr) Apr 18, 2000 FLUENT 6.2 (2d, dp, segregated, lsm)      Contours of Isotherms Apr 18, 2000 FLUENT 6.2 (2d, dp, segregated, lsm)



Contours of Stream Function (l/sr) Apr 18, 2000 FLUENT 6.2 (2d, dp, segregated, lsm)      Contours of Isotherms Apr 18, 2000 FLUENT 6.2 (2d, dp, segregated, lsm)

Figure 5.46: Contours of Streamlines and isotherms at  $Re=600$ ,  $A=1$  and  $\Phi=45^\circ$ , Aiding Flow

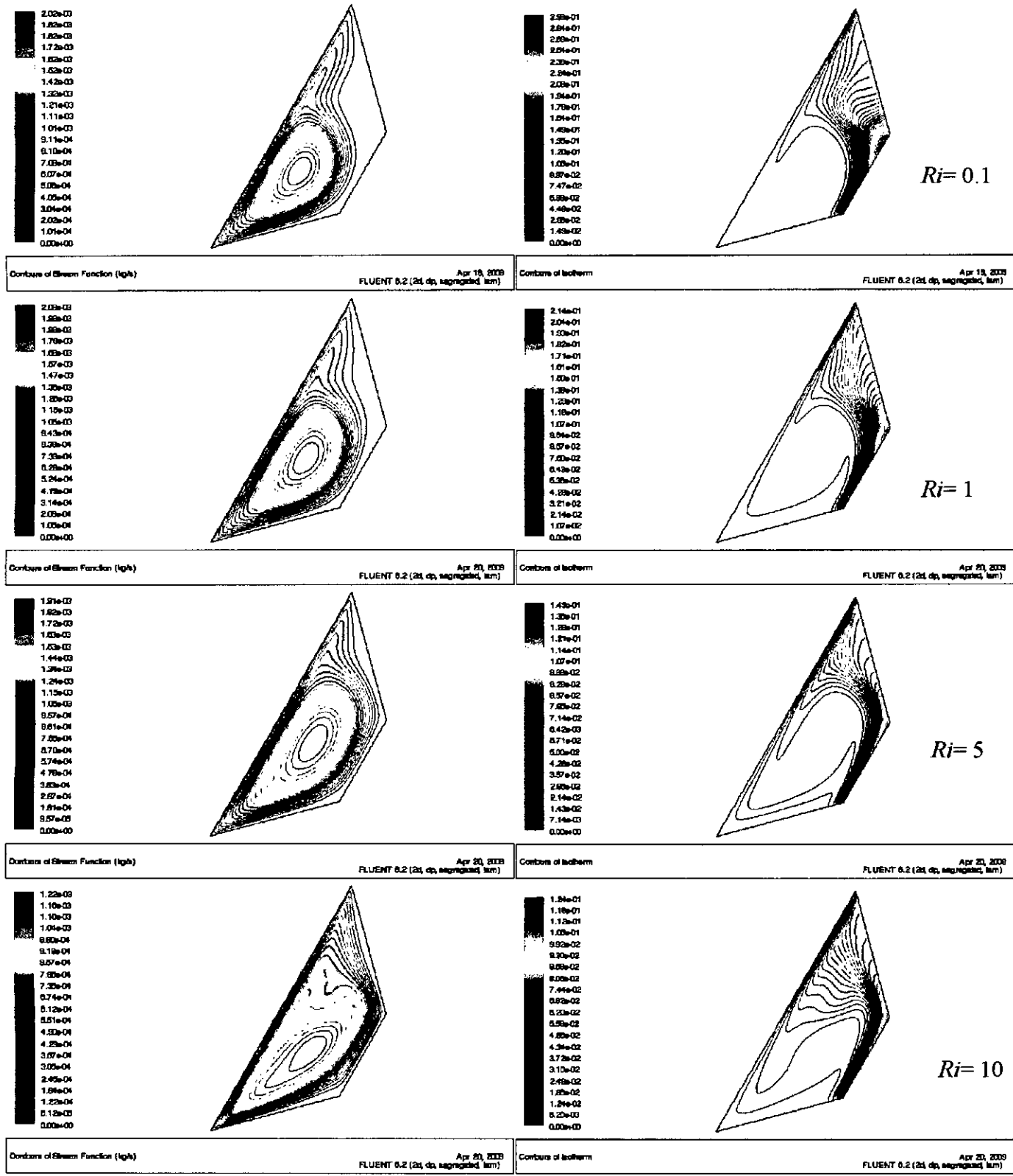


Figure 5.47: Contours of Streamlines and isotherms at  $Re=600$ ,  $A=1$  and  $\Phi=60^\circ$ , Aiding Flow

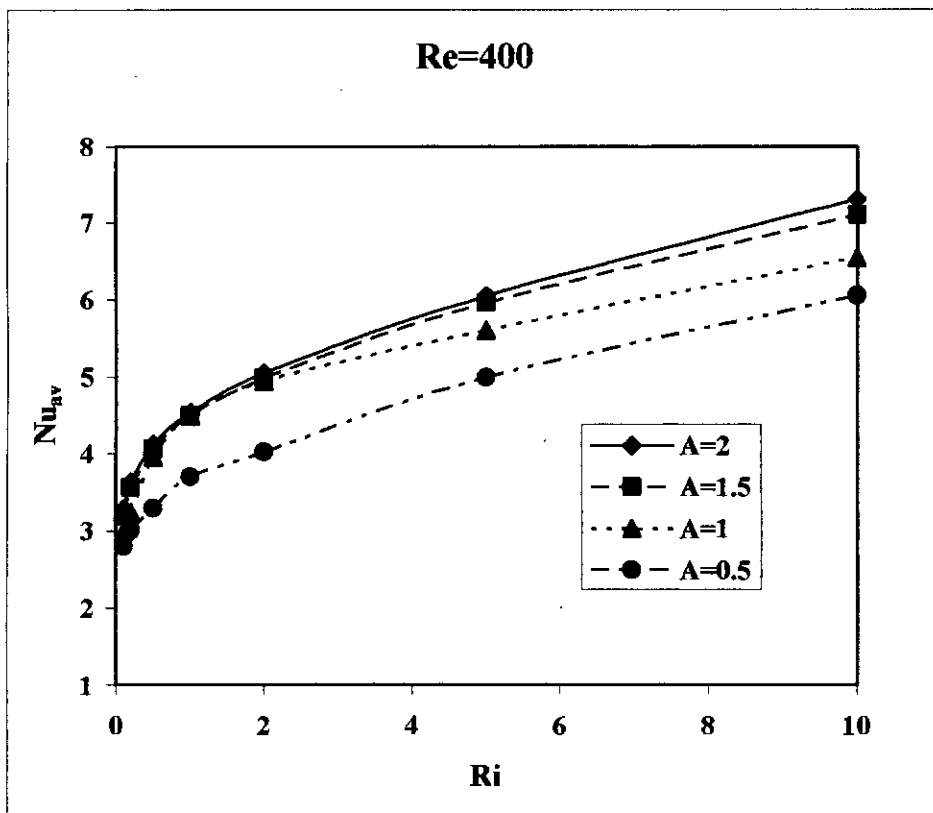


Figure 5.48: Variation of  $Nu_{av}$  with  $Ri$  at  $\Phi=30^\circ$ ,  $Re=400$ , Opposing Flow

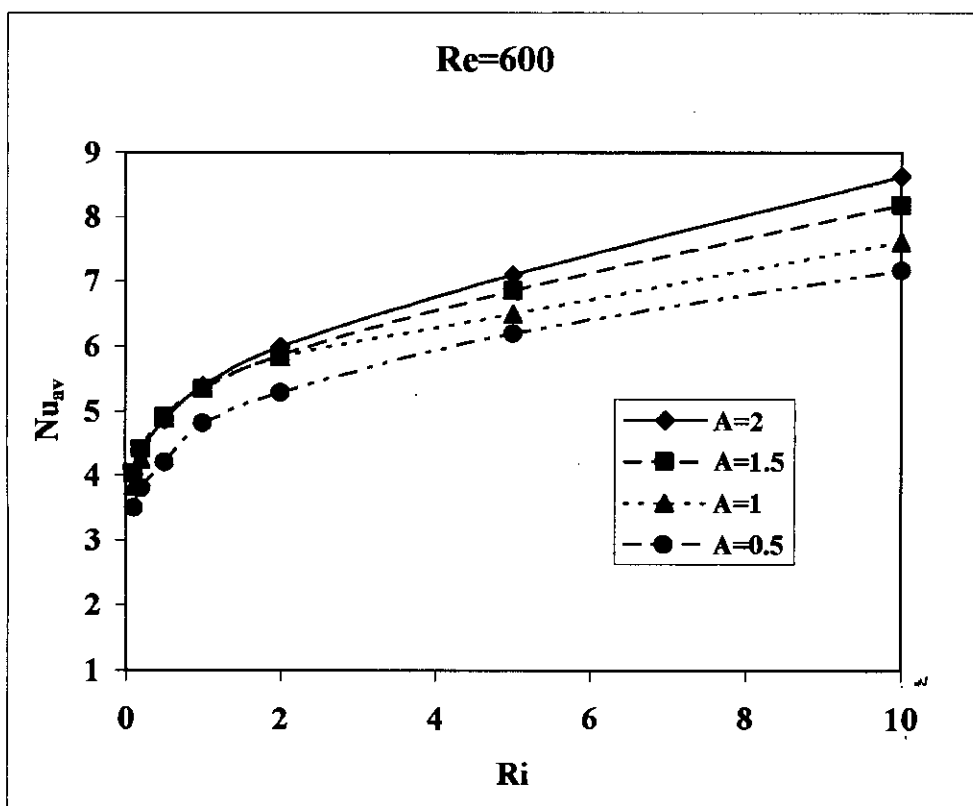


Figure 5.49: Variation of  $Nu_{av}$  with  $Ri$  at  $\Phi=30^\circ$ ,  $Re=600$ , Opposing Flow

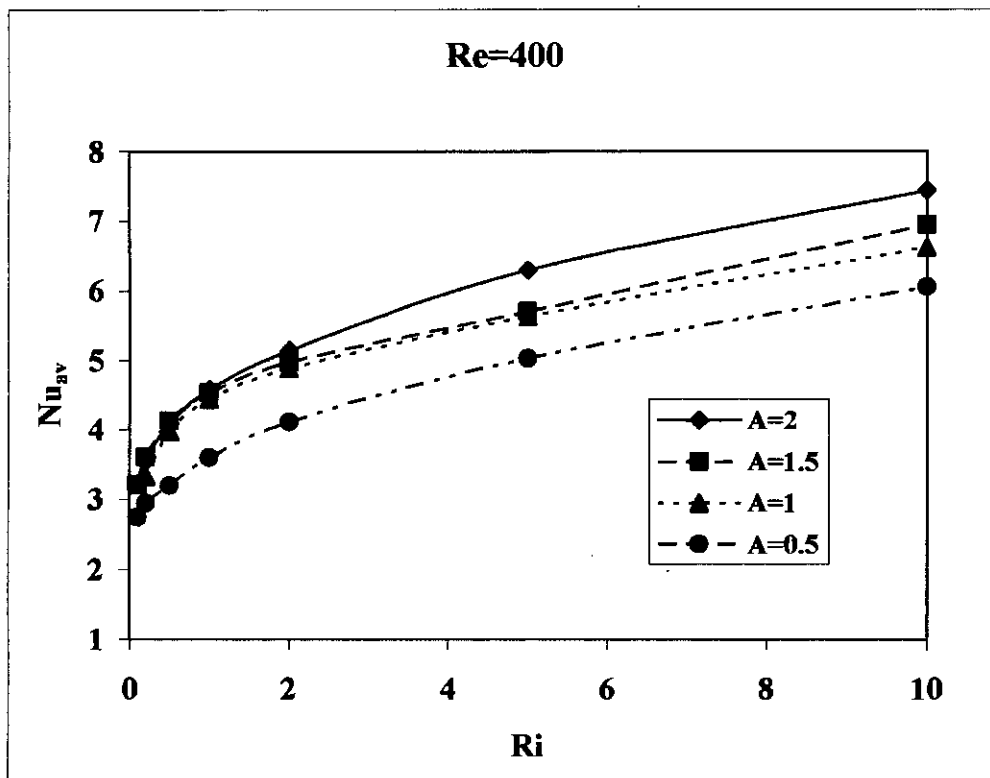


Figure 5.50: Variation of  $Nu_{av}$  with  $Ri$  at  $\Phi=45^\circ$ ,  $Re=400$ , Opposing Flow

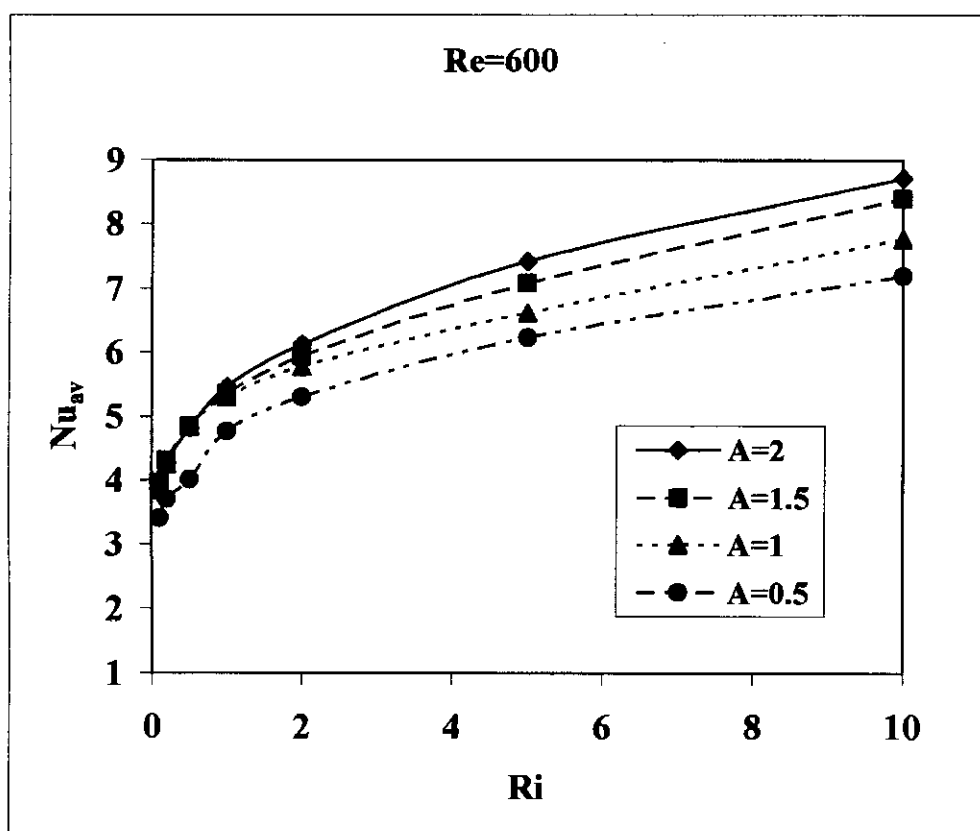


Figure 5.51: Variation of  $Nu_{av}$  with  $Ri$  at  $\Phi=45^\circ$ ,  $Re=600$ , Opposing Flow



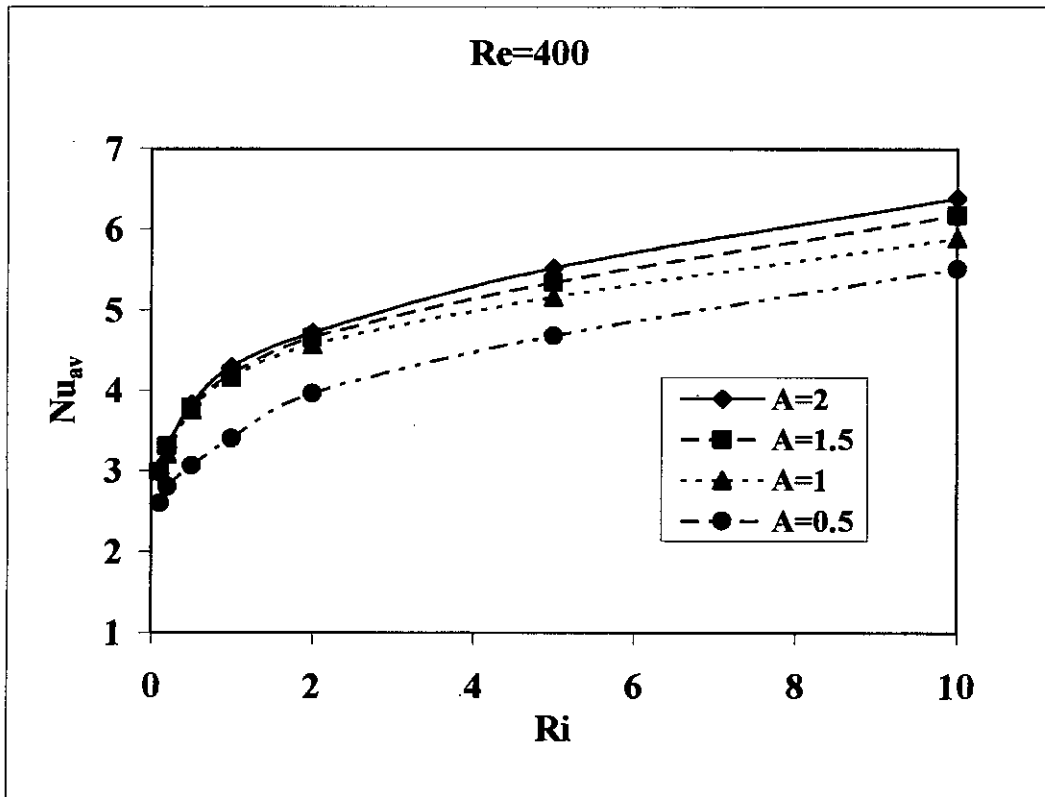


Figure 5.52: Variation of  $Nu_{av}$  with  $Ri$  at  $\Phi=60^\circ$ ,  $Re=400$ , Opposing Flow

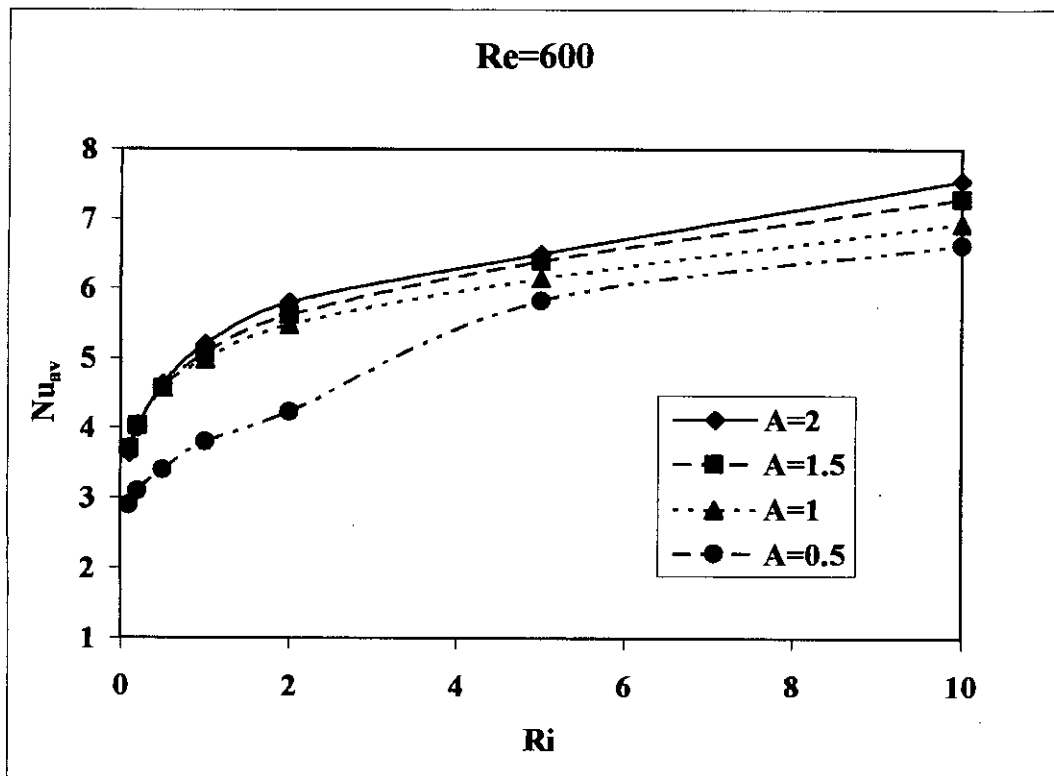


Figure 5.53: Variation of  $Nu_{av}$  with  $Ri$  at  $\Phi=60^\circ$ ,  $Re=600$ , Opposing Flow

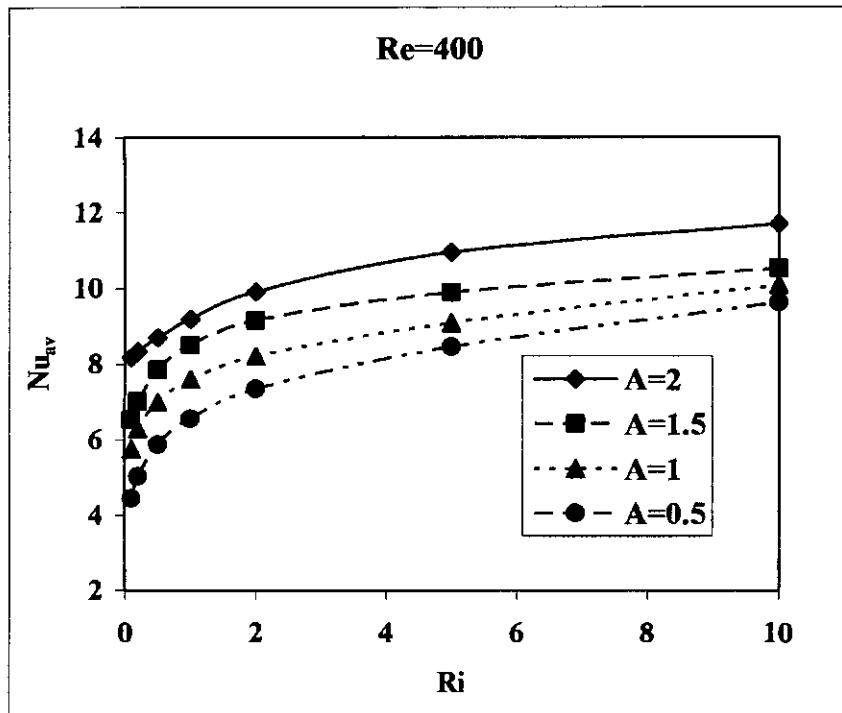


Figure 5.54: Variation of  $Nu_{av}$  with  $Ri$  at  $\Phi=30^\circ$ ,  $Re=400$ , Aiding Flow

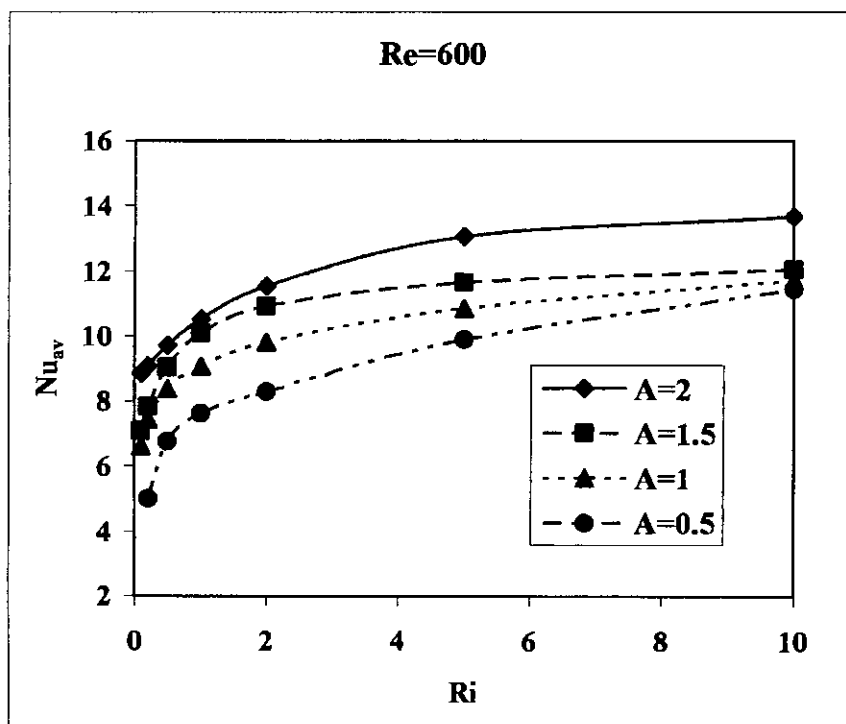


Figure 5.55: Variation of  $Nu_{av}$  with  $Ri$  at  $\Phi=30^\circ$ ,  $Re=600$ , Aiding Flow

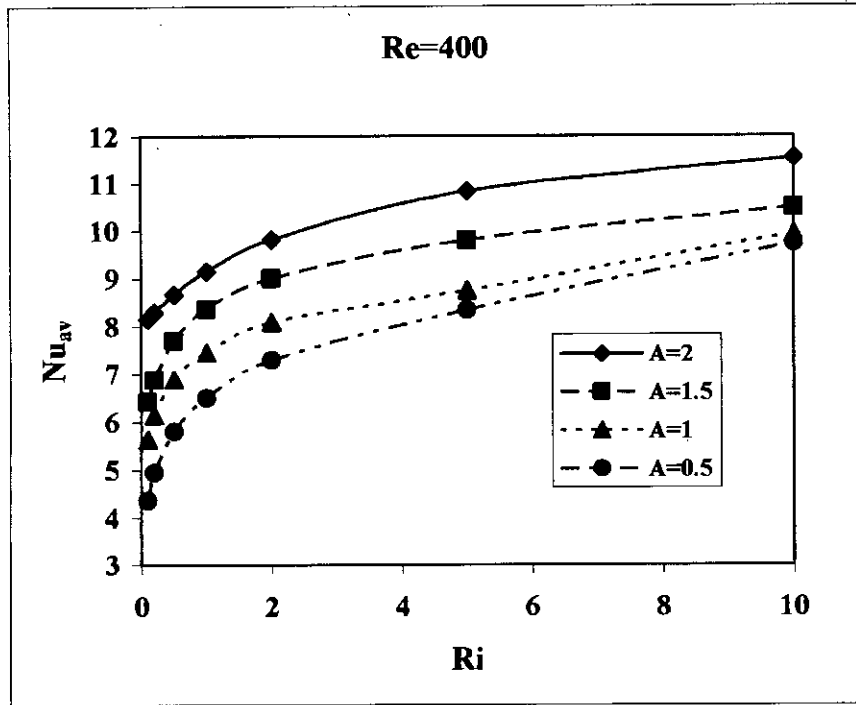


Figure 5.56: Variation of  $Nu_{av}$  with  $Ri$  at  $\Phi=45^\circ$ ,  $Re=400$ , Aiding Flow

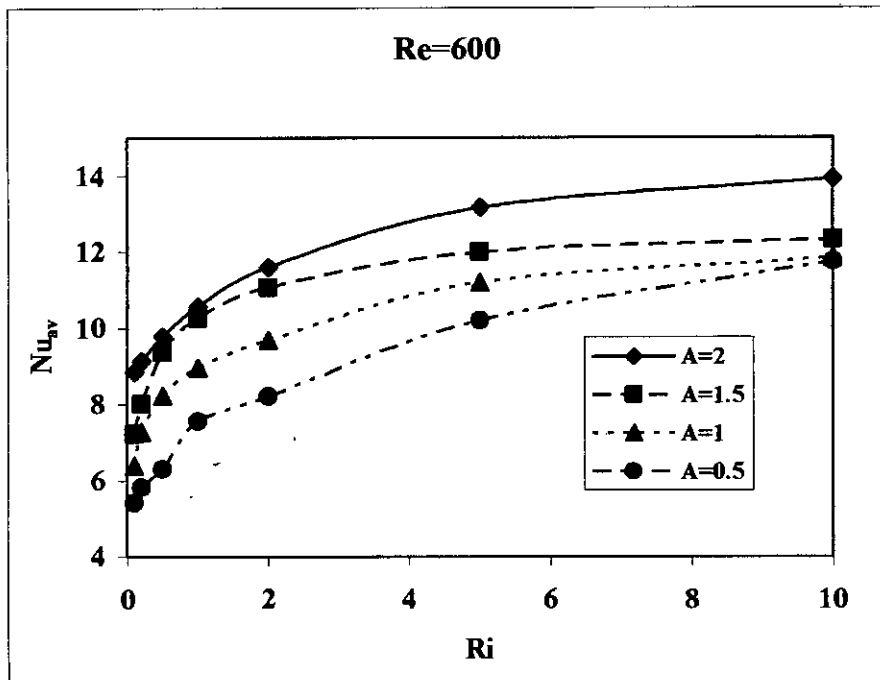


Figure 5.57: Variation of  $Nu_{av}$  with  $Ri$  at  $\Phi=45^\circ$ ,  $Re=600$ , Aiding Flow

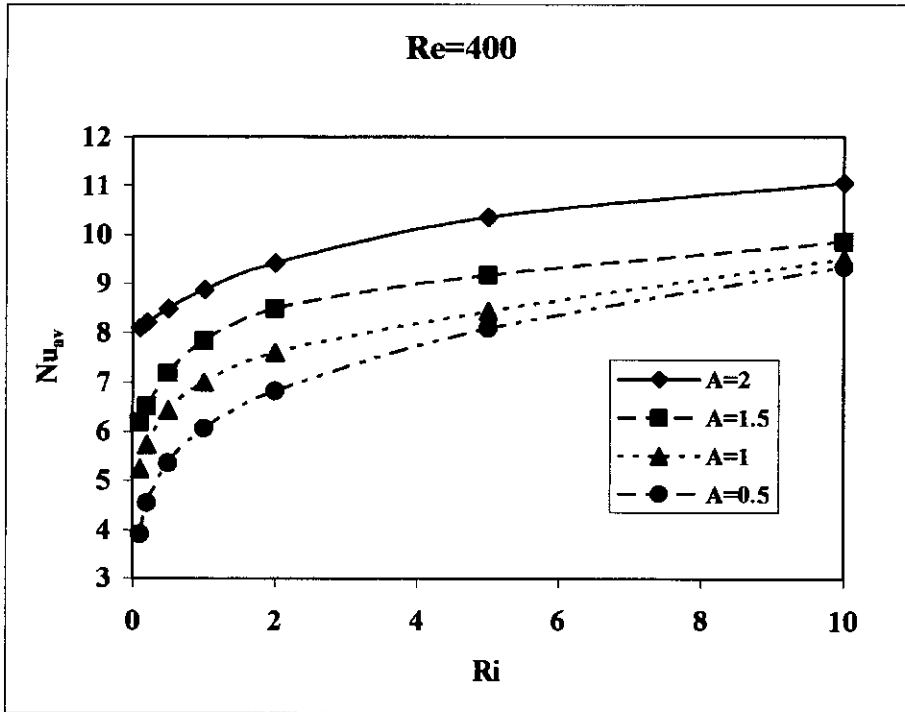


Figure 5.58: Variation of  $Nu_{av}$  with  $Ri$  at  $\Phi=60^\circ$ ,  $Re=400$ , Aiding Flow

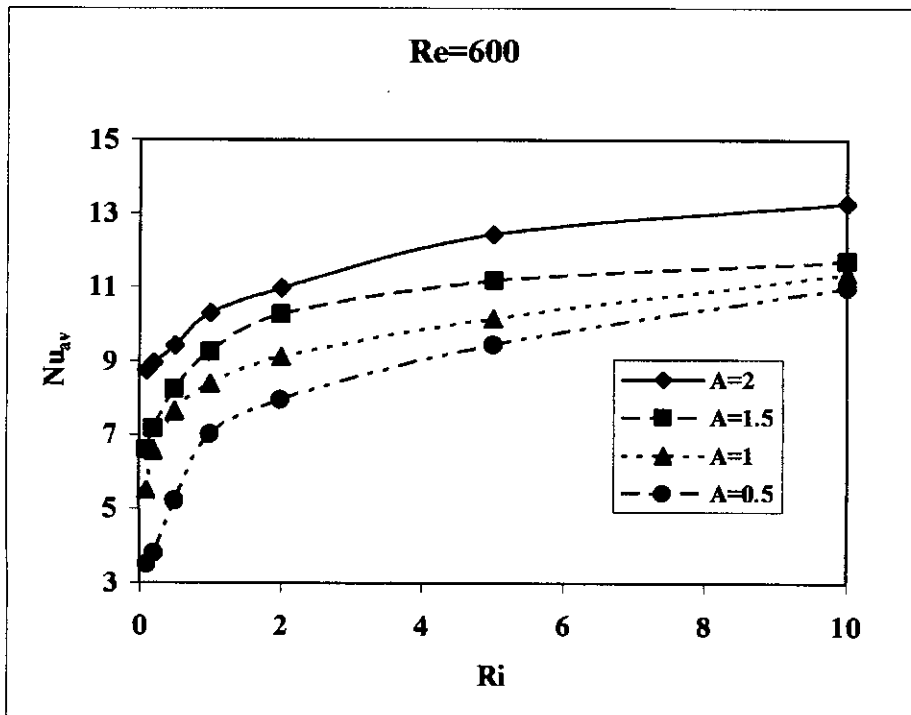


Figure 5.59: Variation of  $Nu_{av}$  with  $Ri$  at  $\Phi=60^\circ$ ,  $Re=600$ , Aiding Flow

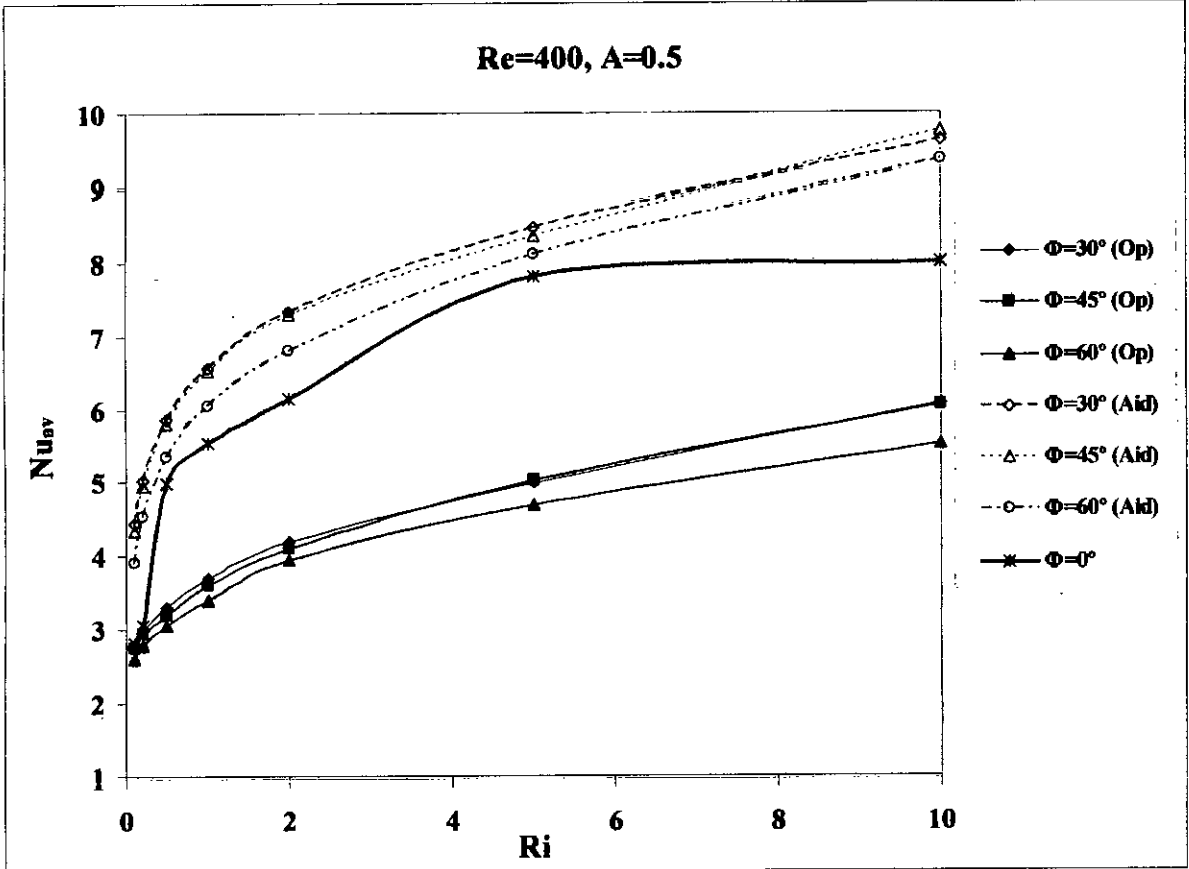


Figure 5.60: Variation of  $Nu_{av}$  with  $Ri$  at  $A=0.5$ ,  $Re=400$

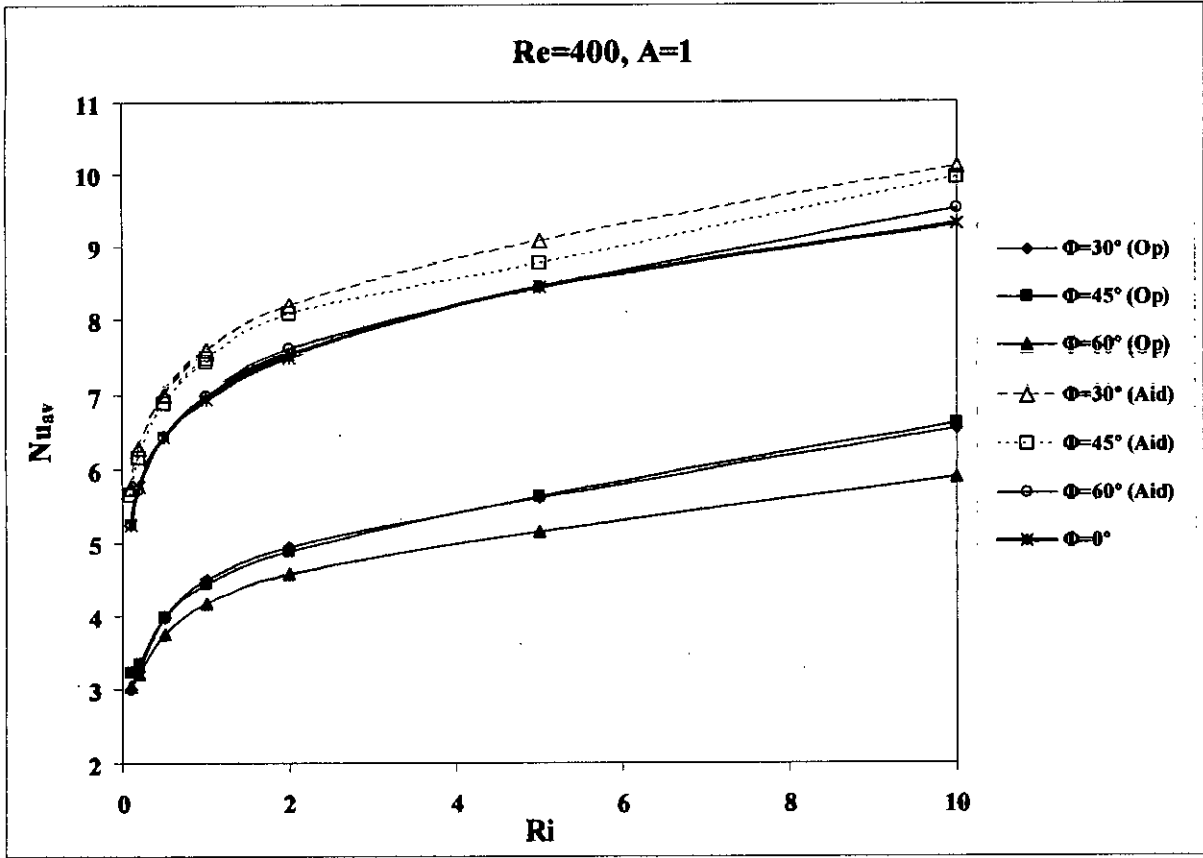


Figure 5.61: Variation of  $Nu_{av}$  with  $Ri$  at  $A=1$ ,  $Re=400$

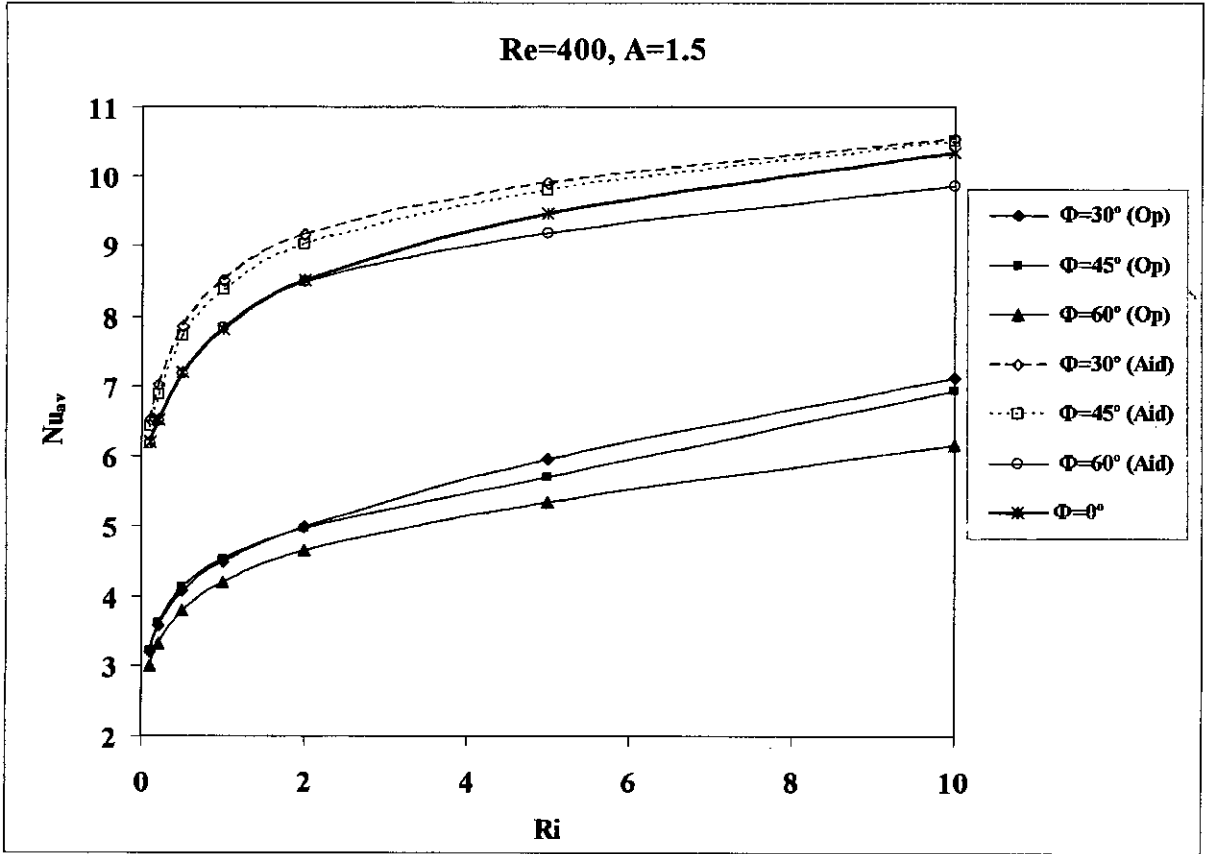


Figure 5.62: Variation of  $Nu_{av}$  with  $Ri$  at  $A=1.5$ ,  $Re=400$

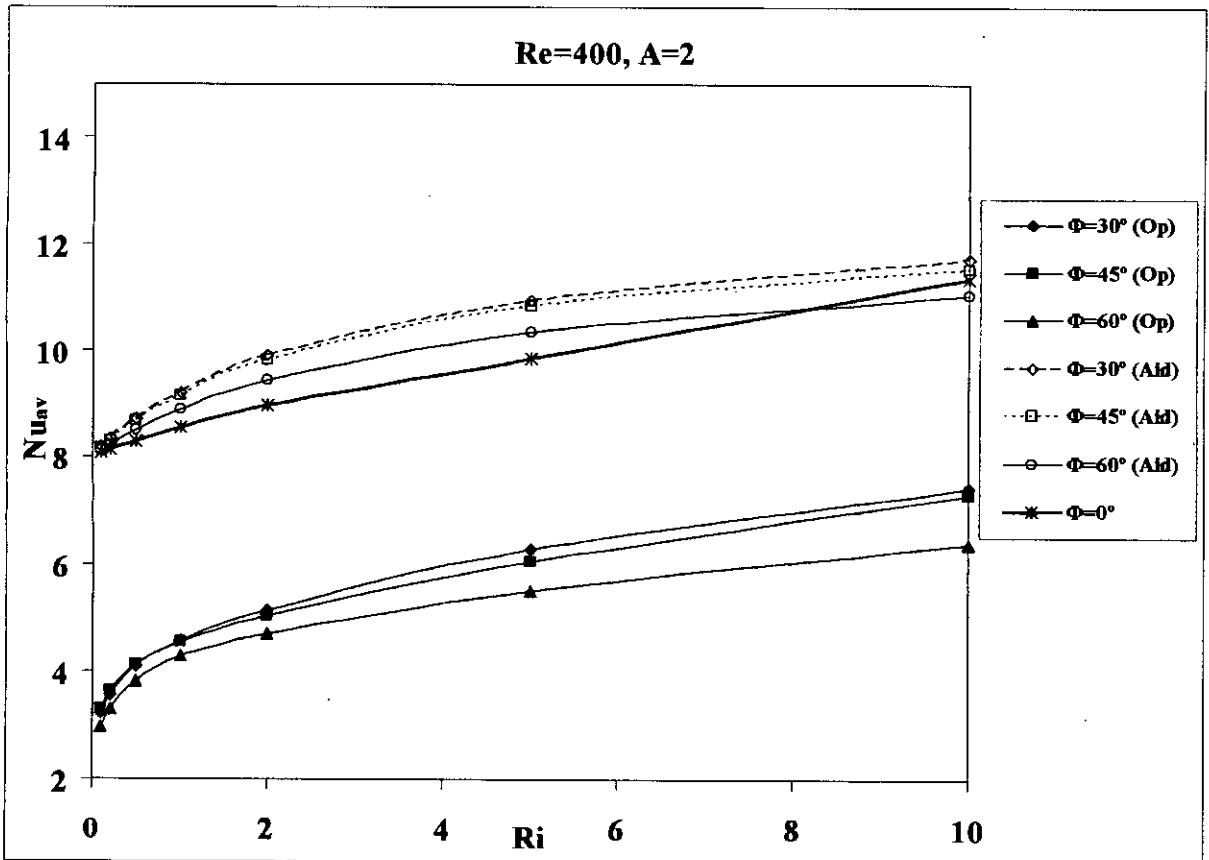


Figure 5.63: Variation of  $Nu_{av}$  with  $Ri$  at  $A=2$ ,  $Re=400$

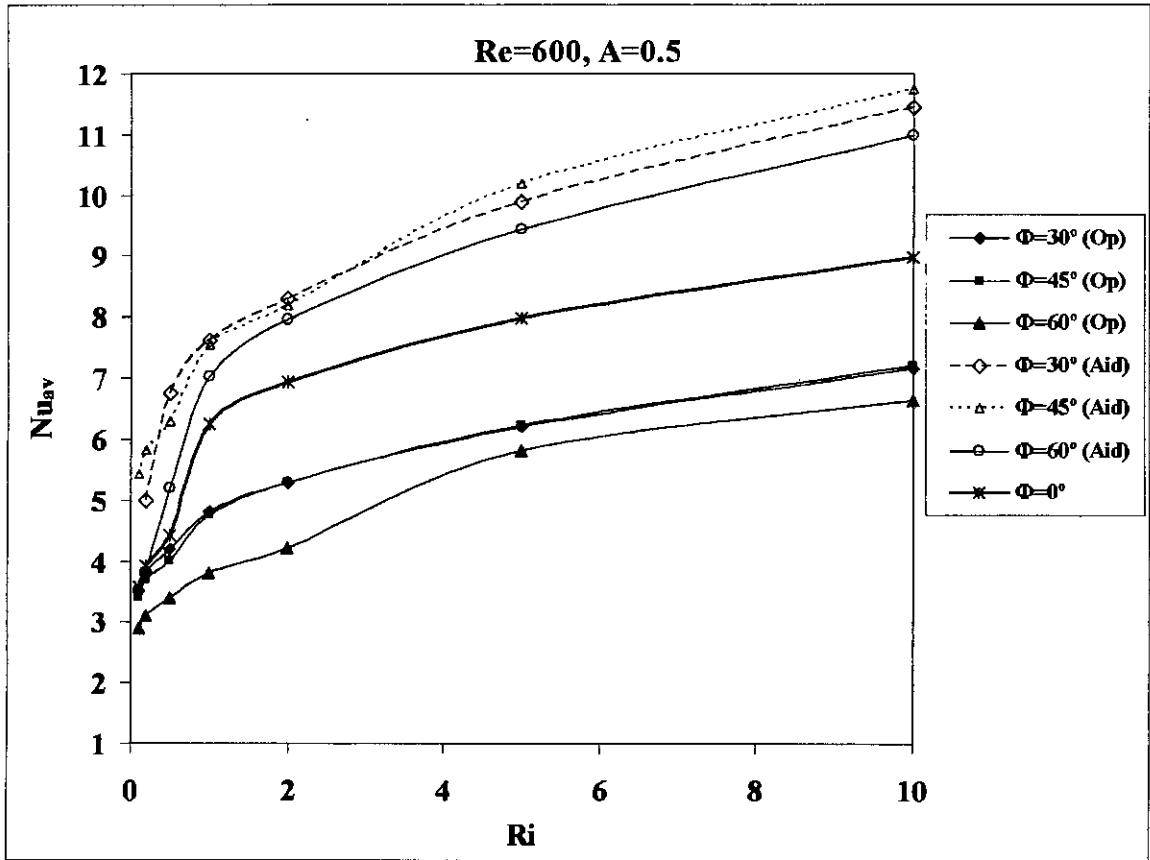


Figure 5.64: Variation of  $Nu_{av}$  with  $Ri$  at  $A=0.5$ ,  $Re=600$

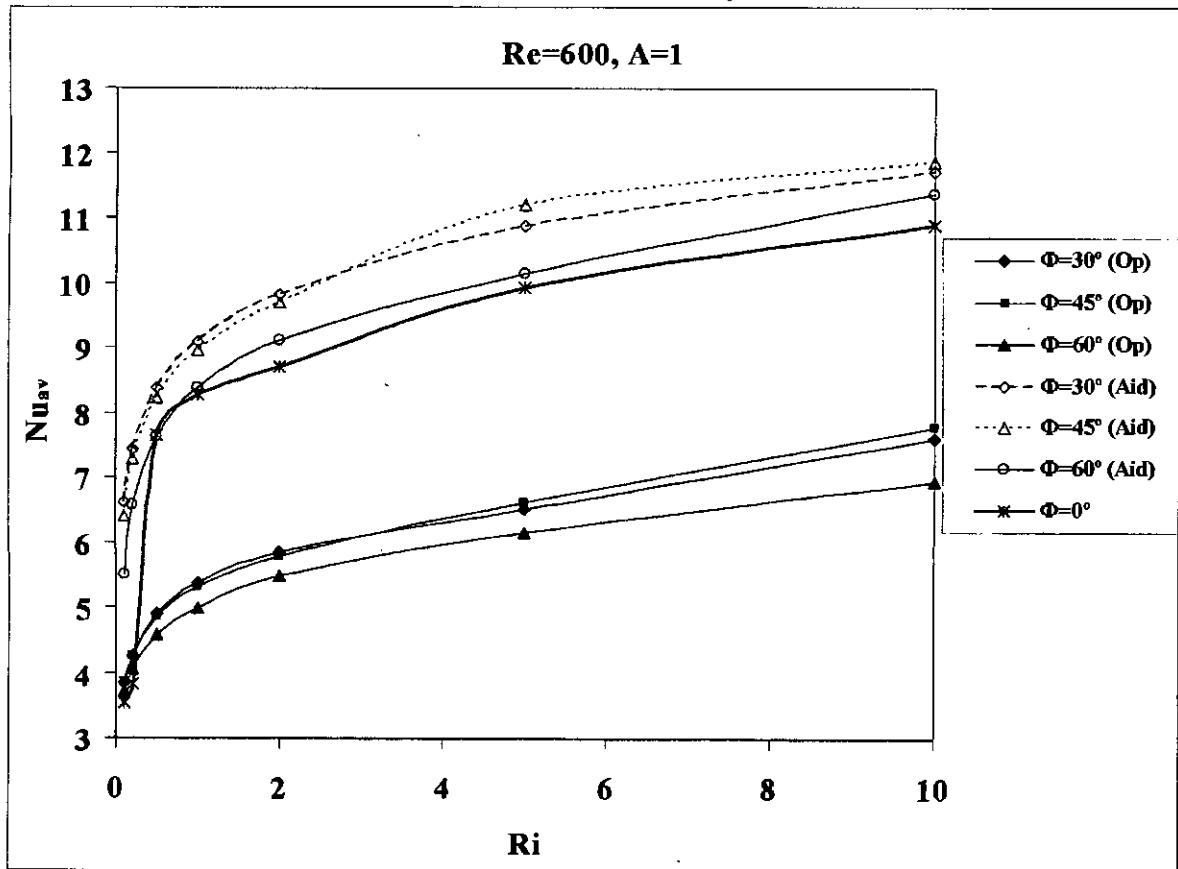


Figure 5.65: Variation of  $Nu_{av}$  with  $Ri$  at  $A=1$ ,  $Re=600$

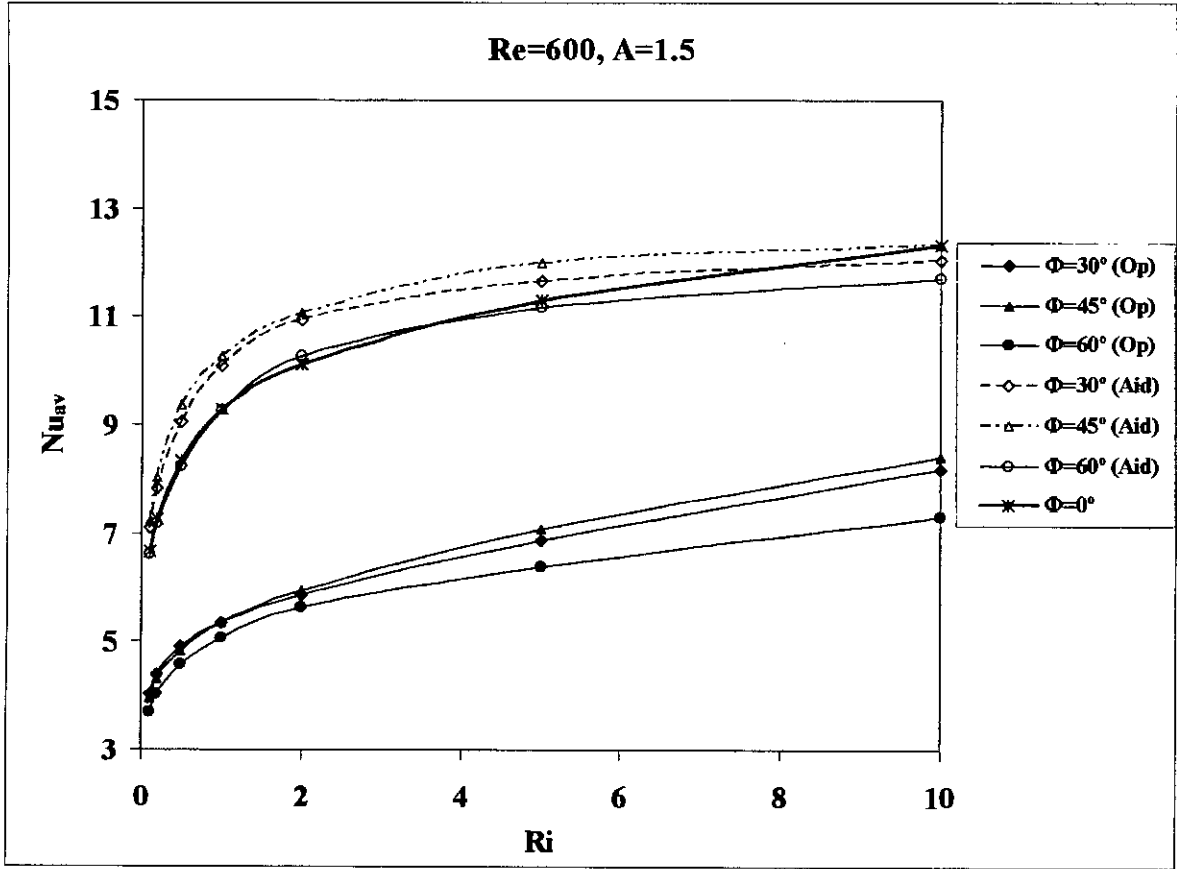


Figure 5.66: Variation of  $Nu_{av}$  with  $Ri$  at  $A=1.5$ ,  $Re=600$

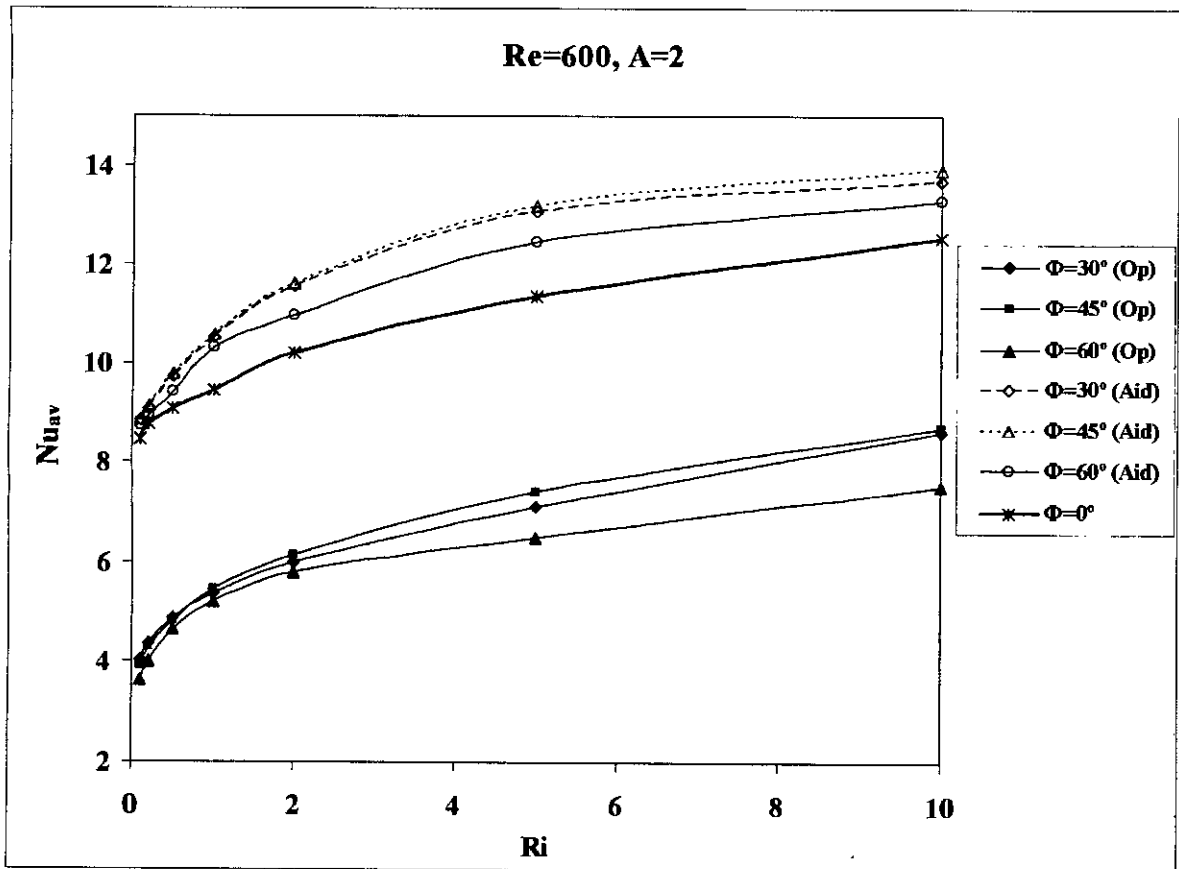


Figure 5.67: Variation of  $Nu_{av}$  with  $Ri$  at  $A=2$ ,  $Re=600$





## CHAPTER 6

# CONCLUSION

---

The conclusions that can be drawn from this study are listed below:

### General Conclusions

1. As the Richardson number increases the  $Nu_{av}$  increases accordingly at all Aspect ratios, because at higher Richardson number natural convection dominates the forced convection.
2. As Aspect Ratio increases from 0.5 to 2.0, the heat transfer rate increases. This is due to the fact that the cavity volume increases with aspect ratio and more volume of cooling air is involved in cooling the heat source leading to better cooling effect.

### Specific Conclusions from This Study

3. The optimum configuration of the trapezoidal enclosure has been obtained at  $\gamma=45^\circ$ , as at this configuration the  $Nu_{av}$  was maximum at all Richardson number.
4. The direction of the motion of the lid also affects the heat transfer phenomena. Aiding flow condition always gives better heat transfer rate than opposing flow condition. Because at aiding flow condition, the shear driven flow aids the natural convective flow, resulting a much stronger convective current that leads to better heat transfer.
5. The  $Nu_{av}$  is also sensitive to rotational angle  $\Phi$ . Nusselt number decreases as the rotational angle,  $\Phi$  increases from  $0^\circ$  for opposing flow condition. For aiding flow condition,  $Nu_{av}$  increases up to  $\Phi=30^\circ$ , and then it starts decreasing.  $Nu_{av}$  increases marginally at  $\Phi=30^\circ$  from  $\Phi=45^\circ$  but at  $\Phi=60^\circ$ ,  $Nu_{av}$  drops significantly for all the aspect ratios.

## CHAPTER 7

# FURTHER RECOMMENDATIONS

---

The following recommendation can be put forward for the further work on this present research.

1. Numerical investigation can be carried out by incorporating different physics like radiation effects, internal heat generation/ absorption.
2. Double diffusive natural convection can be analyzed through including the governing equation of concentration conservation.
3. Investigation can be performed by using magnetic fluid or electrically conducting fluid within the trapezoidal cavity and changing the boundary conditions of the cavity's wall.
4. Investigation can be performed by moving the other lids of the enclosure and see the heat transfer effect.
5. Investigation can be carried out by changing the Prandtl number of the fluid inside the trapezoidal enclosure.
6. Investigation can be carried out by using a porous media inside the trapezoidal cavity instead of air.

## REFERENCES

- [1] H. Benard, "Fouration de centers de gyration a L'arriere d'cen obstacle en movement", *Compt. Rend*, vol. 147, pp. 416-418, 1900.
- [2] L. Rayleigh, "On convection currents in a horizontal layer of fluid when the higher temperature is on the underside", *Philos. Mag.*, vol. 6, no. 32, pp. 529-546, 1916.
- [3] H. Jeffreys, "Some cases of instabilities in fluid motion", *Proc. R. Soc. Ser.A*, vol. 118, pp. 195-208, 1928.
- [4] F.P. Incropera, Convection heat transfer in electronic equipment cooling, *J.Heat Transfer* 110 (1988) 1097-1111.
- [5] C. K. Cha and Y. Jaluria, Recirculating mixed convection flow for energy extraction, *Int. j. Heat Mass Transfer* 27.1801-1810 (1984).
- [6] J. Imberger and P. F. Hamblin, Dynamics of lakes, reservoirs, and cooling ponds, *A. Rev. Fluid Mech.* 14, 153-187 (1982).
- [7] F. J. K. Ideriah, Prediction of turbulent cavity flow driven by buoyancy and shear, *J. Mech. Engng Sci.* 22, 287-295 (1980).
- [8] L. A. B. Pilkington, Review lecture: The float glass process, *Proc. R. Sot. Lond., IA* 314, 1-25 (1969).
- [9] O. Aydin, W.J. Yang, Mixed convection in cavities with a locally heated lower wall and moving sidewalls, *Numer. Heat Transfer, Part A* 37 (2000) 695-710.
- [10] K. Torrance, R. Davis, K. Eike, P. Gill, D. Gutman, A. Hsui, S. Lyons, H. Zien, Cavity flows driven by buoyancy and shear, *J. Fluid Mech.* 51 (1972) 221-231.
- [11] E. Papanicolaou, Y. Jaluria, Mixed convection from and isolated heat source in a rectangular enclosure, *Numer. Heat Transfer, Part A* 18 (1990) 427-461
- [12] E. Papanicolaou, Y. Jaluria, Transition to a periodic regime in mixed convection in a square cavity, *J. Fluid Mech.* 239 (1992) 489-509
- [13] E. Papanicolaou, Y. Jaluria, Mixed convection from a localized heat source in a cavity with conducting walls: A numerical study, *Numer. Heat Transfer, Part A* 23 (1993) 463-484
- [14] E. Papanicolaou, Y. Jaluria, Mixed convection from simulated electronic components at varying relative positions in a cavity *J. Heat Transfer*, 116 (1994) 960-970
- [15] J. R. Kosef and R. L. Street, The Lid-Driven Cavity Flow: A Synthesis of Quantitative and Qualitative Observations, *ASME J. Fluids Engng.*, 106(1984) 390-398.

- [16] K. Khanafer and A. J. Chamkha, Mixed convection flow in a lid-driven enclosure filled with a fluid saturated porous medium, *Int. J. Heat Mass Transfer*, 36 (1993) 1601-1608.
- [17] G. A. Holtzman, R. W. Hill, K. S. Ball, Laminar natural convection in isosceles triangular enclosures heated from below and symmetrically cooled from above, *J. Heat Transfer* 122 (2000) 485-491.
- [18] H. Asan, L. Namli, The laminar natural convection in a pitched roof of triangular cross-section for summer day boundary conditions, *Energy and Buildings* 33 (2001) 753-757.
- [19] M.K. Moallemi, K.S. Jang, Prandtl number effects on laminar mixed convection heat transfer in a lid-driven cavity, *Int. J. Heat Mass Transfer* 35 (1992) 1881-1892.
- [20] A.A. Mohammad, R. Viskanta, Laminar flow and heat transfer in Rayleigh-Benard convection with shear, *Phys. Fluids A* 4 (1992) 2131-2140.
- [21] A.A.Mohammad,R.Viskanta,Flow structures and heat transfer in a lid-driven cavity filled with liquid gallium and heated from below, *Exp. Thermal Fluid Sci.* 9 (1994) 309-319.
- [22] R.B. Mansour, R. Viskanta, Shear-opposed mixed-convection flow heat transfer in a narrow, vertical cavity, *Int. J. Heat Fluid Flow* 15 (1994) 462-469.
- [23] R. Iwatsu, J.M. Hyun, K. Kuwahara, Mixed convection in a driven cavity with a stable vertical temperature gradient, *Int. J. Heat Mass Transfer* 36 (1993) 1601-1608.
- [24] R. Iwatsu, J.M. Hyun, Three-dimensional driven cavity flows with a vertical temperature gradient, *Int. J. Heat Mass Transfer* 38 (1995) 3319-3328.
- [25] A. A. Mohammad, R. Viskanta, Flow and heat transfer in a lid-driven cavity filled with a stably stratified fluid, *Appl. Math. Model.* 19 (1995) 465-472.
- [26] A.K. Prasad, J.R. Koseff, Combined forced and natural convection heat transfer in a deep lid-driven cavity flow, *Int. J. Heat Fluid Flow* 17 (1996) 460-467.
- [27] T.H. Hsu, S.G. Wang, Mixed convection in a rectangular enclosure with discrete heat sources, *Numer. Heat Transfer, Part A* 38 (2000) 627-652.
- [28] O. Aydin, W.J. Yang, Mixed convection in cavities with a locally heated lower wall and moving sidewalls, *Numer. Heat Transfer, Part A* 37 (2000) 695-710.
- [29] P.N. Shankar, V.V. Meleshko, E.I. Nikiforovich, Slow mixed convection in rectangular containers, *J. Fluid Mech.* 471 (2002) 203-217.
- [30] H.F. Oztop, I. Dagtekin, Mixed convection in two-sided lid-driven differentially heated square cavity, *Int. J. Heat Mass Transfer* 47 (2004) 1761-1769.
- [31] M. A. R. Sharif, Laminar mixed convection in shallow inclined driven cavities with hot moving lid on top and cooled from bottom, *Applied Thermal Engineering* 27 (2007) 1036-1042.

[32] G. Guo, M. A. R. Sharif, Mixed convection in rectangular cavities at various aspect ratios with moving isothermal sidewalls and constant flux heat source on the bottom wall, *Int. J. Thermal Sciences* 43 (2004) 465–475.

# APPENDIX

## AVERAGE NUSSELT NUMBER FOR TRAPEZOIDAL ENCLOSURE

Optimum Inclination Angle,  $\gamma$ :

Table 1: Average Nusselt number,  $Nu_{av}$  at Different Reynolds number,  $Re$  and Richard number,  $Ri$

Ri	30°		45°		60°	
	Re=400	Re=600	Re=400	Re=600	Re=400	Re=600
0.1	3.057	3.5	5.243	3.534	4.96	5.94
0.2	3.091	3.65	5.755	3.82	5.1	6.0554
0.5	5.01	5.75	6.426	7.646	5.52	6.41
1	6.02	6.8	6.95	8.27	5.766	6.74
2	7.1	7.95	7.53	8.7	6.17	7.185
5	8.15	9.44	8.442	9.93	7.03	7.9489
10	9.05	10.23	9.32	10.89	7.839	8.6847

Table 2: Average Nusselt number,  $Nu_{av}$  at  $\Phi=0^\circ$  and  $Re=400$

Ri	A=0.5	A=1.0	A=1.5	A=2.0
0.1	2.81	5.243	6.2	8.076
0.2	3.063	5.755	6.527	8.13
0.5	4.988	6.426	7.2	8.305
1	5.533	6.95	7.82	8.556
2	6.14	7.53	8.511	8.965
5	7.811	8.442	9.47	9.85
10	8	9.32	10.35	11.355

Table 3: Average Nusselt number,  $Nu_{av}$  at  $\Phi=0^\circ$  and  $Re=600$

Ri	A=0.5	A=1	A=1.5	A=2
0.1	3.57	3.534	6.66	8.47
0.2	3.925	3.82	7.25	8.76
0.5	4.42	7.646	8.33	9.065
1	6.245	8.27	9.274	9.44
2	6.94	8.7	10.12	10.2
5	7.986	9.93	11.3	11.344
10	8.98	10.89	12.31	12.54

Table 4: Average Nusselt number,  $Nu_{av}$  at  $\Phi=30^\circ$  and  $Re=400$ , opposing flow condition

<b>Ri</b>	<b>A=0.5</b>	<b>A=1.0</b>	<b>A=1.5</b>	<b>A=2.0</b>
0.1	2.8	3	3.197	3.23
0.2	3.01	3.243	3.568	3.568
0.5	3.3	3.97	4.07	4.099
1	3.7	4.5	4.493	4.5797
2	4.2	4.94	4.98	5.1348
5	4.9925	5.6	5.959	6.2845
10	6.06	6.55	7.11	7.437

Table 5: Average Nusselt number,  $Nu_{av}$  at  $\Phi=30^\circ$  and  $Re=600$ , opposing flow condition

<b>Ri</b>	<b>A=0.5</b>	<b>A=1</b>	<b>A=1.5</b>	<b>A=2</b>
0.1	3.5	3.8298	4.028	4.023
0.2	3.8	4.25	4.4	4.36
0.5	4.2	4.889	4.91	4.863
1	4.8	5.359	5.34	5.374
2	5.28	5.83	5.86	5.987
5	6.2	6.5	6.85	7.1
10	7.165	7.61	8.184	8.63

Table 6: Average Nusselt number,  $Nu_{av}$  at  $\Phi=45^\circ$  and  $Re=400$ , opposing flow condition

<b>Ri</b>	<b>A=0.5</b>	<b>A=1</b>	<b>A=1.5</b>	<b>A=2</b>
0.1	2.75	3.22	3.223	3.288
0.2	2.95	3.338	3.615	3.6358
0.5	3.2	3.98	4.13	4.12
1	3.6	4.44	4.53	4.536
2	4.1	4.876	4.97	5.05
5	5.02	5.62	5.7	6.05
10	6.05	6.62	6.94	7.316

Table 7: Average Nusselt number,  $Nu_{av}$  at  $\Phi=45^\circ$  and  $Re=600$ , opposing flow condition

<b>Ri</b>	<b>A=0.5</b>	<b>A=1</b>	<b>A=1.5</b>	<b>A=2</b>
0.1	3.4	3.85	3.96	3.916
0.2	3.7	4.25	4.31	4.265
0.5	4.01	4.845	4.84	4.81
1	4.76	5.297	5.35	5.46
2	5.3	5.77	5.9316	6.1175
5	6.229	6.613	7.075	7.423
10	7.19677	7.766	8.395	8.71



Table 8: Average Nusselt number,  $Nu_{av}$  at  $\Phi=60^\circ$  and  $Re=400$ , opposing flow condition

Ri	A=0.5	A=1	A=1.5	A=2
0.1	2.6	3.039	2.9929	2.974
0.2	2.8	3.2078	3.31	3.288
0.5	3.06	3.752	3.785	3.826
1	3.4	4.16	4.2	4.2945
2	3.9581	4.563	4.654	4.713
5	4.68	5.155	5.34	5.523
10	5.51	5.89	6.171	6.382

Table 9: Average Nusselt number,  $Nu_{av}$  at  $\Phi=60^\circ$  and  $Re=600$ , opposing flow condition

Ri	A=0.5	A=1	A=1.5	A=2
0.1	2.9	3.719	3.7	3.634
0.2	3.1	4.044	4.026	4.003
0.5	3.4	4.5698	4.563	4.63
1	3.8	4.98	5.0655	5.193
2	4.225	5.4713	5.614	5.79
5	5.82	6.145	6.383	6.5
10	6.627	6.93	7.289	7.54

Table 10: Average Nusselt number,  $Nu_{av}$  at  $\Phi=30^\circ$  and  $Re=400$ , Aiding flow condition

Ri	A=0.5	A=1	A=1.5	A=2
0.1	4.44	5.75	6.518	8.1755
0.2	5.02	6.278	7.01	8.34
0.5	5.86	7	7.85	8.7
1	6.56	7.58	8.51	9.2
2	7.34	8.2	9.16	9.9169
5	8.46	9.09	9.9	10.95
10	9.63	10.1	10.533	11.72

Table 11: Average Nusselt number,  $Nu_{av}$  at  $\Phi=30^\circ$  and  $Re=600$ , Aiding flow condition

Ri	A=0.5	A=1	A=1.5	A=2
0.1		6.62	7.09	8.84
0.2	5	7.43	7.82	9.08
0.5	6.748	8.37	9.048	9.72
1	7.61	9.08	10.089	10.52
2	8.3	9.825	10.92	11.543
5	9.899	10.867	11.658	13.06
10	11.45	11.72	12.05	13.67

Table 12: Average Nusselt number,  $Nu_{av}$  at  $\Phi=45^\circ$  and  $Re=400$ , Aiding flow condition

Ri	A=0.5	A=1	A=1.5	A=2
0.1	3.91	5.237	6.177	8.112
0.2	4.543	5.73225	6.5051	8.225
0.5	5.357	6.43	7.171	8.497
1	6.05	6.991	7.835	8.88
2	6.81	7.6	8.498	9.43
5	8.1	8.44	9.18	10.354
10	9.35	9.52	9.8639	11.057

Table 13: Average Nusselt number,  $Nu_{av}$  at  $\Phi=45^\circ$  and  $Re=600$ , Aiding flow condition

Ri	A=0.5	A=1	A=1.5	A=2
0.1	3.5	5.5	6.606	8.75
0.2	3.8	6.57	7.17	8.94
0.5	5.2	7.63	8.24	9.42
1	7.016	8.38	9.25	10.3
2	7.96	9.11	10.255	10.959
5	9.44	10.15	11.169	12.437
10	11	11.37	11.7	13.283

Table 14: Average Nusselt number,  $Nu_{av}$  at  $\Phi=60^\circ$  and  $Re=400$ , Aiding flow condition

Ri	A=0.5	A=1	A=1.5	A=2
0.1	2.6	3.039	2.9929	2.974
0.2	2.8	3.2078	3.31	3.288
0.5	3.06	3.752	3.785	3.826
1	3.4	4.16	4.2	4.2945
2	3.9581	4.563	4.654	4.713
5	4.68	5.155	5.34	5.523
10	5.51	5.89	6.171	6.382

Table 15: Average Nusselt number,  $Nu_{av}$  at  $\Phi=60^\circ$  and  $Re=600$ , Aiding flow condition

Ri	A=0.5	A=1	A=1.5	A=2
0.1	2.9	3.719	3.7	3.634
0.2	3.1	4.044	4.026	4.003
0.5	3.4	4.5698	4.563	4.63
1	3.8	4.98	5.0655	5.193
2	4.225	5.4713	5.614	5.79
5	5.82	6.145	6.383	6.5
10	6.627	6.93	7.289	7.54

